

Chapter 5

Annual Mean Sea Level

5.1 Observational Background

While concluding the Great Trigonometrical Survey of India, Colonel S. G. Burrard made the following observation [quoted after Ghildyal and Kumar, 1984].

Whilst therefore the levelling operations 1858–1909 have proved that the mean surface of the Arabian Sea and the Bay of Bengal are very nearly at the same elevation, they have also given rise to a suspicion, that the Bay of Bengal may be perhaps slightly higher of the two. It is but a suspicion, the accuracy of the levelling does not warrant us in pronouncing the divergence to be proved. It will be for our successors to show by means of future lines, whether the suspicion is well-founded, or whether the divergence is a result of levelling errors.

The Great Trigonometrical Survey of India was carried out during 1858–1909 to map the surface topography of the Indian subcontinent, and was, in its time, the most detailed and accurate survey of its kind ever undertaken. It is in the course of this survey that a difference of about 30 cm was noticed between the mean sea level¹ in the Bay of Bengal and the Arabian Sea, an observation that was confirmed during the Adjustment of the First Level Net of India [Ghildyal and Kumar, 1984]. The observations show that the mean sea level at Vishakhapatnam is 32 cm higher than that at Mumbai and that the mean sea level at Chennai is 17 cm higher than that at Mangalore. The permitted error in levelling over 1080 km, the distance along the levelling lines between Chennai and Mangalore, is 9.8 cm; thus, even after accounting for possible errors in levelling, the mean sea level along the east coast of India is higher than that along the west coast [Ghildyal and Kumar, 1984].

¹By mean sea level, Ghildyal and Kumar mean annual sea level, which is the same as annual mean sea level.

5.2 Theoretical Background

The only study of this difference in mean sea level that we are acquainted with is the one by Ghildyal and Kumar [1984]. They state that “enough levelling data have accumulated to carry forward the investigation from the stage where Colonel Burrard left it for us to complete. The divergence in mean sea level is apparent and this is not due to errors of levelling alone but other factors also.” They compute the difference in sea level for several choices of levelling lines before reaching this conclusion. The difference in mean sea level between Chennai and Mangalore is attributed to the lower surface salinity at Chennai (6.7 cm) and higher sea surface temperature (SST) at Chennai (8 cm), with the lower atmospheric pressure at Mangalore reducing the difference by 5 cm. These three factors together account for a difference of about 7 cm between Chennai and Mangalore, less than the permissible error due to levelling. Ghildyal and Kumar state that the apparent difference in mean sea level between the two coasts can be accounted for by these corrections and levelling errors, and that this implies that the mean sea level is not different along these two coasts! The authors are surveyors, and their discomfort at the possibility of a variation in mean sea level along the boundary of the open sea is evident. Hence, though Ghildyal and Kumar on the right track as far as discerning the causes of the observed difference are concerned, their aim is to explain away the difference.

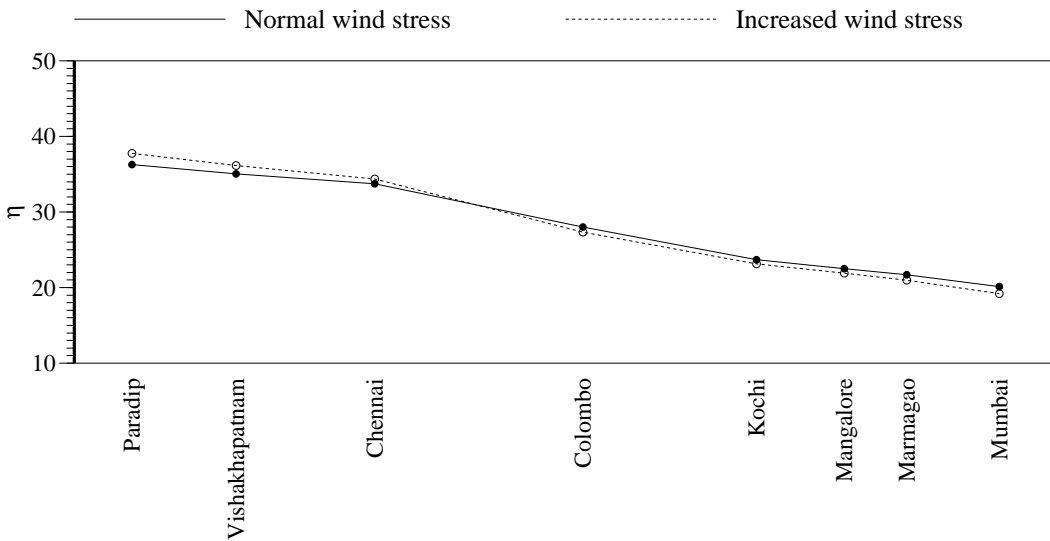
There is no reason for assuming that such a difference in mean sea level cannot exist between the east and west coasts of India. The observations suggest that there is a mean alongshore gradient of sea level along the coast of India. Hence, we accept the observation of Colonel Burrard, confirmed by Ghildyal and Kumar, and see we can discern the causes. As we saw earlier, both wind-forced coastal currents and salinity make a significant contribution to the seasonal cycle of sea level along the coast of India. Of these, salinity is invoked by Ghildyal and Kumar too, except that they use only the surface salinity (and temperature). This is not correct because dynamic heights are determined with respect to a level of no motion, and hence depend on the vertical profile of temperature and salinity between this level and the sea surface, as in the reduced-gravity model.

5.3 Effect of Wind-Forced Coastal Currents

The effect of wind-forced coastal currents on the seasonal cycle of coastal sea level was examined in Section 4.1 using a dynamical $1\frac{1}{2}$ -layer reduced-gravity model. The annual sea level² from this simulation is plotted for the coastal stations in Figure 5.1. There is an alongshore gradient in sea level, the annual sea level at Vishakhapatnam being higher than that at Mumbai by about 15 cm

²Having described the background for this chapter, we return to our preferred terminology.

Figure 5.1 Effect of wind-forced coastal currents on annual sea level η along the coast. The figure shows annual sea level (cm) for two simulations with the $1\frac{1}{2}$ -layer model. The first simulation is with the wind-stress climatology of Hellerman and Rosenstein [1983], as in the earlier chapters. The second simulation is for a “more vigorous monsoon circulation”, the wind stress of Hellerman and Rosenstein having been multiplied by 1.2. A stronger wind forcing amplifies the alongshore sea-level gradient; the annual sea level behaves like a see-saw along the coast, with its pivot at the southern tip of Sri Lanka.



and the annual sea level at Chennai being higher than that at Mangalore by about 11 cm. These values, though lower than the observations, are of the same order. The sea level slopes down continuously along the coast, with highest sea level at Paradip, in the northwestern corner of the Bay of Bengal, and lowest sea level at Mumbai, the northernmost station along the west coast.

In the above simulation, the model was forced by the wind-stress climatology of Hellerman and Rosenstein [1983]. The climatology is an average of data collected over several years, and hence, represents an average, or “normal”, monsoon. To see what a more vigorous monsoon would do to the alongshore gradient in sea level, we run a test case with the wind stress of Hellerman and Rosenstein multiplied by 1.2, implying a 10% increase in the strength of the wind all over the basin. The resulting annual sea level is also plotted in Figure 5.1. The sea level is now higher on the east coast, but lower on the west coast, the increase in the difference between Vishakhapatnam and Mumbai being about 13%, and that in the difference between Chennai and Mangalore being about 11%. The annual sea level see-saws along the coast, with its pivot at the southern tip of Sri Lanka. The see-saw goes up in the east if the winds are *uniformly* stronger over the basin throughout the year; it goes down in the east if the winds are weaker.

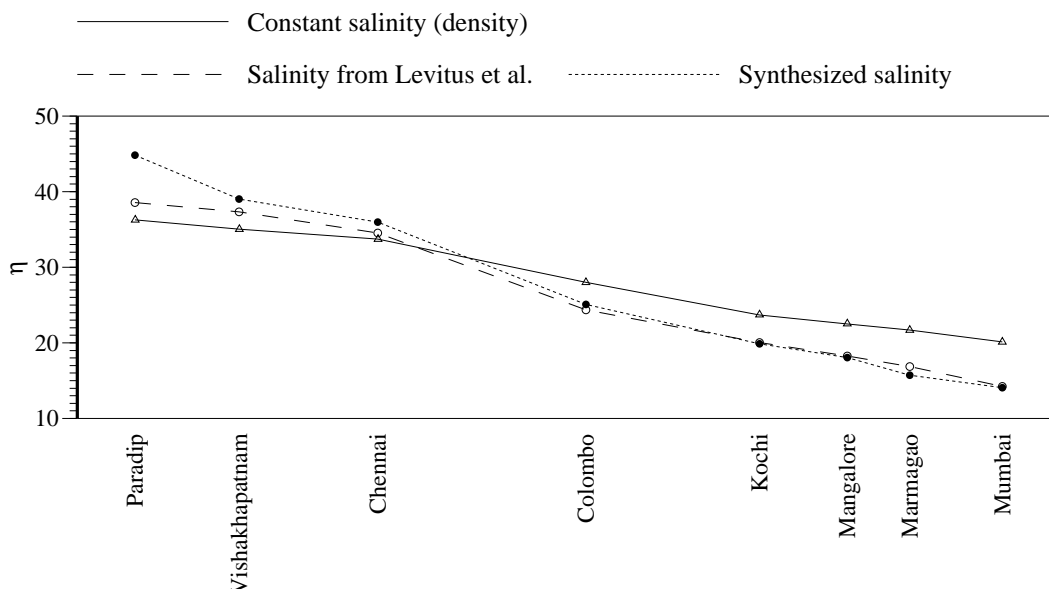
The observations of Colonel Burrard and Ghildyal and Kumar do not represent a climatology,

unlike our simulation. The observed difference in annual sea level between the two coasts is for a particular year, but it still gives an idea of the alongshore variability. The above simulations show that purely wind-forced circulation accounts for about half the observed difference.

5.4 Effect of the Alongshore Gradient in Salinity

Variations in temperature, as we saw earlier, have only a minor impact on the sea level along the Indian coast; hence, we ignore their effect on annual sea level and examine the contribution of salinity to the alongshore gradient in annual sea level. The effect of salinity is shown in Figure 5.2, which shows the annual sea level along the coast based on the simulation with the climatologies of Levitus and Boyer [1994] and Levitus et al. [1994] (Section 4.3.1) and the simulation with the synthesized climatology (Section 4.3.4). The difference in annual sea level between the two coasts

Figure 5.2 Effect of salinity on the annual sea level η along the coast. The figure shows annual sea level (cm) for three simulations with the $1\frac{1}{2}$ -layer model, all forced by the wind-stress climatology of Hellerman and Rosenstein [1983]. In the first simulation, density is constant in the active upper layer. In the second, temperature and salinity are prescribed from the climatologies of Levitus and Boyer [1994] and Levitus et al. [1994]. The third simulation is identical to the second, but the salinity field is modified along the coast from the northeastern corner of the Bay of Bengal to Veraval on the west coast of India, as described in Section 4.3.3. The alongshore gradient in salinity forces an alongshore gradient in annual sea level. The alongshore variations in salinity account for about half the difference in annual sea level between the east and west coasts of India.

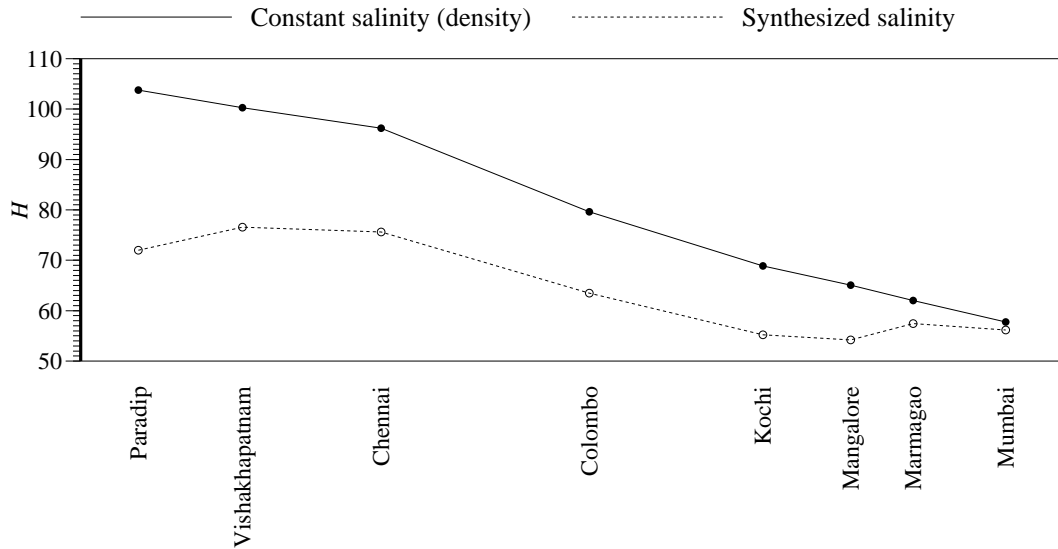


increases because of salinity; there is a marginal decrease in sea level along the west coast because

of a decrease in the annual mean Γ , but there is a large increase along the east coast because of a large increase in the annual mean Γ . The difference in sea level between Vishakhapatnam and Mumbai is now 25 cm and that between Chennai and Mangalore is 18 cm, closer to the observations. There is not much difference between the simulations with and without the modifications in salinity along the coast. This is because the annual mean coastal salinity in the climatology of Levitus et al. [1994] is not very different from that in the synthesized climatology; it is only the seasonal cycle of monthly climatology that departs considerably from observations.

In the presence of horizontal variations in salinity, there is a baroclinic contribution to the average pressure gradient in the upper layer³ from the horizontal density gradient in the layer. Since the pressure gradient has to vanish in the deeper layer, the presence of the low-salinity plume along the east coast also reduces the upper layer thickness (Figure 5.3). The decrease in layer

Figure 5.3 Effect of salinity on the annual upper layer thickness H along the coast. The figure shows annual upper layer thickness (m) for two simulations with the $1\frac{1}{2}$ -layer model, both forced by the wind-stress climatology of Hellerman and Rosenstein [1983]. In the first simulation, density is constant in the active upper layer. In the second, temperature and salinity are prescribed from the climatologies of Levitus and Boyer [1994] and Levitus et al. [1994], except along the coast of the Indian subcontinent from the northeastern corner of the Bay of Bengal to Veraval on the west coast of India, where it is modified as described in Section 4.3.3. The alongshore variation in salinity changes not only the alongshore gradient of annual sea level, but also that of upper layer thickness.



thickness along the east coast reduces the difference in layer thickness between the east and west coasts of India. In the purely wind-forced model, the upper layer is much thicker along the east

³See Appendix A.

coast. The presence of the low-salinity plume decreases it, but the layer thickness is still greater in the bay than in the Arabian Sea. Since the thickness of the upper layer is a measure of the thickness of the mixed layer, the higher thickness in the bay contradicts observations. This points to one of the limitations of the reduced-gravity model. It is a discrete model of a continuously stratified system. The large horizontal gradient in salinity, and hence in density, in the north Indian Ocean implies that the vertical structure is coupled to the horizontal structure; a simple decomposition into discrete vertical modes, as in the $1\frac{1}{2}$ -layer reduced-gravity model, is not possible, and if attempted, leads to the errors described above. The model is incapable of simulating the higher sea level in the Bay of Bengal without simulating a thicker upper layer also. These simulations show that the lower salinity in the Bay of Bengal, especially in the coastal waters of India, is the likely cause of the thinner mixed layers observed in the bay.

In conclusion, the simulations support the observation of Colonel Burrard, subsequently verified by Ghildyal and Kumar, that the annual sea level is higher on the east coast of India than on the west coast. Both wind-forced coastal currents and salinity contribute to this alongshore gradient in sea level. The impact of winds and salinity on annual sea level and the coupling that exists between the ocean, the atmosphere, and land imply that variability associated with the monsoon must lead to sea-level variability at lower frequencies; these lower frequencies form the subject of the following chapter.

Chapter 6

Interannual and Interdecadal Variability

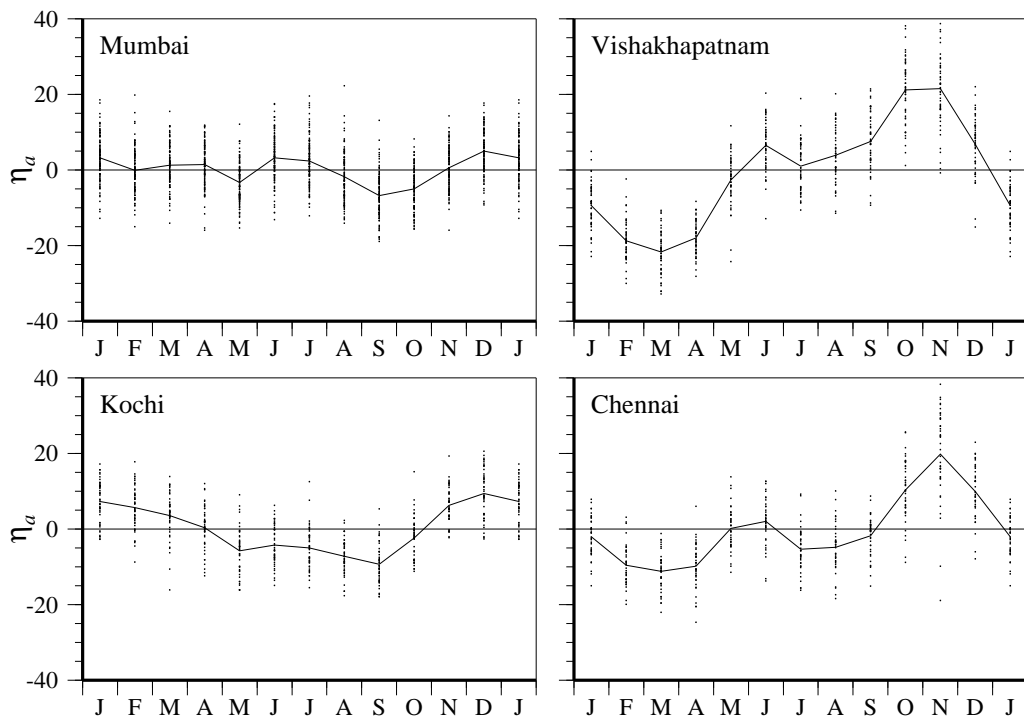
The striking aspect of the climate of the Indian subcontinent is the monsoon. The word *monsoon* is derived from the Arabic word *mausam*, which means “season”; it is used to describe the regular reversal of winds with season that determines the climate of the subcontinent. There are two facets of the monsoon. First, the change in weather with season is regular. For example, 1 June is the normal date of onset of the monsoon over southwest India. The seasonal cycle associated with the monsoon is so regular that a departure of more than a few days from this mean date of onset is sufficient cause for concern in the country. It is no different with the progress of the monsoon across the subcontinent; this too follows a definite pattern and is tracked in India by the official herald, the India Meteorological Department. This regular, rhythmic change in winds is responsible for the significant climatological seasonal cycle of sea level along the coast of India (Chapter 4). Thus, regularity, bordering on predictability, is one facet of the monsoon. Second, the monsoon is fickle: it varies a lot from one year to another. Associated with the seasonal changes in winds, which define the monsoonal climate, are changes in atmospheric pressure and, most important, rainfall. Since agriculture is the lifeblood of the subcontinent, it is the variability of rainfall that has the maximum impact and it has aroused interest for a long time, leading to rainfall becoming the best documented climatic variable in the subcontinent. There is considerable interannual and interdecadal variability in the rainfall records; since rainfall directly affects salinity in the ocean, it is inevitable that the interannual variability of the monsoon should lead to interannual variability in sea level along the coast of India. There is evidence for such variability in the tide-gauge record at Mumbai (Figure 1.3). In this chapter, we describe the interannual and interdecadal variations in the sea level along the coast of India and determine their possible causes.

6.1 Interannual Variability of Sea Level Along the Coast

6.1.1 Variability of the Seasonal Cycle

The regularity of the monsoon makes the seasonal cycle a major signal in the sea-level records along the coast of India. We begin our description of interannual variability by examining how the seasonal cycle varies from one year to another. One difficulty in studying sea-level variability at periods greater than a year is the short length of several records. Of the eight tide-gauge records used earlier, only those at Vishakhapatnam (52 years), Chennai (43 years), Kochi (50 years), and Mumbai (111 years) are longer than 40 years. Therefore, we restrict our attention just to these four stations¹. The anomalies of monthly sea level, computed by subtracting the mean of the time series from the sea level for each month, are plotted in Figure 6.1, which also shows the climatological seasonal cycle. There is considerable scatter about the climatology, the anomalies

Figure 6.1 Anomalies of uncorrected monthly sea level, η_a (cm). The continuous line is the climatological seasonal cycle. The dots represent the anomalies of monthly sea level, computed by subtracting the mean of the time series from the monthly sea level. There is considerable scatter about the climatology, indicating significant interannual variability of sea level along the coast of India.



¹The 40-year cutoff is arbitrary, but, as we shall see, even 40 years is not enough.

of monthly sea level being comparable to the range of the seasonal cycle. Therefore, there is considerable interannual variability in the sea level along the coast of India. The sea-level data used in Figure 6.1 include the effect of atmospheric pressure, which has a strong effect on the seasonal cycle; for example, it changes the sea level by about 10 cm in June at Mumbai. We apply the Inverse-Barometer (IB) approximation (Section 2.2.1) to correct for this effect, using monthly atmospheric-pressure data from the Global Historical Climate Network (GHCN); unfortunately, the GHCN data also have gaps and are not available for the entire span of the sea-level records (Table 6.1), thereby truncating them. In applying the IB approximation, we assume that the average monthly sea-level pressure over the world oceans does not change from year to year, this assumption being necessary since we have only climatological data (from COADS) for the average pressure. The resulting anomalies are plotted in Figure 6.2; there still is considerable scatter about the climatology.

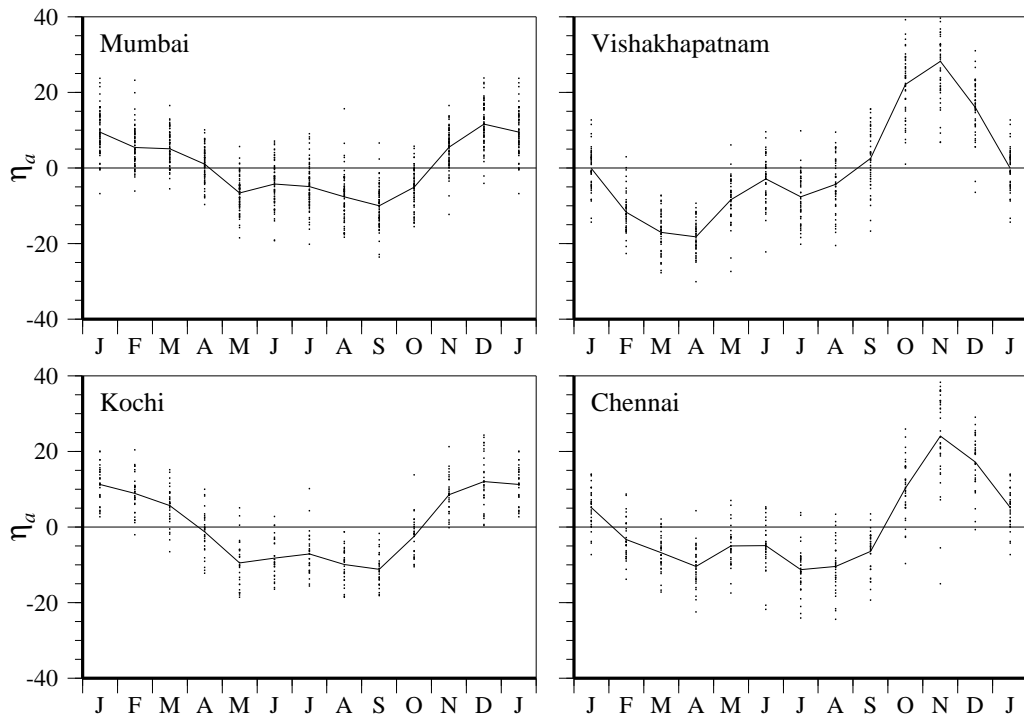
Table 6.1 Sea-level pressure data from the Global Historical Climate Network (GHCN). N_{yr} is the number of years of data available.

| Station | Longitude (°E) | Latitude (°N) | Time span | N_{yr} |
|-----------------------|-------------------|------------------|-----------|-----------------|
| Vishakhapatnam | 83.23 | 17.72 | 1941–1988 | 48 |
| Chennai (Minambakkam) | 80.18 | 13.00 | 1941–1988 | 48 |
| Kochi (Fort Cochin) | 76.20 | 10.00 | 1941–1973 | 33 |
| Mumbai (Colaba) | 72.82 | 18.90 | 1921–1988 | 68 |

Given that there are large changes in monthly sea level from year to year, how robust is the seasonal cycle? In other words, is the interannual variability such that it warps the seasonal cycle, or does the seasonal cycle repeat almost every year², with interannual changes merely perturbing it? One way to determine this is to check the timing of the extrema of the seasonal cycle. Histograms of the month of occurrence of the extrema of the seasonal cycle of sea level, not corrected for the effect of atmospheric pressure, are shown in Figure 6.3. The histograms show that the seasonal cycle is extremely robust on the east coast, there not being much variation in the timing of the maximum; the maximum occurs mostly in October or November at Vishakhapatnam and in November at Chennai. The scatter is more for the minimum, but it occurs mostly during February–April, when the anticyclonic gyre, with a poleward, upwelling-favourable western

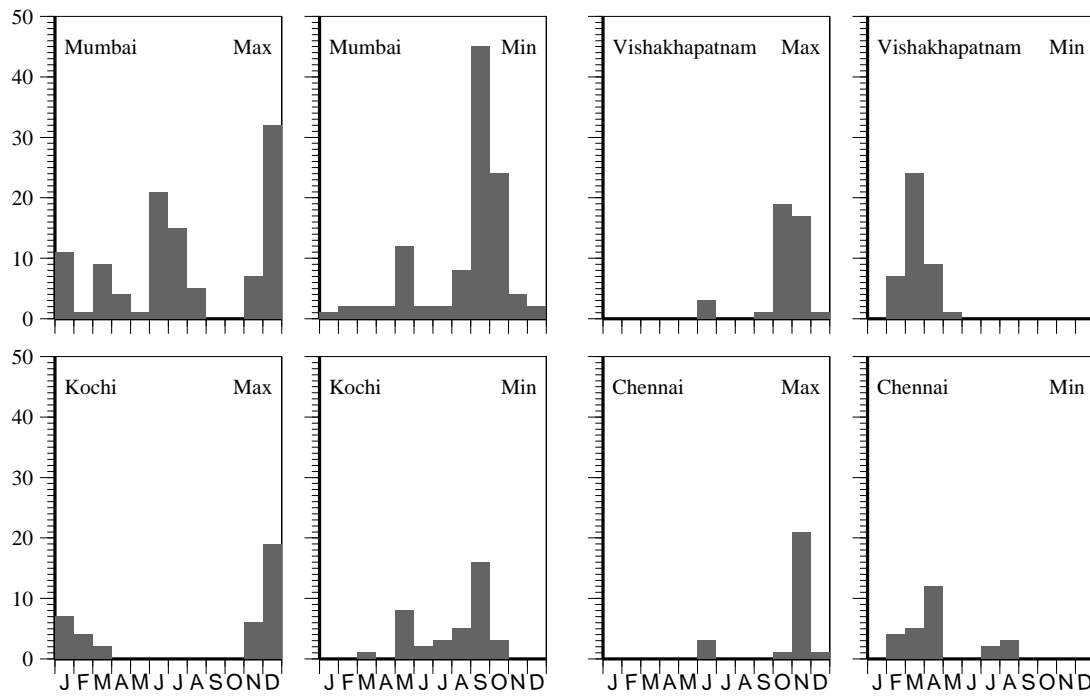
²For computations related to sea level, the year is defined from July of a given year to June of the following year in the rest of this chapter, unless otherwise stated. This is done because of the effect that salinity has on sea level along the coast of India. Since the changes in salinity are linked to monsoon rainfall, it seems more reasonable to define the year such that the monsoon rains occur “early in the year”, rather than in the middle; with this definition, rainfall for a given calendar year has an effect on sea level throughout the “year”. Another possible definition would start the year after the monsoon rains, say in October. Note that the calendar year is still used for computations involving rainfall.

Figure 6.2 Anomalies of corrected monthly sea level, η_a (cm). The continuous line is the climatological seasonal cycle. The dots represent the anomalies of monthly sea level, computed by subtracting the mean of the time series from the monthly sea level. There is considerable scatter about the climatology, indicating significant interannual variability of sea level along the coast of India.



boundary current, forms in the Bay of Bengal. Since Chennai lies close to the southern limit of the gyre and the size of the gyre depends on the wind field over the bay, the greater scatter there is not surprising. Along the west coast, however, there is considerable variation in the timing of the extrema, the scatter increasing poleward along the coast to Mumbai. At Kochi, the maximum occurs mostly during November–January, when the climatological seasonal cycle peaks there. The minimum occurs mostly in May, before the southwest monsoon, or in September, towards the end of the southwest monsoon; this reflects the existence of a minor secondary maximum during the southwest monsoon. At Mumbai, the extrema of the seasonal cycle can occur in almost any month of the year. The maximum occurs during winter, or during the southwest monsoon, or in March, reflecting the multiple peaks of the seasonal cycle before it is corrected for the effect of atmospheric pressure (Figure 4.1). The prominence of the semiannual signal is also reflected in the timing of the minimum, which usually occurs either towards the end of the southwest monsoon, or in May.

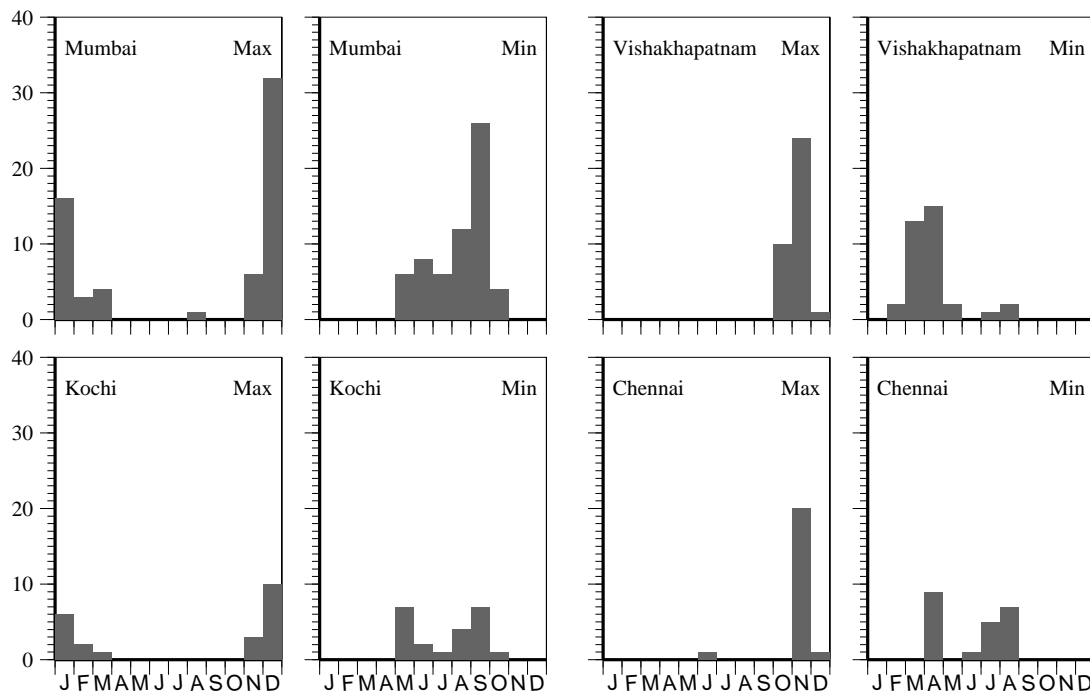
Figure 6.3 Histograms of the time of occurrence of the extrema of the seasonal cycle of uncorrected sea level. The number of occurrences of the extremum in a given month is plotted on the ordinate and the month during which the extremum occurs is plotted on the abscissa. The scatter in the timing of the extrema is more on the west coast, implying that the seasonal cycle is more robust along the east coast of India.



Since the effect of atmospheric pressure on the seasonal cycle is not small, it is necessary to determine how robust the corrected seasonal cycle is. The resulting histograms are shown in Figure 6.4; for comparison, the histograms for the uncorrected sea level are repeated in Figure 6.5, retaining only those years that contribute to Figure 6.4. These figures show that the seasonal cycle is much more robust when corrected for atmospheric pressure. There is a large decrease in the scatter in the timing of the extrema, especially at Mumbai, where the corrected seasonal cycle peaks almost always in winter.

Therefore, the seasonal cycle of sea level, when corrected for the effect of atmospheric pressure, is robust and the basic pattern of the seasonal cycle does not show significant interannual variations, reflecting the regularity with which the monsoon winds and salinity along the coast of India change. Nevertheless, there must be interannual variability in the annual sea level along the coast of India because the anomalies of monthly sea level with respect to the climatological seasonal cycle are not small (Figures 6.1 and 6.2).

Figure 6.4 Histograms of the time of occurrence of the extrema of the seasonal cycle of corrected sea level. The number of occurrences of the extremum in a given month is plotted on the ordinate and the month during which the extremum occurs is plotted on the abscissa. The scatter in the timing of the extrema is much less when the sea level is corrected for the effect of atmospheric pressure. The corrected seasonal cycle is more robust throughout the coast.



6.1.2 Variability of Annual Sea Level

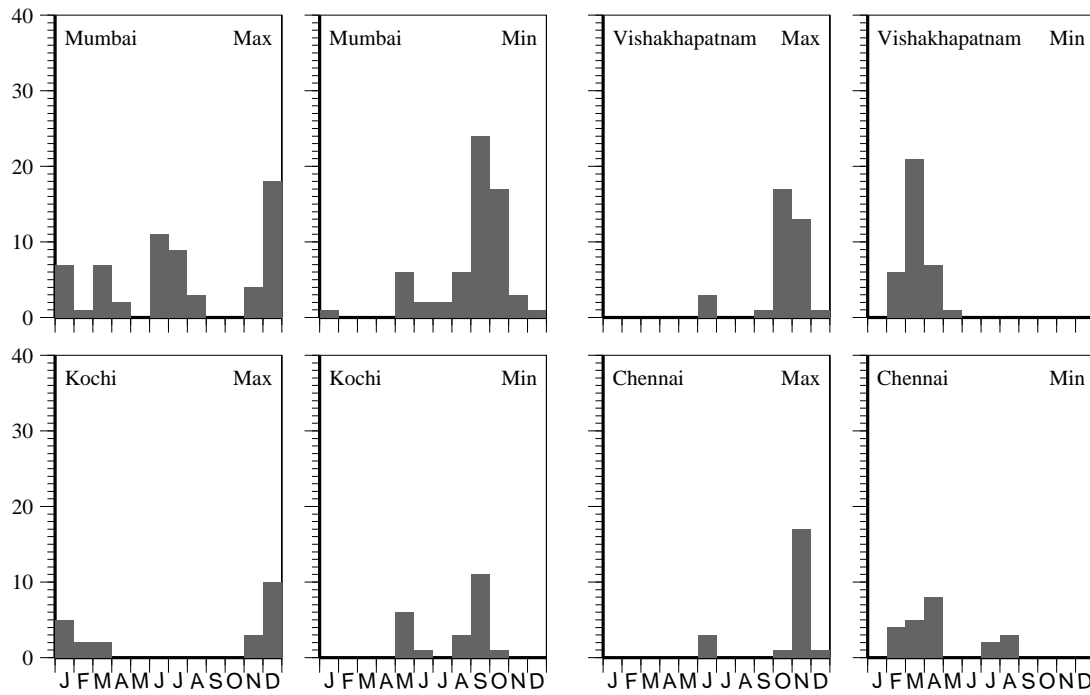
Annual sea level³ at a location is computed by averaging monthly sea level over a year. The sea-level records at the four stations are with respect to a given datum, the Revised Local Reference (RLR); hence, it is possible to average the annual sea level over the length of the record and compute anomalies of annual sea level. These anomalies, like the monthly anomalies, can be compared along the coast⁴, but, since the reference datum at each station is local to that station and is not linked to that at the others, it is not possible to compute absolute sea level at a station.

The anomalies of annual sea level are plotted in Figure 6.6; the monthly sea level used to compute the annual sea level for this figure are not corrected for the effect of atmospheric pressure. The annual sea level along the coast exhibits significant interannual variability, the range of

³Annual sea level is also called “annual mean”, or just “mean”, sea level in this chapter; the qualification is necessary at times because the annual extrema are also considered along with the annual mean. Nevertheless, “annual sea level”, when used as such, still refers to the annual mean.

⁴The difference in the length of the sea-level records, however, introduces some errors.

Figure 6.5 Histograms of the time of occurrence of the extrema of the seasonal cycle of uncorrected sea level, but for the same period as in Figure 6.4. The number of occurrences of the extremum is plotted on the ordinate and the month during which the extremum occurs is plotted on the abscissa. This figure is similar to Figure 6.3, except that the data cover only those years that contribute to Figure 6.4. The scatter in the timing of the extrema is more than for the corrected seasonal cycle, especially at Mumbai, reflecting the significant contribution made by atmospheric pressure to the seasonal cycle there.



the variation being comparable to that of the climatological seasonal cycle at each station. The anomalies of annual sea level are also coherent along the coast, and this coherence remains when the monthly sea level is corrected for atmospheric pressure before computing the annual sea level (Figure 6.7). This coherence is not just visual; the anomalies are also statistically well correlated⁵ along the coast (Table 6.2). The only exception seems to be the tide gauge at Kochi, where sea level rises sharply from the 1940s to 1960; the variation at the other stations is not similar, and this reduces the correlations for Kochi. Annual sea level at Kochi is best correlated with that at Chennai, but this is owing to the absence of data at Chennai during the 1940s.

This coherence along the coast is also seen in the variation of the annual extrema (Figures 6.8, 6.9). The maximum and minimum sea level during a year are in phase with the annual mean; they increase (decrease) when the mean increases (decreases). The correlation between the

⁵See Appendix C for the method used to compute the significance levels.

Table 6.2 Linear correlation statistics for annual sea level. η_V , η_C , η_K , and η_M denote the sea level anomalies at Vishakhapatnam, Chennai, Kochi, and Mumbai; the subscript “m” implies annual mean sea level. r is the linear correlation coefficient between the variables in the first two columns (at zero lag). r_s is the linear correlation at the $P\%$ significance level for the required number of degrees of freedom; if the column for P is blank, then r_s is the correlation at the 90% significance level, but the two variables are not correlated even at this level. A “C” in the last column implies that the sea-level data are corrected for the effect of atmospheric pressure (default is no correction). The correlation between Chennai and Kochi for corrected sea level is not computed because only seven degrees of freedom are available.

| | | r | r_s | P | |
|--------------|--------------|-------|-------|------|---|
| $\eta_{V,m}$ | $\eta_{C,m}$ | 0.779 | 0.561 | 99.0 | |
| $\eta_{V,m}$ | $\eta_{K,m}$ | 0.772 | 0.575 | 99.0 | C |
| $\eta_{V,m}$ | $\eta_{M,m}$ | 0.572 | 0.449 | 99.0 | |
| $\eta_{V,m}$ | $\eta_{C,m}$ | 0.482 | 0.444 | 95.0 | C |
| $\eta_{V,m}$ | $\eta_{K,m}$ | 0.401 | 0.316 | 95.0 | |
| $\eta_{V,m}$ | $\eta_{M,m}$ | 0.474 | 0.436 | 99.0 | C |
| $\eta_{C,m}$ | $\eta_{K,m}$ | 0.687 | 0.590 | 99.0 | |
| $\eta_{C,m}$ | $\eta_{M,m}$ | 0.593 | 0.505 | 99.0 | |
| $\eta_{C,m}$ | $\eta_{V,m}$ | 0.548 | 0.433 | 95.0 | C |
| $\eta_{K,m}$ | $\eta_{M,m}$ | 0.216 | 0.292 | | |
| $\eta_{K,m}$ | $\eta_{V,m}$ | 0.398 | 0.390 | 90.0 | C |

annual mean and the annual extrema is excellent (Table 6.3). It is not just the annual extrema that are in phase with the annual mean sea level; even the seasonal averages (for February–April, March–May, and July–September along both coasts, for October–December along the east coast, and for November–January along the west coast) are significantly correlated with the annual mean (Table 6.3). This implies that the major change from year to year is in the mean sea level, superimposed on which is the seasonal cycle. The interannual variations in this superimposed seasonal cycle lead to differential variations in the extrema and the seasonal averages of sea level.

6.2 Interdecadal Variability of Sea Level Along the Coast

An implication of the above statistics is that it is not necessary to correct for atmospheric pressure when determining the annual extrema. This is important because applying the correction using the GHCN pressure data truncates the length of the sea-level record. Not applying the correction implies that the sea-level record at Mumbai extends over 111 years (1878–1988), permitting us to use low-pass filters to examine the variability at even lower frequencies. The next longest record, at Vishakhapatnam, is only 52 years long; hence, only the tide gauge at Mumbai is useful for

Figure 6.6 Anomalies of uncorrected annual sea level (cm). The annual sea level was computed by averaging monthly sea level, not corrected for atmospheric pressure, over a year (July–June), and the mean of the time series was removed to obtain the anomalies. The curve for Mumbai is superimposed on those for the other three stations. The anomalies of annual sea level are coherent along the coast, Kochi being the only exception. The sharp rise in annual sea level at Kochi during 1940–1960 is not seen at the other stations.

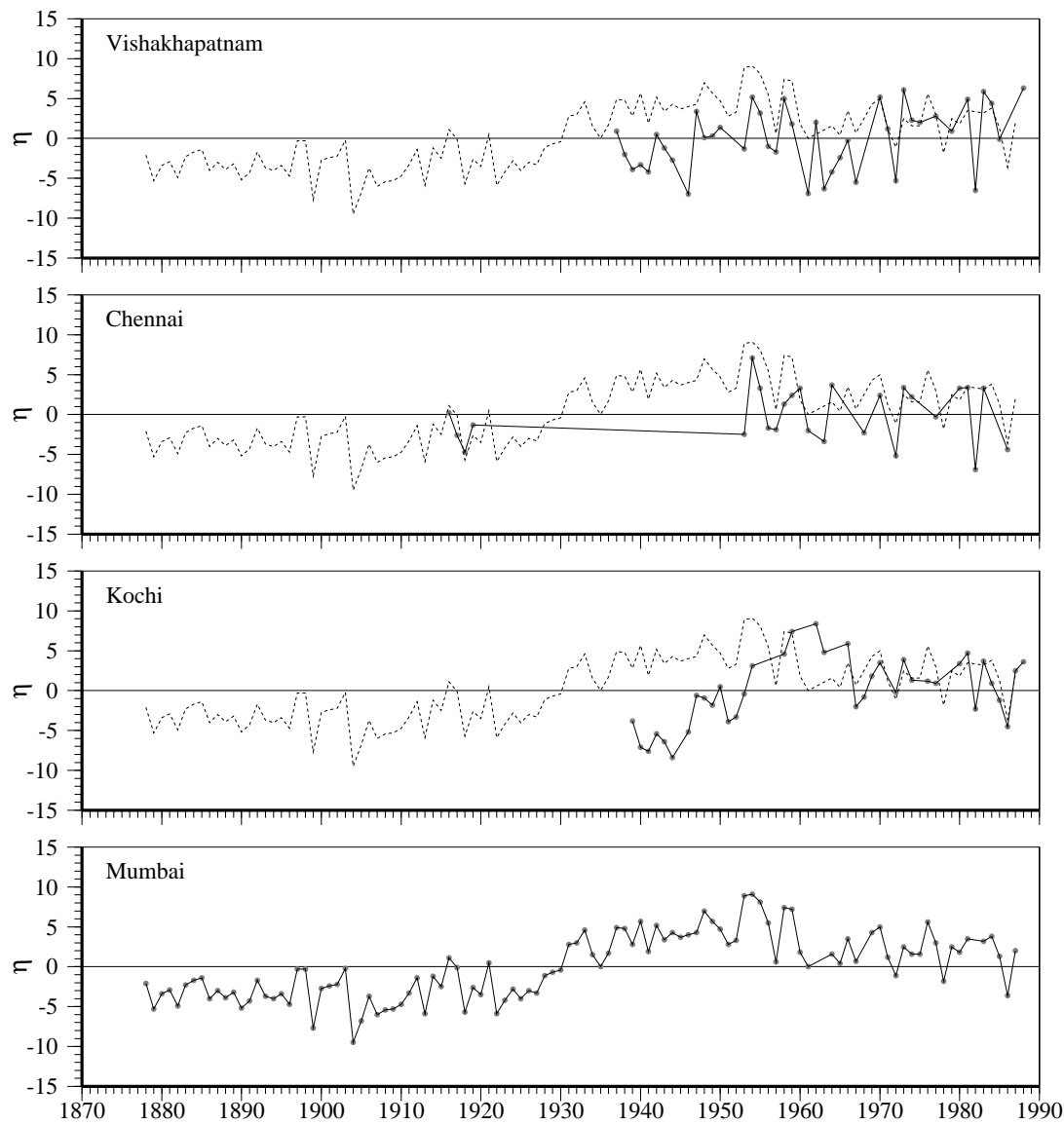


Figure 6.7 Anomalies of corrected annual sea level (cm). The annual sea level was computed by averaging monthly sea level, corrected for the effect of atmospheric pressure, over an year (July–June), and the mean of the time series was removed to obtain the anomalies. The curve for Mumbai is superimposed on those for the other three stations. The corrected annual sea level is also coherent along the coast, Kochi again being the only exception.

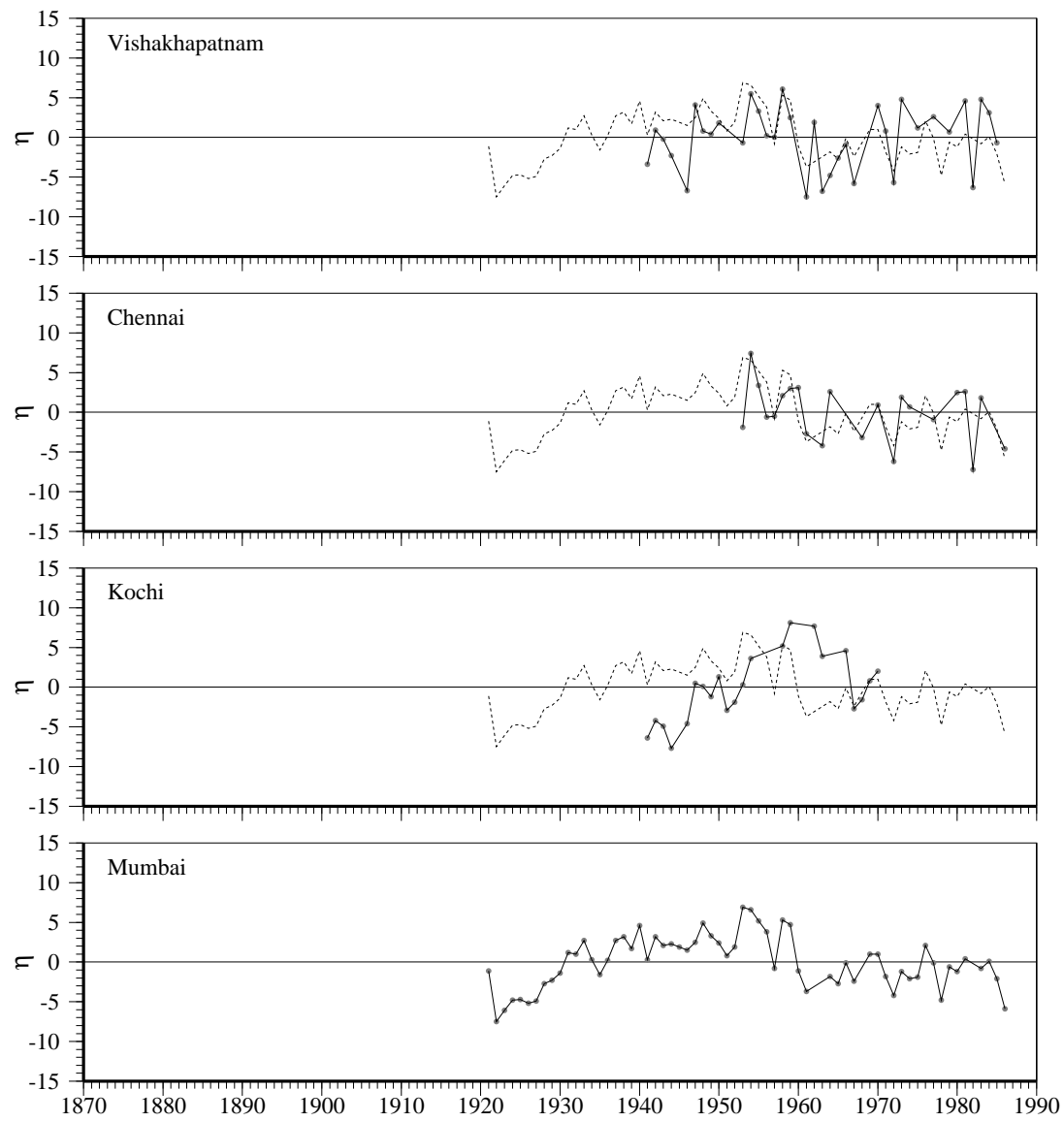


Figure 6.8 Anomalies of the uncorrected annual mean (middle curve), maximum (upper curve), and minimum (lower curve) sea level (cm). The annual mean sea level was computed by averaging monthly sea level, not corrected for atmospheric pressure, over an year (July–June); the annual maximum (minimum) is the maximum (minimum) sea level during July–June. The mean of the time series was removed to obtain the anomalies. The annual extrema are in phase with the annual mean; in general, when the mean sea level increases, so do the maximum and the minimum.

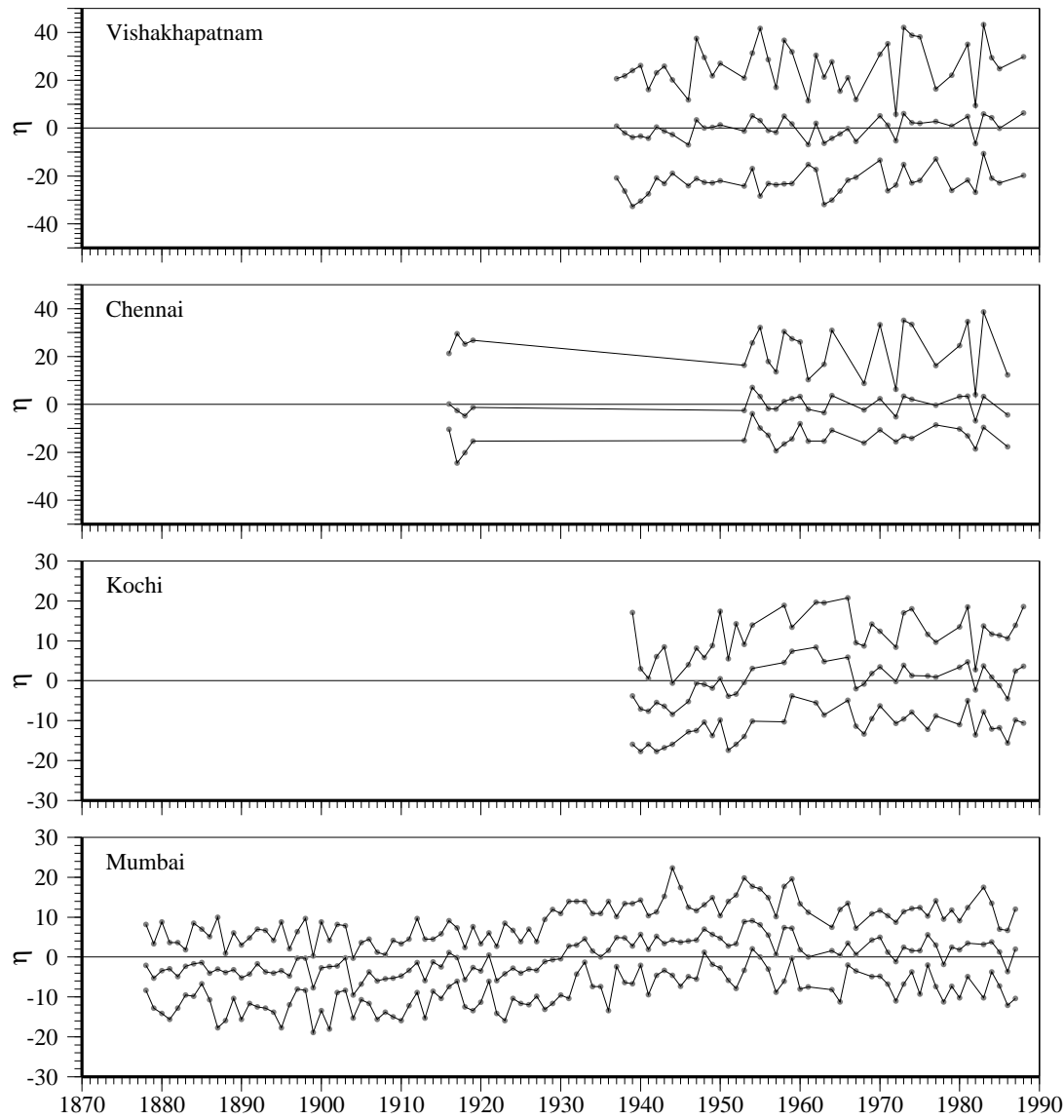


Figure 6.9 Anomalies of the corrected annual mean (middle curve), maximum (upper curve), and minimum (lower curve) sea level (cm). The annual mean sea level was computed by averaging monthly sea level, corrected for atmospheric pressure, over a year (July-June); the annual maximum (minimum) is the maximum (minimum) sea level during July-June. The mean of the time series was removed to obtain the anomalies. The annual extrema of corrected sea level are in phase with the annual mean; in general, when the mean sea level increases, so do the maximum and the minimum.

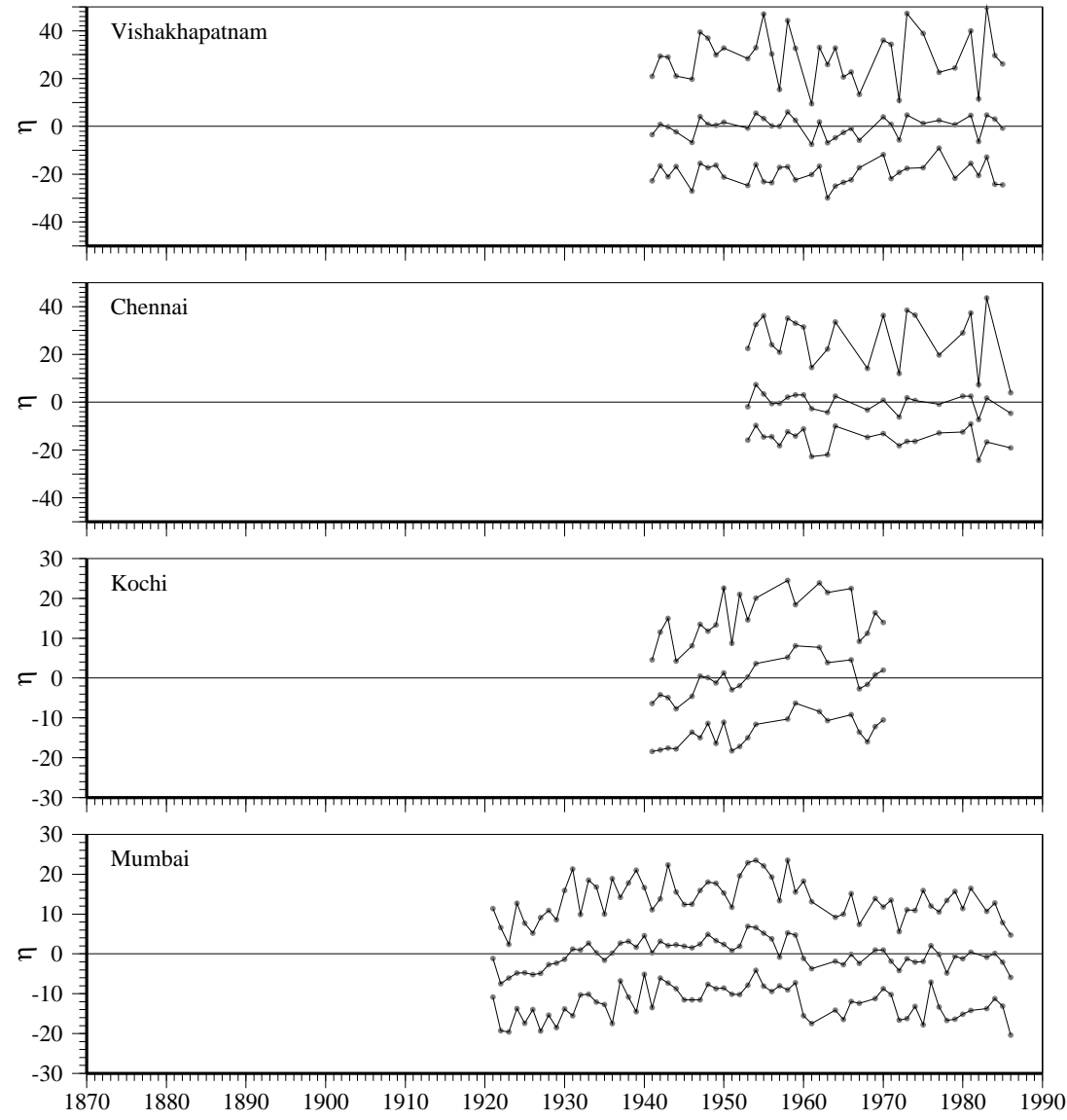


Table 6.3 Linear correlation statistics for annual mean, extrema, and seasonal averages of sea level. η_V , η_C , η_K , and η_M denote the sea level anomalies at Vishakhapatnam, Chennai, Kochi, and Mumbai; the subscripts “m”, “max”, and “min” imply annual mean, maximum, and minimum sea level, and the subscripts “FMA”, “MAM”, “JAS”, “OND”, and “NDJ” imply average sea level for February–April, March–May, July–September, October–December, and November–January. r is the linear correlation coefficient between the variables in the first two columns (at zero lag). r_s is the linear correlation at the $P\%$ significance level for the required number of degrees of freedom; if the column for P is blank, then r_s is the correlation at the 90% significance level, but the two variables are not correlated even at this level. A “C” in the last column implies that the sea-level data are corrected for the effect of atmospheric pressure (default is no correction).

| | | r | r_s | P | |
|--------------|----------------|-------|-------|------|---|
| $\eta_{V,m}$ | $\eta_{V,max}$ | 0.789 | 0.388 | 99.0 | |
| $\eta_{V,m}$ | $\eta_{V,max}$ | 0.798 | 0.418 | 99.0 | C |
| $\eta_{V,m}$ | $\eta_{V,min}$ | 0.530 | 0.388 | 99.0 | |
| $\eta_{V,m}$ | $\eta_{V,min}$ | 0.530 | 0.418 | 99.0 | C |
| $\eta_{V,m}$ | $\eta_{V,FMA}$ | 0.556 | 0.388 | 99.0 | |
| $\eta_{V,m}$ | $\eta_{V,MAM}$ | 0.586 | 0.388 | 99.0 | |
| $\eta_{V,m}$ | $\eta_{V,JAS}$ | 0.746 | 0.388 | 99.0 | |
| $\eta_{V,m}$ | $\eta_{V,OND}$ | 0.800 | 0.388 | 99.0 | |
| $\eta_{C,m}$ | $\eta_{C,max}$ | 0.759 | 0.478 | 99.0 | |
| $\eta_{C,m}$ | $\eta_{C,max}$ | 0.831 | 0.515 | 99.0 | C |
| $\eta_{C,m}$ | $\eta_{C,min}$ | 0.752 | 0.478 | 99.0 | |
| $\eta_{C,m}$ | $\eta_{C,min}$ | 0.789 | 0.515 | 99.0 | C |
| $\eta_{C,m}$ | $\eta_{C,FMA}$ | 0.606 | 0.478 | 99.0 | |
| $\eta_{C,m}$ | $\eta_{C,MAM}$ | 0.505 | 0.478 | 99.0 | |
| $\eta_{C,m}$ | $\eta_{C,JAS}$ | 0.523 | 0.478 | 99.0 | |
| $\eta_{C,m}$ | $\eta_{C,OND}$ | 0.850 | 0.478 | 99.0 | |
| $\eta_{K,m}$ | $\eta_{K,max}$ | 0.796 | 0.402 | 99.0 | |
| $\eta_{K,m}$ | $\eta_{K,max}$ | 0.821 | 0.515 | 99.0 | C |
| $\eta_{K,m}$ | $\eta_{K,min}$ | 0.895 | 0.402 | 99.0 | |
| $\eta_{K,m}$ | $\eta_{K,min}$ | 0.893 | 0.515 | 99.0 | C |
| $\eta_{K,m}$ | $\eta_{K,FMA}$ | 0.891 | 0.402 | 99.0 | |
| $\eta_{K,m}$ | $\eta_{K,MAM}$ | 0.905 | 0.402 | 99.0 | |
| $\eta_{K,m}$ | $\eta_{K,JAS}$ | 0.873 | 0.402 | 99.0 | |
| $\eta_{K,m}$ | $\eta_{K,NDJ}$ | 0.875 | 0.402 | 99.0 | |
| $\eta_{M,m}$ | $\eta_{M,max}$ | 0.879 | 0.247 | 99.0 | |
| $\eta_{M,m}$ | $\eta_{M,max}$ | 0.785 | 0.320 | 99.0 | C |
| $\eta_{M,m}$ | $\eta_{M,min}$ | 0.862 | 0.247 | 99.0 | |
| $\eta_{M,m}$ | $\eta_{M,min}$ | 0.828 | 0.320 | 99.0 | C |
| $\eta_{M,m}$ | $\eta_{M,FMA}$ | 0.887 | 0.247 | 99.0 | |
| $\eta_{M,m}$ | $\eta_{M,MAM}$ | 0.907 | 0.247 | 99.0 | |
| $\eta_{M,m}$ | $\eta_{M,JAS}$ | 0.845 | 0.247 | 99.0 | |
| $\eta_{M,m}$ | $\eta_{M,NDJ}$ | 0.863 | 0.247 | 99.0 | |

studying interdecadal variability in sea level. Since the annual mean and extrema of sea level are coherent along the coast, it is reasonable to assume that the interdecadal variability at Mumbai is representative of that along the coast of India.

6.2.1 Interdecadal Variability of Sea Level at Mumbai

To determine the variability at periods higher than a year, we low-pass-filter the sea-level data at Mumbai (not corrected for atmospheric pressure) with an N -year running mean. The correlations between the filtered annual mean and annual extrema remain statistically significant at the lower frequencies and the coherence between the annual mean and extrema increases as frequency decreases (Table 6.4, Figure 6.10).

Table 6.4 Linear correlation statistics for low-pass-filtered sea level at Mumbai. η_M denotes the anomaly of low-pass-filtered sea level at Mumbai; the subscripts “m”, “max”, and “min” imply mean, maximum, and minimum sea level, respectively. r is the linear correlation coefficient between the variables in the first two columns. An N -year running mean is used to filter the sea-level data before computing the correlations ($N = 1$ implies no running mean). r_s is the linear correlation at the $P\%$ significance level for the required number of degrees of freedom.

| | | r | r_s | P | N |
|--------------|----------------|-------|-------|------|-----|
| $\eta_{M,m}$ | $\eta_{M,max}$ | 0.879 | 0.247 | 99.0 | 1 |
| $\eta_{M,m}$ | $\eta_{M,min}$ | 0.862 | 0.247 | 99.0 | 1 |
| $\eta_{M,m}$ | $\eta_{M,max}$ | 0.927 | 0.304 | 99.0 | 2 |
| $\eta_{M,m}$ | $\eta_{M,min}$ | 0.917 | 0.304 | 99.0 | 2 |
| $\eta_{M,m}$ | $\eta_{M,max}$ | 0.974 | 0.450 | 99.0 | 5 |
| $\eta_{M,m}$ | $\eta_{M,min}$ | 0.968 | 0.450 | 99.0 | 5 |
| $\eta_{M,m}$ | $\eta_{M,max}$ | 0.990 | 0.609 | 99.0 | 10 |
| $\eta_{M,m}$ | $\eta_{M,min}$ | 0.985 | 0.609 | 99.0 | 10 |

The filtered data show that sea level was generally low during 1870–1920; it peaked in the late 1950s, decreasing thereafter. The rise in the first half of this century was about 11 cm, the fall after that being about 4.5 cm. This decrease after 1960 was also noted by Emery and Aubrey [1989], who computed the linear trends in sea level along the coast of India. They considered five stations in their analysis, of which four — Vishakhapatnam, Chennai, Kochi, and Mumbai — showed a rise in sea level relative to land over the duration of the tide-gauge record. At Mangalore, however, they noted a decrease in sea level relative to land. The tide-gauge record at Mangalore spans the period 1952–1976 (Table 2.1), during which sea level at Mumbai also shows a decreasing trend. The coherence in the low-frequency variability of sea level along the coast of India suggests a similar behaviour at Mangalore and also at the other tide-gauge stations.

6.2.2 Significance of the Tide Gauge at Mumbai

This decrease in sea level over a decade or more is puzzling because it does not fit in with the idea of “global sea-level-rise”. Sea level has been recognized as an excellent marker of climate change and “global” sea level appears to be rising relative to land at the rate of 1 mm year⁻¹; this is attributed, in part, to the warming of the globe due to the greenhouse effect [Gornitz et al., 1982]. The warming is expected to affect sea level in two ways. First, it is expected to raise the temperature in the upper ocean; second, it is expected to melt polar ice caps, releasing the large quantities of freshwater trapped in them. Both processes would increase the volume of water in the world oceans, thereby raising sea level all over the globe.

The issue, however, is more complicated, and it is difficult to obtain a single global index for long-term sea-level changes [Barnett, 1984]. Though there is an apparent increase in sea level in most of the world oceans, there are regions that show a different trend, southeast Asia for example. Apart from this, there is the problem of separating natural, low-frequency sea-level variability from that caused by anthropogenic effects; this calls for long sea-level time-series, and such records are not many. Moreover, the available records are not distributed uniformly, most being from Scandinavia. Between the tropics of Cancer and Capricorn, only three records, those at Mumbai, Honolulu, and Balboa, go back at least to the beginning of this century. Of these, only Mumbai is in the Indian ocean, and its tide gauge has been considered representative of the low-frequency sea-level variability in the basin [Gornitz et al., 1982; Barnett, 1984]. The coherence in the interannual variability of sea level along the coast of India supports this assumption.

6.3 Monsoon Variability and Sub-Annual Changes of Sea Level

Given that the ocean and the atmosphere form a coupled system, it is unquestionable that the changes in sea level must reflect changes in climate. The major aspect of the climate of the Indian subcontinent in particular, and of Asia in general, is the monsoon, which is linked to global climate by the planetary-scale processes in the atmosphere and the ocean. Therefore, there must be a relation between the variability of the Indian monsoon and the sub-annual changes in sea level at Mumbai and other stations along the Indian coast. The best record of monsoon variability is contained in rainfall measurements at meteorological stations scattered over the Indian subcontinent. Since rainfall directly influences salinity, which, in turn, influences coastal sea level, the sub-annual variability of sea level along the coast of India must be related to the sub-annual variability of rainfall over India. Hence, we look for a connection between the variability of rainfall and that of sea level.

6.3.1 Correlation Between Local Rainfall and Sea Level

A connection between sea level at a location and the local rainfall was tentatively established by earlier studies [Varadarajulu et al., 1982; Prasad and Reddy, 1985; Shetye and Almeida, 1985]. The seasonal cycle of rainfall over southeast India, including Vishakhapatnam and Chennai, differs from that over the rest of India: southeast India receives more rain during the northeast monsoon. Therefore, the seasonal cycles of both local rainfall and sea level peak in November at Vishakhapatnam and Chennai. This, however, is not true along the west coast of India, or at Paradip in the northern Bay of Bengal. Given that the seasonal cycle of sea level is coherent along the east coast, is there any connection between local rainfall and sea level at sub-annual time scales? We examine the possibility, using annual rainfall⁶ as a measure of rainfall variability to avoid using two indices, one for the southwest monsoon and another for the northeast monsoon.

Monthly rainfall data for Vishakhapatnam, Chennai, Kochi, and Mumbai are available from GHCN (Table 6.5). Annual rainfall for these stations is plotted along with the annual mean and extrema of sea level in Figure 6.11; the corresponding correlations are listed in Table 6.6. Local rainfall is significantly correlated with annual sea level only at Mumbai. At Chennai and Kochi, local rainfall appears to be unrelated to annual sea level.

Table 6.5 Monthly local rainfall data from the Global Historical Climate Network (GHCN). N_{yr} is the number of years of data available. The symbol in the last column is used for the local rainfall at these four stations.

| Station | Longitude (°E) | Latitude (°N) | Time span | N_{yr} | Symbol |
|-----------------------|-------------------|------------------|-----------|-----------------|--------|
| Vishakhapatnam | 83.23 | 17.72 | 1866–1989 | 124 | R_v |
| Chennai (Minambakkam) | 80.18 | 13.00 | 1813–1990 | 178 | R_c |
| Kochi (Willingdon) | 76.27 | 9.95 | 1842–1973 | 132 | R_k |
| Mumbai (Colaba) | 72.82 | 18.90 | 1817–1989 | 173 | R_m |

The local rainfall at these four stations are correlated amongst themselves, but the correlation is high only for Vishakhapatnam and Mumbai, the two stations at which local rainfall and sea level yield a non-negligible correlation. Since the connection between rainfall and sea level is through salinity, this implies that salinity along the coast is not influenced simply by the local rainfall, except, perhaps, in the neighbourhood of Mumbai. The correlation at Mumbai remains significant when the rainfall and sea level are low-pass-filtered (Table 6.6, Figure 6.12). Like annual sea level,

⁶Annual rainfall is defined as the sum of monthly rainfall over a calendar year. As mentioned earlier, we use the calendar year for computing rainfall, but compute the mean and extrema of sea level during July–June; for computing correlations between rainfall and sea level, “zero lag” implies (say) rainfall for 1950 is matched against sea level during July 1950 to June 1951.

Table 6.6 Linear correlation statistics for annual local rainfall and sea level. R_V , R_C , R_K , and R_M denote the anomalies of annual local rainfall at Vishakhapatnam, Chennai, Kochi, and Mumbai, and $\eta_{V,m}$ and $\eta_{M,m}$ the anomalies of annual sea level at Vishakhapatnam and Mumbai. r is the linear correlation coefficient between the variables in the first two columns (at zero lag). r_s is the linear correlation at the $P\%$ significance level for the required number of degrees of freedom; if the column for P is blank, then r_s is the correlation at the 90% significance level, but the two variables are not correlated even at this level. An N -year running mean has been used to filter the data before computing the correlations; $N = 1$ implies no running mean. Correlations for sea level at Chennai and Kochi are not shown because they are negligible.

| | | r | r_s | P | N |
|-------|--------------|-------|-------|------|-----|
| R_V | $\eta_{V,m}$ | 0.183 | 0.272 | | 1 |
| R_M | $\eta_{M,m}$ | 0.492 | 0.247 | 99.0 | 1 |
| R_M | $\eta_{M,m}$ | 0.587 | 0.304 | 99.0 | 2 |
| R_M | $\eta_{M,m}$ | 0.666 | 0.450 | 99.0 | 5 |
| R_M | $\eta_{M,m}$ | 0.752 | 0.609 | 99.0 | 10 |
| R_V | R_M | 0.307 | 0.235 | 99.0 | 1 |
| R_C | R_M | 0.138 | 0.141 | | 1 |
| R_K | R_M | 0.136 | 0.160 | | 1 |
| R_C | R_K | 0.163 | 0.160 | 90.0 | 1 |

rainfall also increases from a low early this century to a peak in the 1950s and then decreases. This implies that there must be a relation between rainfall and sea level, but this relation may not be local.

6.3.2 All-India Rainfall

The lack of correlation between local rainfall and sea level is not surprising because of the strong influence that runoff from the Ganga and the Brahmaputra has on the salinity along the east coast of India (Section 4.3.2). The decrease in salinity along the east coast is mainly due to the runoff from the Ganga and the Brahmaputra, and that along the west coast is due to the runoff from local rivers during the southwest monsoon and the advection of freshwater from the bay during the northeast monsoon. Therefore, the sub-annual variability of salinity along the east coast must be determined by the variability of rainfall in the catchment areas of the Ganga and the Brahmaputra (Figure 6.13), which must also have an effect on the sub-annual variability of salinity along the west coast; the rainfall along the west coast is an additional factor in the variability of salinity there.

There is considerable variation in the rainfall over the Indian subcontinent in both space and time. Nevertheless, meteorologists use an area-weighted average, called “all-India rainfall”, as a popular index of monsoon variability. This is often defined for the southwest monsoon (June–

September), during which a large fraction of the subcontinent receives over 75% of the annual rainfall [Mishra and Gadgil, 1996, and references therein]. The major exception is southeast India, where 70% of the rainfall is during October–December. Since the rainfall during these two seasons is positively correlated [Singh, 1994; Mishra and Gadgil, 1996], annual all-India rainfall is a reasonable measure of the variability of monsoon rainfall over India.

There is a strong biennial component in the variation of all-India rainfall, with a good (poor) monsoon followed by a poor (good) monsoon [Mishra and Gadgil, 1996, and references therein]. This interannual variation is embedded in a decadal-scale variation: there have been distinct epochs in the monsoon rainfall over India and in its variability [Joseph, 1976]. There was a high frequency of droughts and variability was large during the periods 1899–1920 and 1965–1987, whereas very few droughts occurred and the variability was low during 1880–1899 and 1929–1964; since 1988, another epoch with a low frequency of droughts appears to have commenced [Mishra and Gadgil, 1996].

Since all-India rainfall is a derived quantity, estimated as the area-weighted average of annual rainfall at stations covering 29 meteorological subdivisions in India [Parthasarathy et al., 1993, 1995; Mishra and Gadgil, 1996], there exists more than one estimate. We use two time series of annual all-India rainfall, the first spanning 1901–1990 ($R_{I,19}$) and the second spanning 1871–1994 (R_I). The anomalies computed from the two time series agree well with each other (Figure 6.14), but there is a difference of 23 cm in the long-term mean rainfall, and hence, in total annual rainfall; the mean of $R_{I,19}$ is 86.5 cm, and that of R_I is 109.1 cm. In the absence of any reason for preferring one time series to the other, we use both for studying the link between the monsoon and sea level along the coast of India.

We have data from the 1871–1994 time series for 29 meteorological subdivisions in India [Parthasarathy et al., 1995]. Three of these — Konkan and Goa, Coastal Karnataka, and Kerala (Figure 6.15) — lie to the west of the Sahyadri Range in a coastal strip that receives very high rainfall; Mumbai lies in the subdivision Konkan-and-Goa and is close to the northern end of the coastal strip; Kochi lies in Kerala and is close to the southern end of the strip. We combine data from these three subdivisions, using an area-weighted average to estimate “West-Coast rainfall” (R_{WC}), which has a mean of 281 cm. Its anomaly is plotted along with that of R_I in Figure 6.14.

It is more difficult to estimate the rainfall in the catchment areas of the Ganga and the Brahmaputra because the catchment areas of these two rivers and their tributaries covers a vast area of India and spans several meteorological subdivisions; it also includes Bangladesh, for which we have no rainfall data. We pick eight of these subdivisions — North Assam, South Assam, Sub-Himalayan West Bengal, Gangetic West Bengal, Bihar Plateau, Bihar Plains, East Uttar Pradesh, and West Uttar Pradesh Plains (Figure 6.15) — and combine the data from them, using an area-weighted average to estimate “Ganga-Brahmaputra rainfall” (R_{GB}), which has a mean of 147 cm.

This gives an idea of the rainfall and its variability in the catchment areas of the Ganga and the Brahmaputra, but is less accurate than West-Coast rainfall because some of the tributaries of the Ganga, especially those flowing south–north, are not accounted for; also ignored in this estimate are the contributions to runoff from rainfall in the Himalayan foothills and from snow-melt in Tibet and the Himalayas, where the Ganga, the Brahmaputra, and some of their major tributaries originate. The rainfall over hilly regions is also not included in estimates of all-India rainfall because of the difficulty in using station rainfall data to compute area-weighted averages; this is prone to large errors in hilly areas, where the spatial variation is large and rapid, unlike in the plains. The anomaly of R_{GB} is plotted along with that of R_i in Figure 6.14.

Though the variability of all-India rainfall is determined primarily by the variability in north-west India because the coefficient of variation is largest there ($> 50\%$) [Mishra and Gadgil, 1996, and references therein], all-India rainfall is significantly correlated with both West-Coast rainfall and Ganga-Brahmaputra rainfall; so is the local rainfall at Mumbai and Kochi with West-Coast rainfall (Table 6.7). The implication of these correlations is that all-India rainfall, from either time

Table 6.7 Linear correlation statistics for annual rainfall. R_i and $R_{i,19}$ denote the anomalies of all-India rainfall for the 1871–1994 and 1901–1990 time series, R_{WC} and R_{GB} the anomalies of West-Coast and Ganga-Brahmaputra rainfall, and R_v , R_k , and R_m the anomalies of annual local rainfall at Vishakhapatnam, Mumbai, and Kochi. r is the linear correlation coefficient between the variables in the first two columns (at zero lag). r_s is the linear correlation at the $P\%$ significance level for the required number of degrees of freedom; if the column for P is blank, then r_s is the correlation at the 90% significance level, but the two variables are not correlated even at this level. Rainfall at Chennai is not correlated with all-India rainfall, and hence, the correlation is not listed.

| | | r | r_s | P |
|-----------------|-----------------|-------|-------|------|
| R_i | $R_{i,19}$ | 0.941 | 0.267 | 99.0 |
| R_i | R_{WC} | 0.641 | 0.229 | 99.0 |
| R_i | R_{GB} | 0.587 | 0.229 | 99.0 |
| $R_{i,19}$ | R_{WC} | 0.670 | 0.267 | 99.0 |
| $R_{i,19}$ | R_{GB} | 0.378 | 0.267 | 99.0 |
| R_i | R_v | 0.384 | 0.239 | 99.0 |
| R_i | R_k | 0.199 | 0.194 | 95.0 |
| R_i | R_m | 0.478 | 0.235 | 99.0 |
| $R_{i,19}$ | R_v | 0.265 | 0.213 | 99.0 |
| $R_{i,19}$ | R_k | 0.195 | 0.198 | |
| $R_{i,19}$ | R_m | 0.549 | 0.272 | 99.0 |
| R_{WC} | R_{GB} | 0.177 | 0.175 | 95.0 |
| R_{WC} | R_m | 0.557 | 0.235 | 99.0 |
| R_{WC} | R_k | 0.574 | 0.253 | 99.0 |

series, is a reasonable measure of the rainfall over the west coast of India and in the catchment

areas of the Ganga and the Brahmaputra. Therefore, its variability must influence that of salinity, and hence, of sea level along the coast of India.

6.3.3 Correlation Between All-India Rainfall and Sea Level

The anomalies of the annual mean and extrema of sea level are visually correlated with R_i and $R_{i,19}$ (Figures 6.16, 6.17, 6.18, and 6.19). The corresponding correlations are listed in Table 6.8. Except at Kochi, the annual mean sea level is significantly correlated with R_i and $R_{i,19}$. The correlation is best for Mumbai, which is significantly correlated at the 99% significance level irrespective of the all-India-rainfall time series used. At Vishakhapatnam and Chennai, the correlations are better when $R_{i,19}$ is used, and when the correction is applied for the effect of atmospheric pressure. The correlations at these two stations improve considerably when the sea-level data for 1961 are dropped, this year being an outlier. The annual all-India rainfall during 1961 is the second highest for the series $R_{i,19}$ and the fourth highest for R_i . Despite this, the lowest annual mean sea level was recorded in 1961 at Vishakhapatnam; at Chennai, the annual mean was the sixth lowest in 1961 (sea level corrected for atmospheric pressure). We treat this data point as an outlier for the time being, but return to it in Section 6.4.4.

Table 6.8 also lists the correlations between all-India rainfall and the annual extrema; the annual extrema at Kochi also are not correlated with all-India rainfall. At Mumbai, both the maximum and minimum are significantly correlated with both R_i and $R_{i,19}$. At Vishakhapatnam and Chennai, the maximum is significantly correlated with all-India rainfall, the correlation being significant at the 99% significance level when the sea-level data for 1961 are dropped. The minimum at Vishakhapatnam is better correlated with $R_{i,19}$ than with R_i ; at Chennai, in either case, the correlation falls just short of the 90% significance level. Therefore, the annual mean and extrema of sea level along the coast of India, Kochi being an exception, are significantly correlated with all-India rainfall, the correlations being lower for the minimum; the best correlations are obtained for the sea level at Mumbai, which has the longest tide-gauge record.

The correlations at Mumbai retain their significance (Table 6.9) when the data are low-pass-filtered with a running mean (Figures 6.20 and 6.21). Annual sea level at Mumbai is significantly correlated with the all-India rainfall from the 1901–1990 data, $R_{i,19}$. Though the filtered rainfall is noisier than the filtered sea level, both rainfall and sea level were low in the first two decades of this century, rose to a peak in the 1950s, and declined thereafter. Annual sea level at Mumbai, however, is not as well correlated with the 1871–1994 all-India rainfall, R_i . R_i was above normal during 1871–1899 and dropped to a low during 1900–1915, but the annual sea level at Mumbai during 1878–1899 was just 2 cm higher than that during 1900–1920; eliminating the data during 1871–1900 improves the correlation. Annual sea level at Mumbai is also correlated with West-Coast rainfall R_{WC} , but not with Ganga-Brahmaputra rainfall R_{GB} ; eliminating the data during

Figure 6.10 Low-pass-filtered variability of sea level (cm) at Mumbai. The annual mean (middle curve), maximum (upper curve), and minimum (lower curve) are plotted after the data are low-pass-filtered with a running mean. Plots are shown for no running mean, 2-year running mean, 5-year running mean, and 10-year running mean. The coherence between the annual mean and annual extrema increases as frequency decreases. The interdecadal changes in sea level are apparent even for a 2-year running mean, but are clearer for 5-year and 10-year running means. Sea level at Mumbai was generally low during 1870–1920; it peaked in the late 1950s, decreasing thereafter.

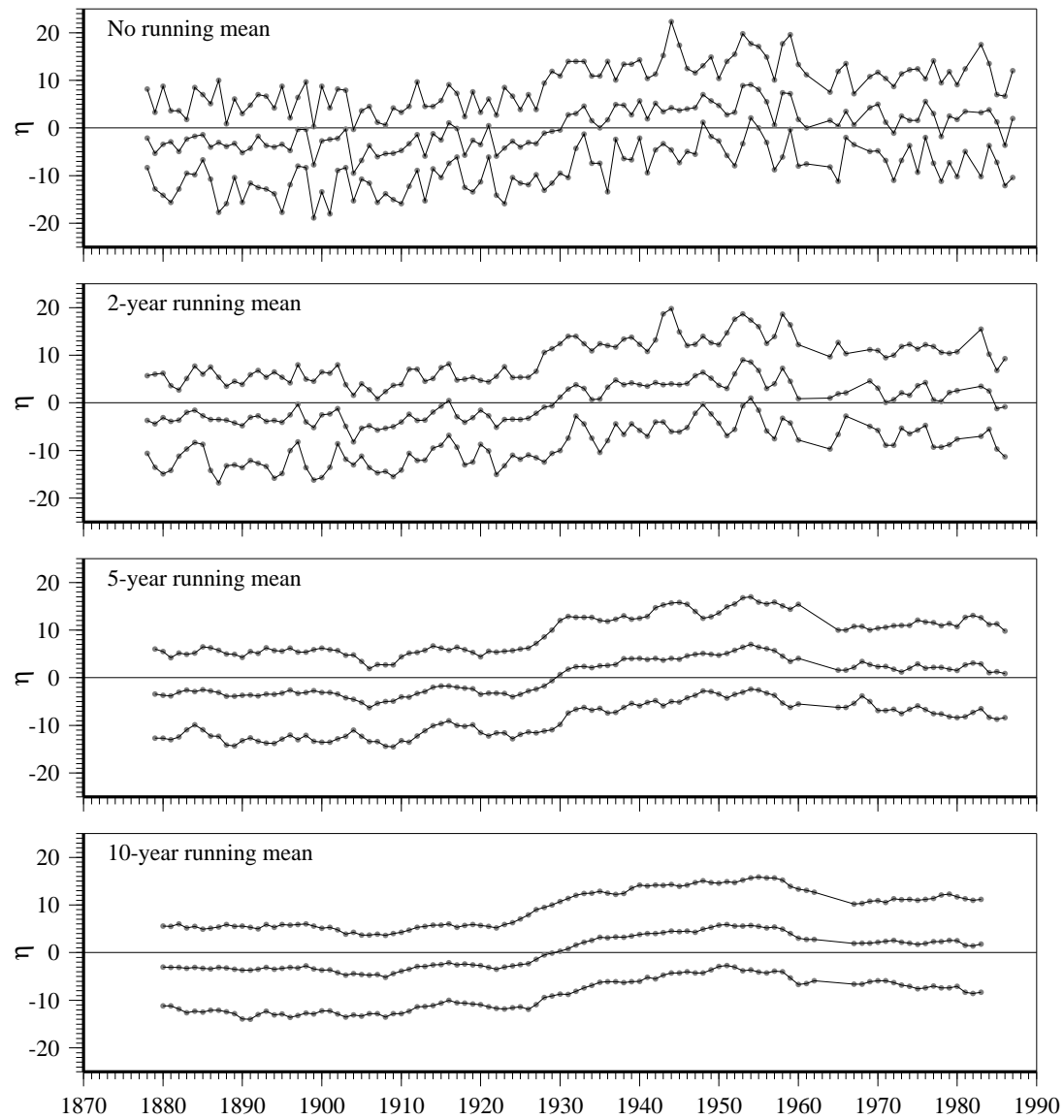


Figure 6.11 Anomalies of local annual rainfall and the annual mean and extrema of sea level at Vishakhapatnam, Chennai, Kochi, and Mumbai. Anomalies of sea level (cm) and rainfall (cm) are plotted on the ordinate and time (year) is on the abscissa. The dashed curve is for rainfall and the solid curves are for the annual mean (middle curve), annual maximum (upper curve) and annual minimum (lower curve) of sea level.

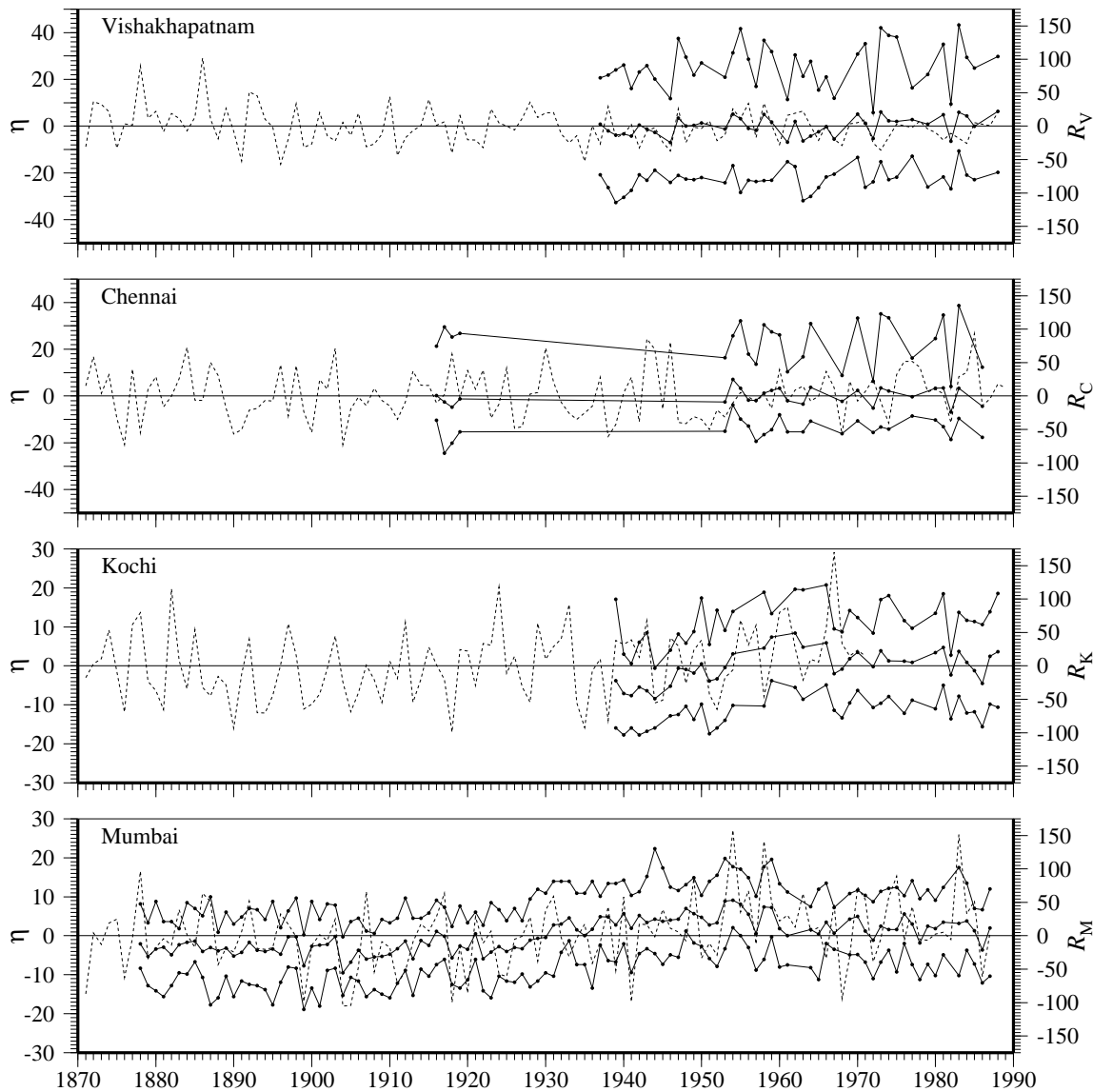


Figure 6.12 Low-pass-filtered variability of local annual rainfall and sea level at Mumbai. Anomalies of sea level (cm) and rainfall (cm) are plotted on the ordinate and time (year) is on the abscissa. The dashed curve is for rainfall and the solid curves are for the annual mean (middle curve), annual maximum (upper curve) and annual minimum (lower curve) of sea level. The data are filtered with a running mean. Plots are shown for no running mean, 2-year running mean, 5-year running mean, and 10-year running mean. Local annual rainfall and the annual mean and extrema of sea level are significantly correlated at Mumbai, the correlation increasing when the data are low-pass-filtered. Like annual sea level, rainfall also increases from a low early this century to a peak in the 1950s and then decreases.

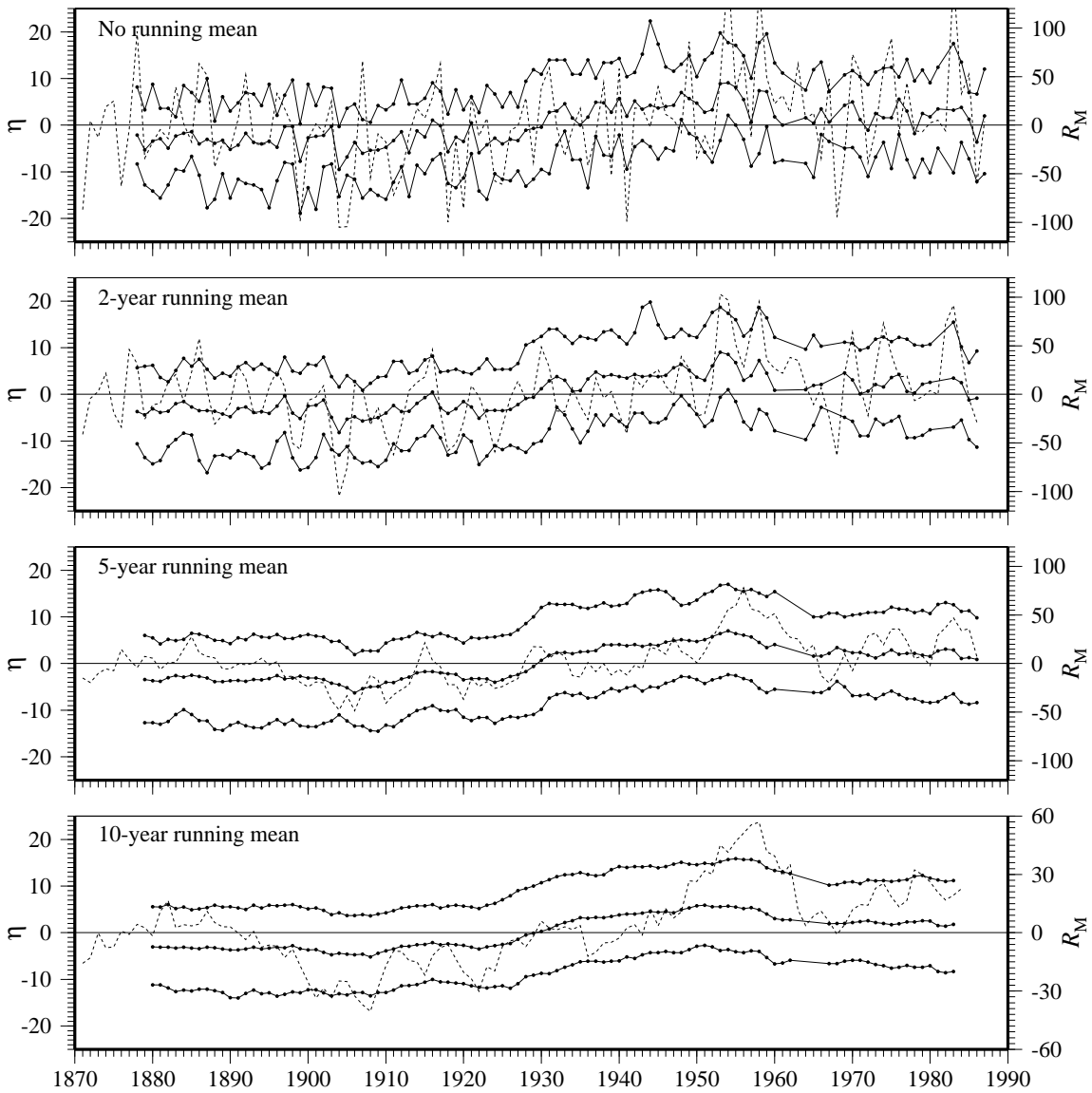


Figure 6.13 The major rivers of India are marked on the map; the dashed line shows the 200 m isobath. Most of the big rivers flow into the Bay of Bengal. The highest runoff is that of the Ganga and Brahmaputra, which together empty about $7.2 \times 10^{11} \text{ m}^3$ into the northern bay during June–October. Most of these rivers originate either in the Himalayas or in the Sahyadri range (Western Ghats), which is about 1 km high and runs parallel to the west coast of India. Smaller, swift streams flow westward from the Sahyadris into the Arabian Sea, and their combined runoff is about 30% that of the Ganga and the Brahmaputra. The runoff into the Arabian Sea is assumed to be 80% of the total rainfall over the three meteorological subdivisions along the west coast of India; this coastal belt stretches from the southern tip of India to just north of Mumbai and is bounded in the east by the Sahyadri range. The abbreviations used in the figure are as follows: EICC, East India Coastal Current; WICC, West India Coastal Current; NMC, Northeast Monsoon Current; LH, Lakshadweep High; R.G., River Ganga; R.B., River Brahmaputra. The currents are plotted for December, when the EICC flows equatorward and the WICC flows poleward. Together, they transport low-salinity water from the northern bay to the west coast of India.

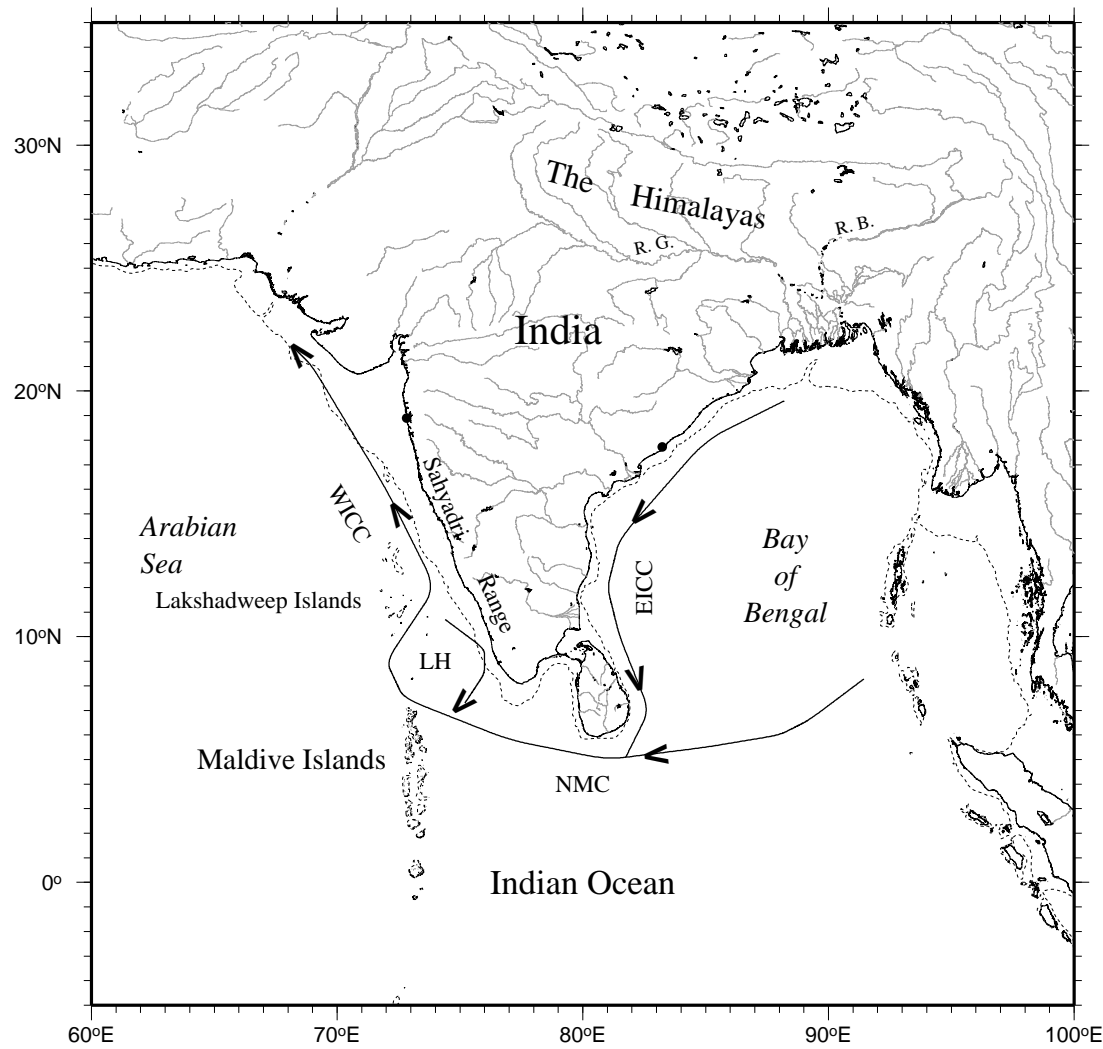


Figure 6.14 Anomalies of annual all-India, West-Coast, and Ganga-Brahmaputra rainfall. The anomalies (cm), are plotted as a function of time (year). The two series of all-India annual rainfall yield different long-term means; the mean of the 1871–1994 (R_I) series is 109.1 cm, and that of the 1901–1990 series ($R_{I,19}$) is 86.5 cm. Though there is a difference in the total rainfall, the anomalies are comparable (top panel). West-Coast rainfall (R_{WC}) is an area-weighted average of annual rainfall over three meteorological subdivisions along the west coast of India — Konkan and Goa, Coastal Karnataka, and Kerala. Anomalies of R_{WC} are correlated with those of R_I (middle panel). Ganga-Brahmaputra rainfall (R_{GB}) is an area-weighted average of annual rainfall over eight meteorological subdivisions in India — North Assam, South Assam, Sub-Himalayan West Bengal, Gangetic West Bengal, Bihar Plateau, Bihar Plains, East Uttar Pradesh, and West Uttar Pradesh Plains. Anomalies of R_{GB} are also correlated with those of R_I (lower panel).

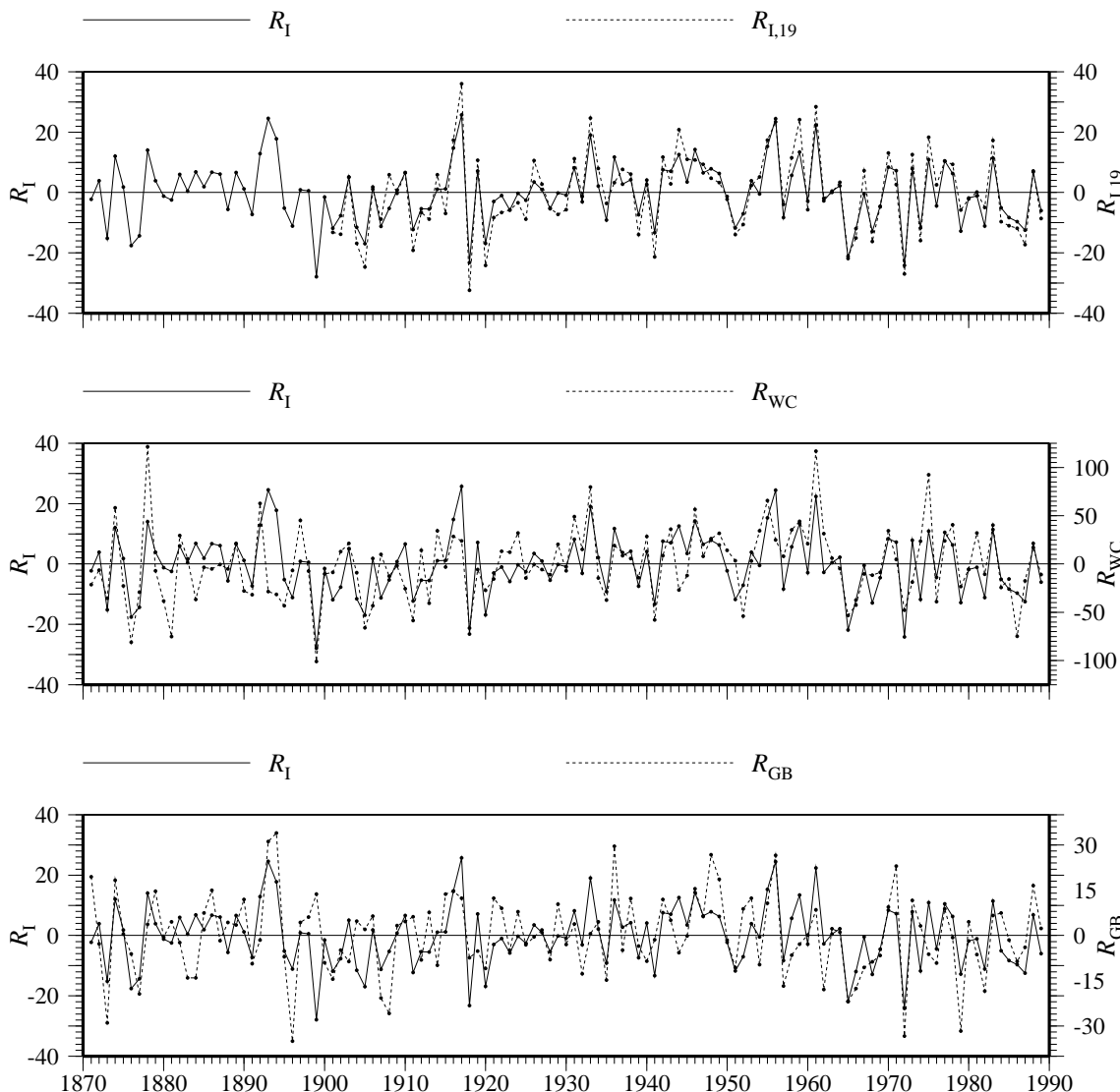


Figure 6.15 The meteorological subdivisions of India referred to in the text. The abbreviations used in the figure are as follows: R.G., River Ganga; R.B., River Brahmaputra; NA, North Assam; SA, South Assam; SHWB, Sub-Himalayan West Bengal; GWB, Gangetic West Bengal; BPn, Bihar Plains; BPu, Bihar Plateau; EUP, East Uttar Pradesh; WUPP, West Uttar Pradesh Plains; KG, Konkan and Goa; CK, Coastal Karnataka; and K, Kerala. The abbreviations, apart from the two for the rivers, refer to meteorological subdivisions of the India Meteorological Department. The first eight of these subdivisions are used to estimate the rainfall in the catchment areas of the Ganga and the Brahmaputra and this estimate is called “Ganga-Brahmaputra rainfall” (R_{GB}). The last three subdivisions are used to estimate the rainfall along the west coast of India till just north of Mumbai and this estimate is called “West-Coast rainfall” (R_{WC}). Both these estimates are significantly correlated with all-India rainfall (R_I and $R_{I,19}$).

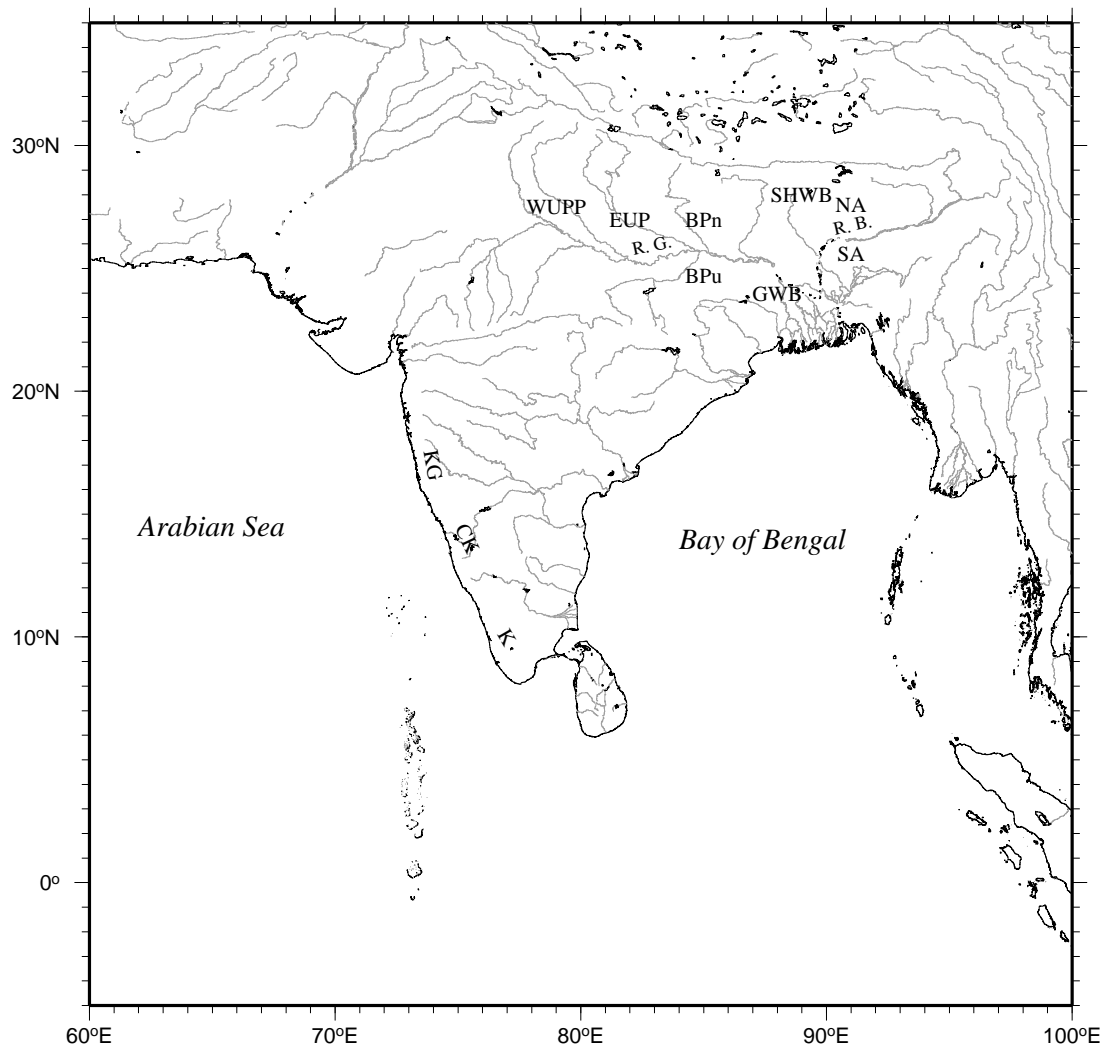


Figure 6.16 Anomalies of annual all-India rainfall ($1871\text{--}1994$) R_1 and the annual mean and extrema of uncorrected sea level at Vishakhapatnam, Chennai, Kochi, and Mumbai. The dashed curve is for rainfall and the solid curves are for the annual mean (middle curve), annual maximum (upper curve) and annual minimum (lower curve) of sea level. Anomalies of sea level (cm) and rainfall (cm) are plotted on the ordinate and time (year) is on the abscissa.

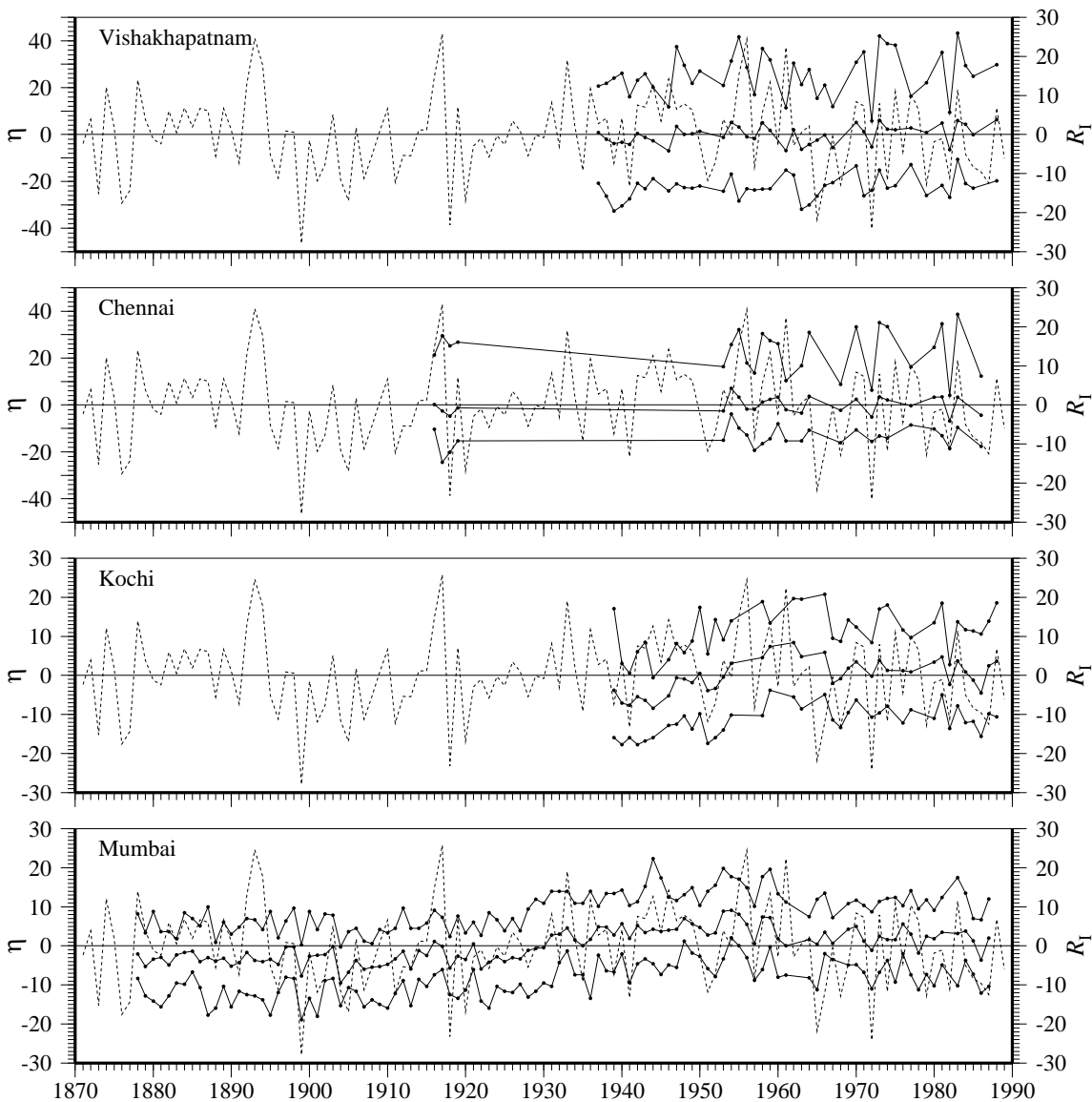


Figure 6.17 Anomalies of annual all-India rainfall (1901–1990) $R_{1,19}$ and the annual mean and extrema of uncorrected sea level at Vishakhapatnam, Chennai, Kochi, and Mumbai. The dashed curve is for rainfall and the solid curves are for the annual mean (middle curve), annual maximum (upper curve) and annual minimum (lower curve) of sea level. Anomalies of sea level (cm) and rainfall (cm) are plotted on the ordinate and time (year) is on the abscissa.

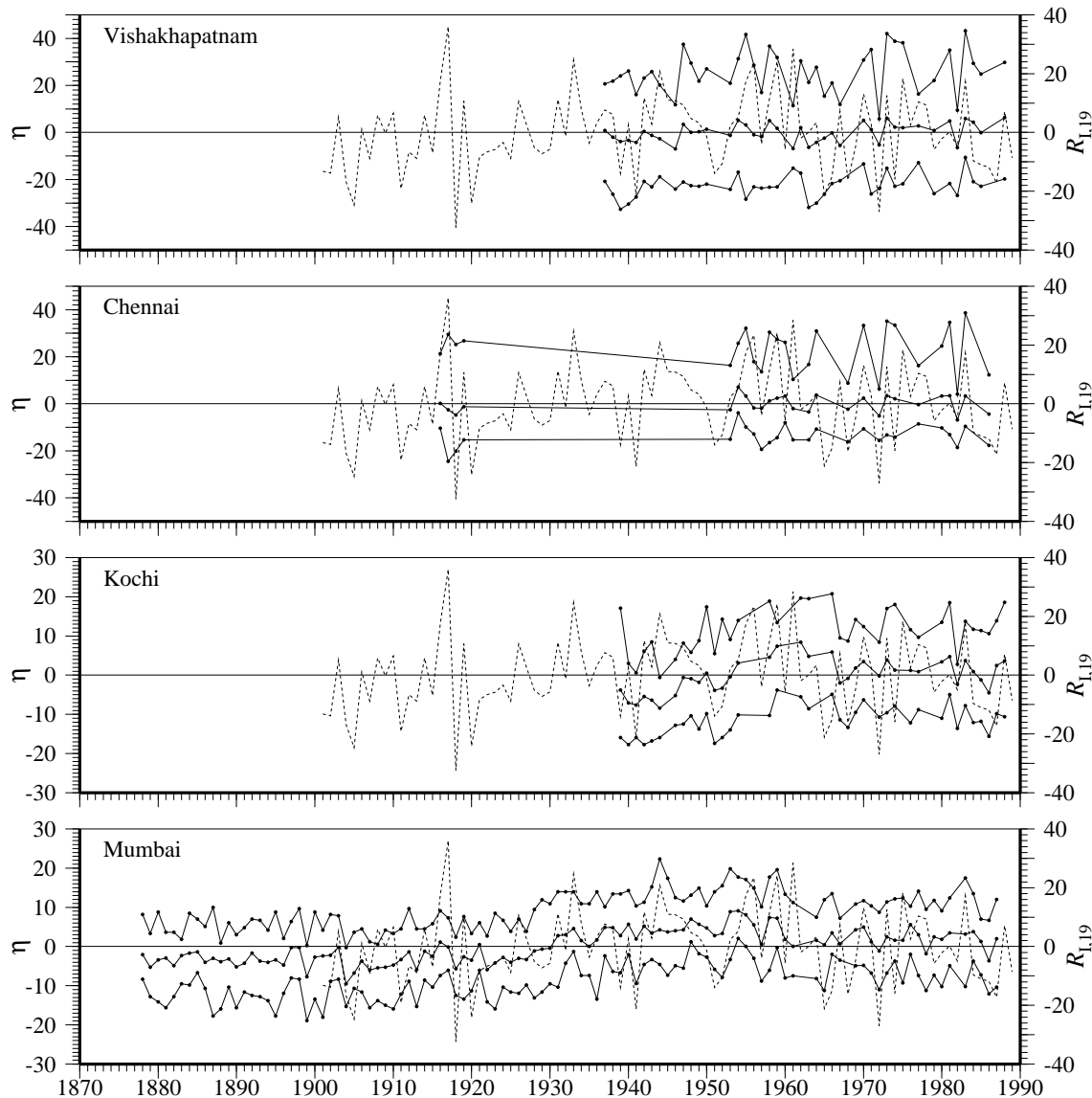


Figure 6.18 Anomalies of annual all-India rainfall (1871–1994) R_1 and the corrected annual mean and extrema of sea level, at Vishakhapatnam, Chennai, Kochi, and Mumbai. The dashed curve is for rainfall and the solid curves are for the annual mean (middle curve), annual maximum (upper curve) and annual minimum (lower curve) of sea level. Anomalies of sea level (cm) and rainfall (cm) are plotted on the ordinate and time (year) is on the abscissa.

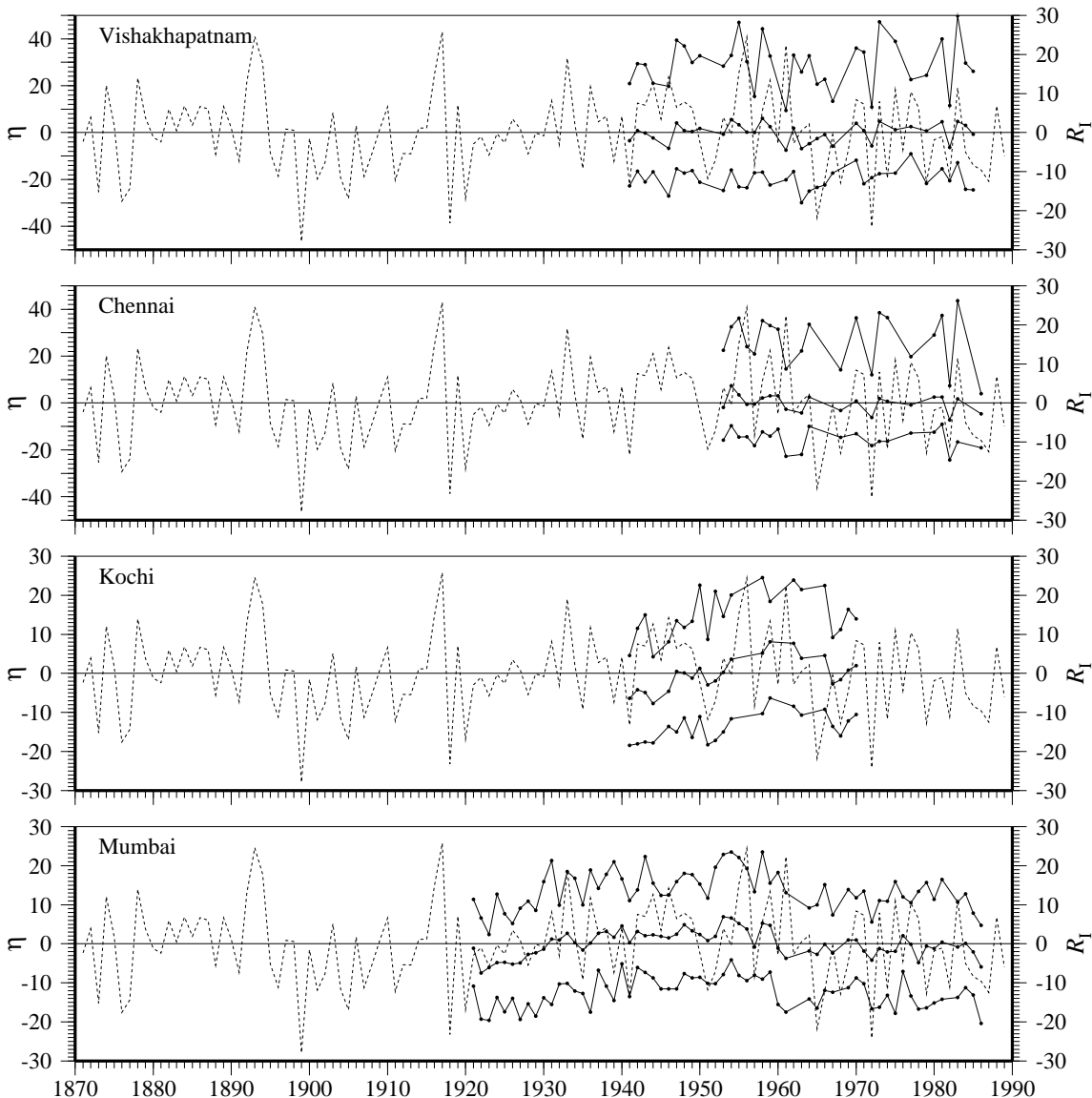


Figure 6.19 Anomalies of annual all-India rainfall ($1901\text{--}1990$) $R_{1,19}$ and the corrected annual mean and extrema of sea level at Vishakhapatnam, Chennai, Kochi, and Mumbai. The dashed curve is for rainfall and the thick solid are for the annual mean (middle curve), annual maximum (upper curve) and annual minimum (lower curve) of sea level. Anomalies of sea level (cm) and rainfall (cm) are plotted on the ordinate and time (year) is on the abscissa.

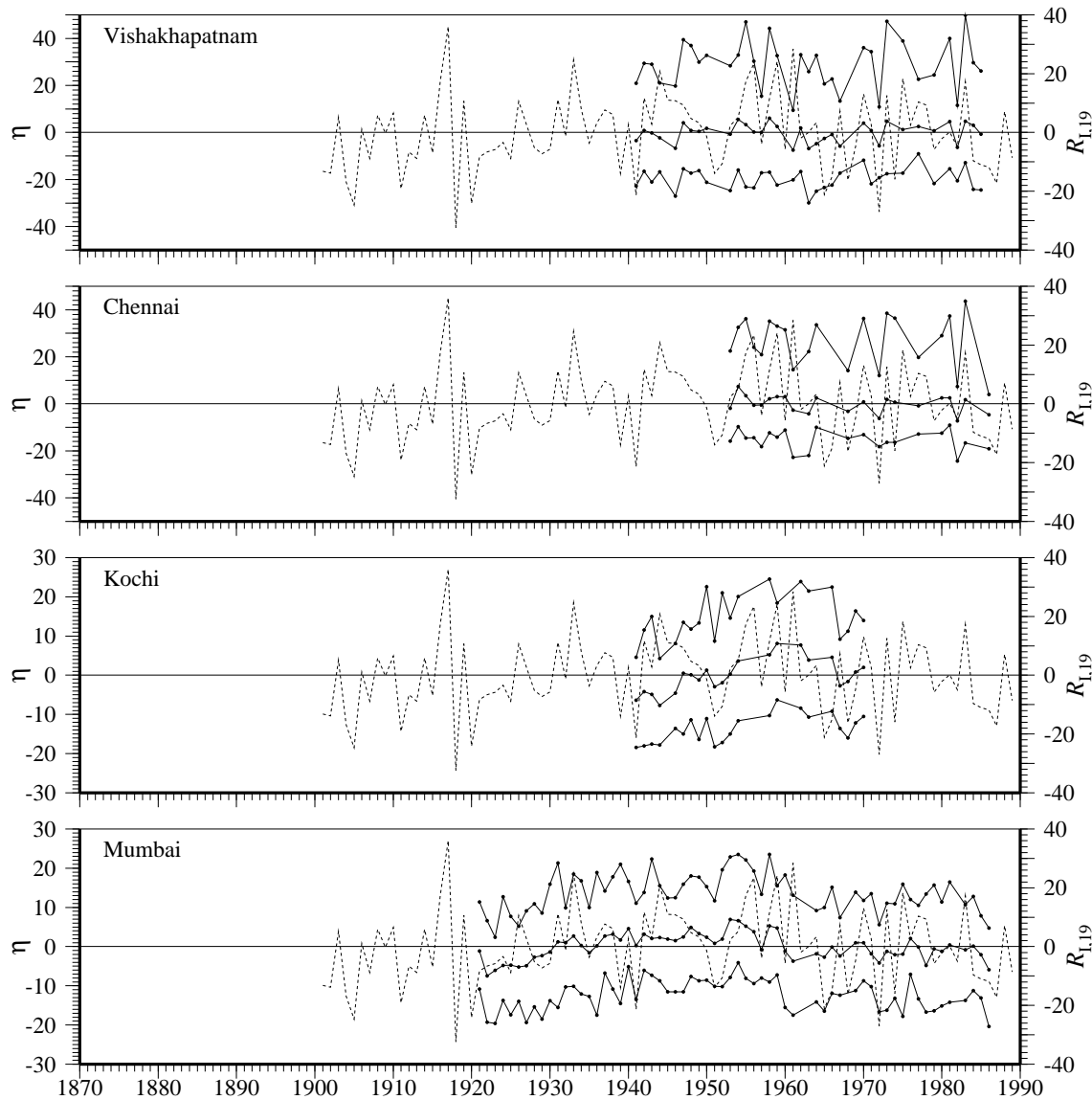


Table 6.8 Linear correlation statistics for annual all-India rainfall and sea level. R_I and $R_{I,19}$ denote the anomalies of annual all-India rainfall (1871–1994 and 1901–1990 time series), and η_V , η_C , η_K , and η_M the anomalies of sea level at Vishakhapatnam, Chennai, Kochi, and Mumbai; the subscripts “m”, “max”, and “min” imply annual mean, maximum, and minimum. r , r_s , and P are as before. A “C” in the sixth column implies that the sea-level data are corrected for atmospheric pressure (default is no correction); an asterisk (*) in the last (seventh) column implies that sea-level data for 1961 have been dropped while computing the correlations. The annual mean and extrema of sea level at Kochi are not correlated with all-India rainfall, and hence, not shown.

| | | r | r_s | P | | |
|------------|----------------|-------|-------|------|---|---|
| R_I | $\eta_{V,m}$ | 0.186 | 0.260 | | | |
| R_I | $\eta_{V,m}$ | 0.211 | 0.283 | | C | |
| R_I | $\eta_{V,m}$ | 0.297 | 0.264 | 90.0 | | * |
| R_I | $\eta_{V,m}$ | 0.352 | 0.329 | 95.0 | C | * |
| R_I | $\eta_{V,max}$ | 0.394 | 0.325 | 95.0 | C | |
| R_I | $\eta_{V,max}$ | 0.550 | 0.424 | 99.0 | C | * |
| R_I | $\eta_{V,min}$ | 0.169 | 0.283 | | C | |
| R_I | $\eta_{V,min}$ | 0.182 | 0.287 | | C | * |
| $R_{I,19}$ | $\eta_{V,m}$ | 0.241 | 0.283 | | C | |
| $R_{I,19}$ | $\eta_{V,m}$ | 0.393 | 0.329 | 95.0 | C | * |
| $R_{I,19}$ | $\eta_{V,max}$ | 0.372 | 0.325 | 95.0 | C | |
| $R_{I,19}$ | $\eta_{V,max}$ | 0.534 | 0.424 | 99.0 | C | * |
| $R_{I,19}$ | $\eta_{V,min}$ | 0.275 | 0.283 | | C | |
| $R_{I,19}$ | $\eta_{V,min}$ | 0.296 | 0.287 | 90.0 | C | * |
| R_I | $\eta_{C,m}$ | 0.308 | 0.329 | | | |
| R_I | $\eta_{C,m}$ | 0.387 | 0.361 | 90.0 | C | |
| R_I | $\eta_{C,m}$ | 0.384 | 0.344 | 90.0 | | * |
| R_I | $\eta_{C,m}$ | 0.520 | 0.423 | 95.0 | C | * |
| R_I | $\eta_{C,max}$ | 0.387 | 0.361 | 90.0 | C | |
| R_I | $\eta_{C,max}$ | 0.545 | 0.537 | 99.0 | C | * |
| R_I | $\eta_{C,min}$ | 0.129 | 0.361 | | C | |
| R_I | $\eta_{C,min}$ | 0.357 | 0.379 | | C | * |
| $R_{I,19}$ | $\eta_{C,m}$ | 0.410 | 0.404 | 95.0 | C | |
| $R_{I,19}$ | $\eta_{C,m}$ | 0.564 | 0.537 | 99.0 | C | * |
| $R_{I,19}$ | $\eta_{C,max}$ | 0.405 | 0.404 | 95.0 | C | |
| $R_{I,19}$ | $\eta_{C,max}$ | 0.578 | 0.537 | 99.0 | C | * |
| $R_{I,19}$ | $\eta_{C,min}$ | 0.086 | 0.361 | | C | |
| $R_{I,19}$ | $\eta_{C,min}$ | 0.325 | 0.379 | | C | * |
| R_I | $\eta_{M,m}$ | 0.321 | 0.247 | 99.0 | | |
| R_I | $\eta_{M,m}$ | 0.356 | 0.320 | 99.0 | C | |
| R_I | $\eta_{M,max}$ | 0.393 | 0.320 | 99.0 | C | |
| R_I | $\eta_{M,min}$ | 0.241 | 0.211 | 90.0 | C | |
| $R_{I,19}$ | $\eta_{M,m}$ | 0.362 | 0.320 | 99.0 | C | |
| $R_{I,19}$ | $\eta_{M,max}$ | 0.336 | 0.320 | 99.0 | C | |
| $R_{I,19}$ | $\eta_{M,min}$ | 0.285 | 0.246 | 95.0 | C | |

Table 6.9 Linear correlation statistics for low-pass-filtered annual rainfall and sea level at Mumbai. R_I and $R_{I,19}$ denote the anomalies of annual all-India rainfall for the 1871–1994 and 1901–1990 time series, R_{WC} and R_{GB} the anomalies of annual West-Coast and Ganga-Brahmaputra rainfall, and $\eta_{M,m}$ the anomalies of low-pass-filtered annual mean sea level at Mumbai. r is the linear correlation coefficient between the variables in the first two columns (at zero lag). r_s is the linear correlation at the $P\%$ significance level for the required number of degrees of freedom; if the column for P is blank, then r_s is the correlation at the 90% significance level, but the two variables are not correlated even at this level. A “T” in the sixth column implies that the rainfall and sea-level data have been truncated and only the data from 1901 onwards have been used to compute the correlations. An N -year running mean has been used to filter the data before computing the correlations; $N = 1$ implies no running mean. The long tide-gauge record at Mumbai yields the best correlations between all-India rainfall and sea level. The correlations at Mumbai retain their significance when the data are low-pass-filtered. $\eta_{M,m}$ is significantly correlated with $R_{I,19}$. Though the filtered rainfall is noisier than the filtered sea level, both rainfall and sea level were low in the first two decades of this century, rose to a peak in the 1950s, and declined thereafter (Figure 6.21). $\eta_{M,m}$, however, is not as well correlated with R_I . R_I was above normal during 1871–1899 and dropped to a low during 1900–1915, but the annual sea level at Mumbai during 1878–1899 was just 2 cm higher than that during 1900–1920 (Figure 6.20); eliminating the data during 1871–1900 improves the correlation. $\eta_{M,m}$ is also correlated with R_{WC} , but not with R_{GB} ; eliminating the data during 1871–1900 improves this correlation also. Since R_M is significantly correlated with R_{WC} , R_I , and $R_{I,19}$ (Table 6.7), and the annual sea level is well correlated along the coast (Table 6.2), this implies that there exists at least a statistical basis for a relation between the sub-annual variability of rainfall over India and that of sea level along her coast. The physical basis for such a relation is the influence of salinity on the seasonal cycle and alongshore variations of sea level along the coast.

| | | r | r_s | P | N |
|------------|--------------|-------|-------|------|------|
| R_I | $\eta_{M,m}$ | 0.321 | 0.247 | 99.0 | 1 |
| R_I | $\eta_{M,m}$ | 0.334 | 0.304 | 99.0 | 2 |
| R_I | $\eta_{M,m}$ | 0.328 | 0.299 | 90.0 | 5 |
| R_I | $\eta_{M,m}$ | 0.464 | 0.424 | 90.0 | 10 |
| $R_{I,19}$ | $\eta_{M,m}$ | 0.437 | 0.278 | 99.0 | 1 |
| $R_{I,19}$ | $\eta_{M,m}$ | 0.501 | 0.344 | 99.0 | 2 |
| $R_{I,19}$ | $\eta_{M,m}$ | 0.556 | 0.506 | 99.0 | 5 |
| $R_{I,19}$ | $\eta_{M,m}$ | 0.752 | 0.677 | 99.0 | 10 |
| R_I | $\eta_{M,m}$ | 0.416 | 0.278 | 99.0 | T 1 |
| R_I | $\eta_{M,m}$ | 0.654 | 0.557 | 95.0 | T 10 |
| R_{WC} | $\eta_{M,m}$ | 0.374 | 0.274 | 99.0 | 1 |
| R_{WC} | $\eta_{M,m}$ | 0.375 | 0.278 | 99.0 | T 1 |
| R_{GB} | $\eta_{M,m}$ | 0.091 | 0.161 | | 1 |
| R_{GB} | $\eta_{M,m}$ | 0.195 | 0.182 | 90.0 | T 1 |

Figure 6.20 Low-pass-filtered variability of all-India annual rainfall ($1871\text{--}1994$) R_i and the annual mean and extrema of sea level at Mumbai. Anomalies of sea level (cm) and rainfall (cm) are plotted on the ordinate and time (year) is on the abscissa. The dashed curve is for rainfall and the solid curves are for the annual mean (middle curve), annual maximum (upper curve) and annual minimum (lower curve) of sea level. The data are filtered with a running mean. Plots are shown for no running mean, 2-year running mean, 5-year running mean, and 10-year running mean.

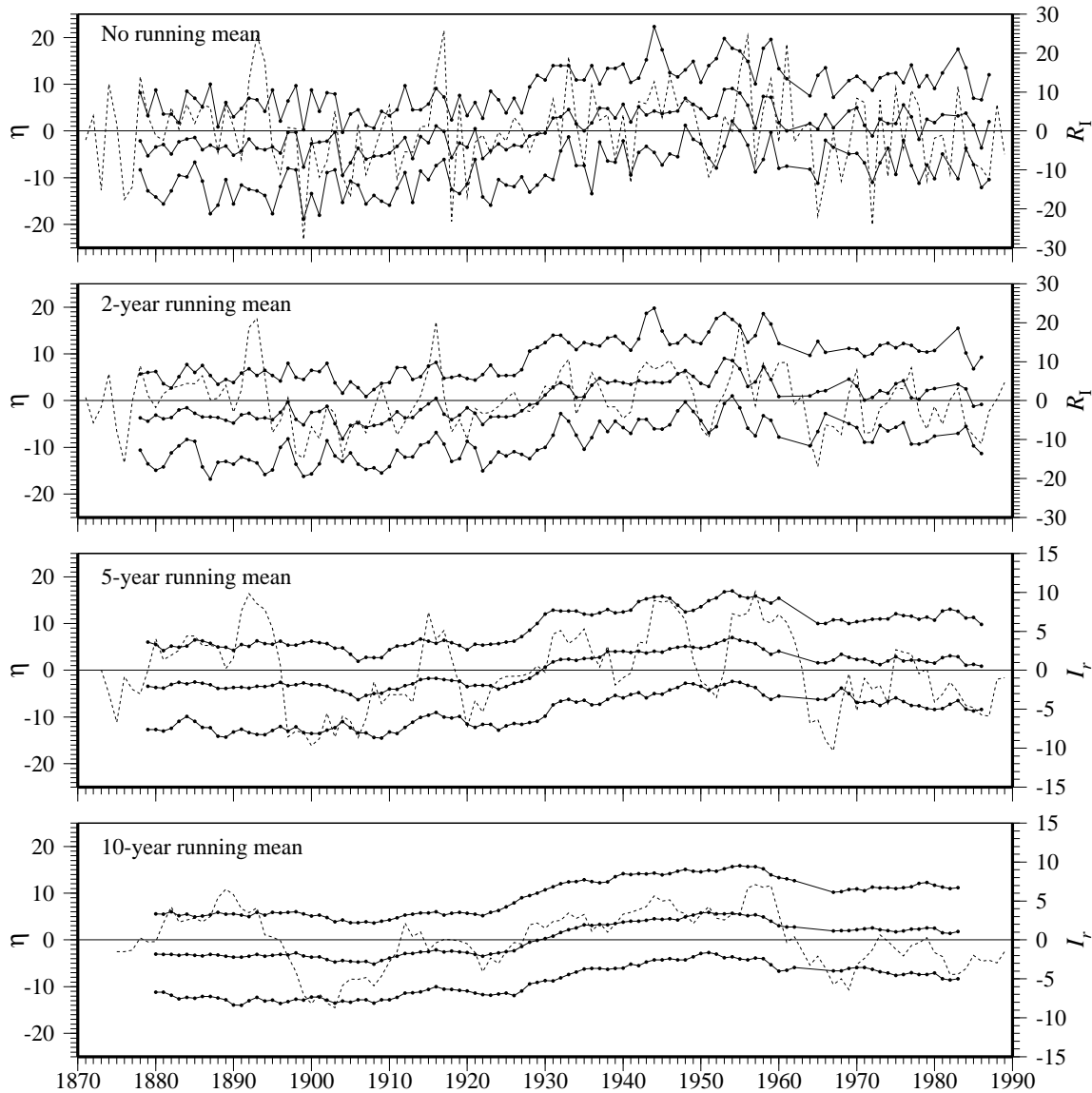
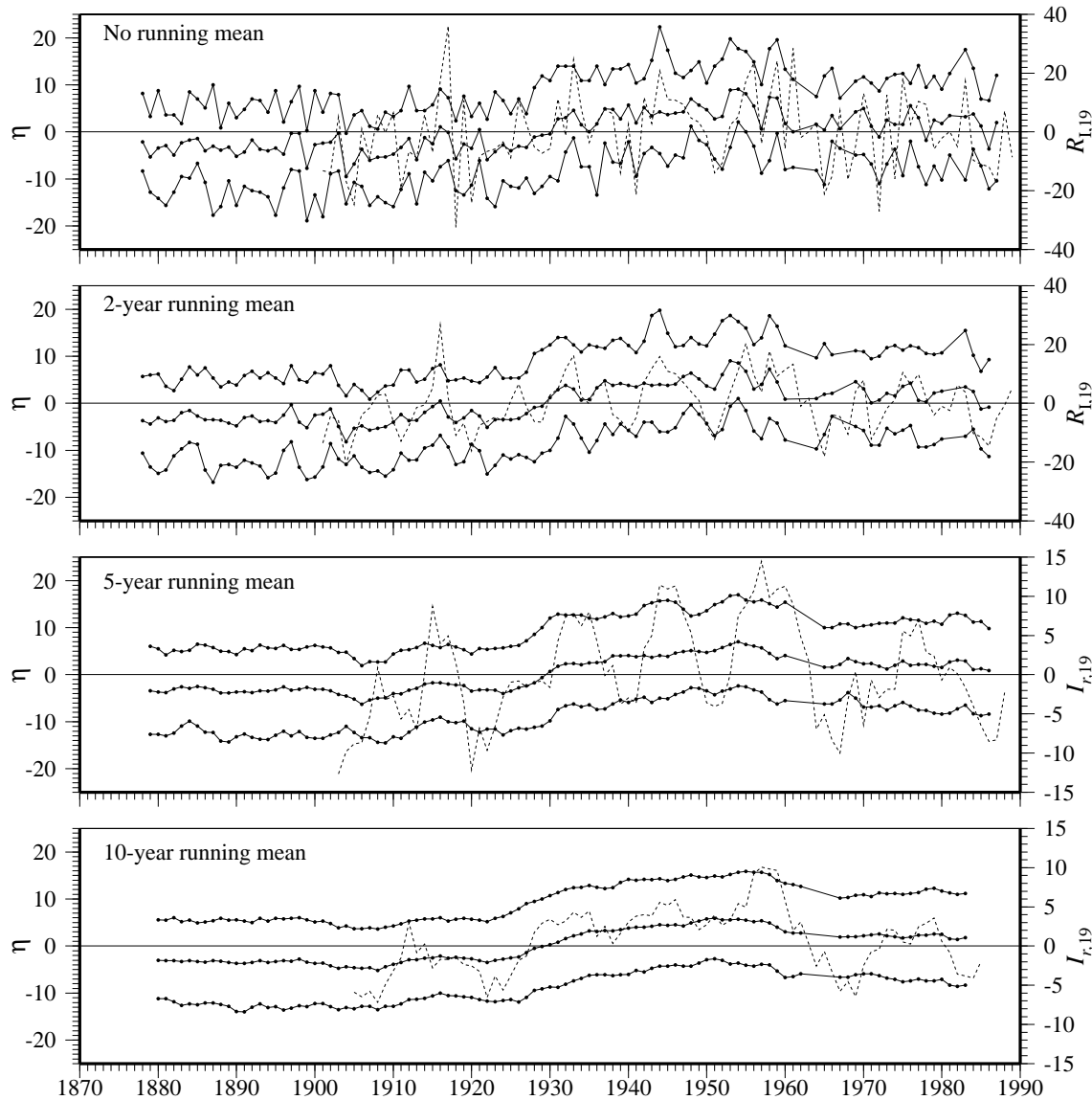


Figure 6.21 Low-pass-filtered variability of all-India annual rainfall ($1901\text{--}1990$) $R_{1,19}$ and the annual mean and extrema of sea level at Mumbai. Anomalies of sea level (cm) and rainfall (cm) are plotted on the ordinate and time (year) is on the abscissa. The dashed curve is for rainfall and the solid curves are for the annual mean (middle curve), annual maximum (upper curve) and annual minimum (lower curve) of sea level. The data are filtered with a running mean. Plots are shown for no running mean, 2-year running mean, 5-year running mean, and 10-year running mean.



1871–1900 improves this correlation also.

Since R_M is significantly correlated with R_{WC} , R_I , and $R_{I,19}$ (Table 6.7), and the annual sea level is well correlated along the coast (Table 6.2), this implies that there exists at least a statistical basis for a relation between the sub-annual variability of rainfall over India and that of sea level along her coast. The physical basis for such a relation is the influence of salinity on the seasonal cycle and alongshore variations of sea level along the coast.

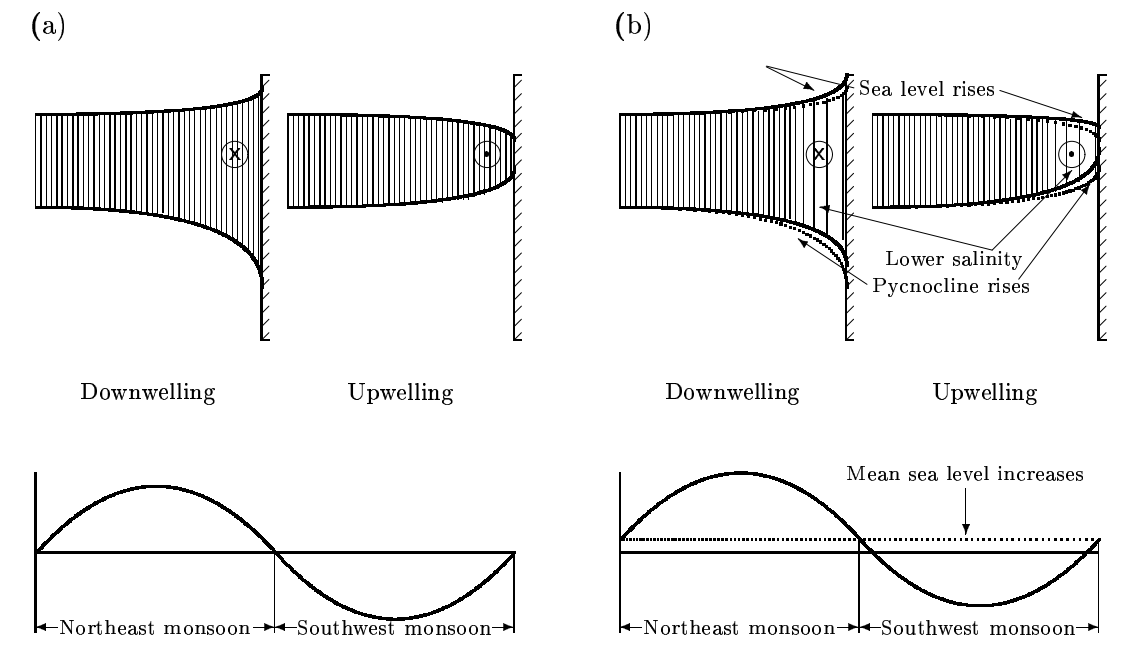
6.3.4 A Hypothesis Linking Monsoon Rainfall and Sea Level Along the Coast

Our hypothesis is that the seasonal inflow of the monsoon rainfall into the seas around India and the dynamics of currents (EICC and WICC) along her coast provide the link between all-India rainfall and coastal sea level, with the coastal salinity field playing an intermediate role. A simple model for the seasonally reversing EICC and WICC is an annual Kelvin wave, which favours upwelling during the southwest monsoon and downwelling during the northeast monsoon (Section 3.4). Under the influence of such a wave, the currents and sea level at the coast undergo a seasonal cycle; a coastal current favouring downwelling (upwelling) implies an increase (decrease) in coastal sea level (Figure 6.22a). The seasonal cycle of currents alone, however, cannot explain the link between all-India rainfall and the sea level at Mumbai on the interdecadal time scale (Figures 6.12, 6.20 and 6.21), just as it could not explain the seasonal cycle of sea level; the salinity along the coast has a significant effect on sea level (Section 4.3). The changes in coastal salinity are a consequence of the spreading of river runoff along the coast by the seasonal EICC and WICC. The result of the spreading and mixing of this low-salinity water is a gradient of salinity normal to the coast; the time scale associated with the temporal variability of this gradient is much longer than a season or a year because mixing is slow in the ocean. We propose that it is this cross-shore gradient of salinity that drives a weak, quasi-steady circulation (Figure 6.22b), providing the link between the interdecadal variability of all-India rainfall and that of sea level at Mumbai. In the next section, we put together a simple dynamical framework to justify this proposition.

6.4 Mechanics of Interdecadal Sea-Level Change Along the Coast of India

Our primary aim is to examine how the currents and sea level associated with an annual coastal Kelvin wave, which is a good description of the conditions along the coast of India, are modified by a cross-shore variation in density. We begin with the linearized $1\frac{1}{2}$ -layer model (Section A.1) that has proven useful in understanding the seasonal cycle of circulation along the coast of India, and then constrain it to reflect the weak, quasi-steady forcing that arises because of the cross-shore

Figure 6.22 (a) Schematic of a section normal to the coast, showing the relation between currents and sea level along the coast of India. The current shown by “X” (“.”) within a circle is into (out of) the plane of the paper. When there is downwelling (upwelling) at the coast, the current flows with the coast on its right (left), sea level rises (falls) at the coast, and the pycnocline (the top of which is shown by the line marking the bottom of the hatched area) slopes down (up) towards the coast. Along the west coast of India, there is downwelling (upwelling) during the northeast (southwest) monsoon. (b) Schematic to show how, according to our hypothesis, the conditions depicted in (a) are modified when salinity near the coast is lower than that farther offshore. Wider spacing of the hatched lines indicates lower salinity. The salinity (hence, density) gradient normal to the coast drives a weak, quasi-steady surface current that moves with the coast on its right, introducing a quasi-steady rise in sea level at the coast.



salinity gradient. The density of the active upper layer may vary in space (because of a variation in salinity); it is not allowed to vary in time, implying that the time scale associated with density changes is much longer than the transient motions such as Kelvin waves that are supported by the model. This is because our interest is in the long-term effects of changes in the coastal salinity field: how is the annual Kelvin wave modified by a quasi-steady cross-shore salinity gradient?

6.4.1 The $1\frac{1}{2}$ -Layer Model

Consider a coastal Kelvin wave propagating south–north along a meridional eastern boundary. The basic state is one of no motion and constant density in each of the two model layers. This state is perturbed by prescribing a density that is a function of space alone; we solve the equations

for a free Kelvin wave in this perturbed medium. The relevant equations are (A.13), with some constraints. First, since we are considering a coastal Kelvin wave, there is no cross-shore velocity, i.e., $u = 0$. Second, since we are interested only in a Kelvin wave, it is not necessary to solve the equations on a β -plane; hence, the Coriolis parameter f is a constant. Third, since salinity and density vary only in space, $\gamma = \gamma(x, y)$; hence, $q = 0$. Fourth, since we are interested in a free wave, $\tau^x = \tau^y = 0$. Then, dropping the Rayleigh friction coefficient, i.e., setting $r = 0$, and dropping the subscript “0” (which indicates that these are the zeroth-order perturbation equations), we obtain

$$-fv = -g\bar{\Gamma}\frac{\partial h}{\partial x} - \frac{g\bar{H}}{2}\frac{\partial \gamma}{\partial x}, \quad (6.1a)$$

$$\frac{\partial v}{\partial t} = -g\bar{\Gamma}\frac{\partial h}{\partial y} - \frac{g\bar{H}}{2}\frac{\partial \gamma}{\partial y}, \quad (6.1b)$$

$$\frac{\partial h}{\partial t} = -\bar{H}\frac{\partial v}{\partial y}, \quad (6.1c)$$

$$\eta = \bar{\Gamma}h + \bar{H}\gamma. \quad (6.1d)$$

\bar{H} and $\bar{\Gamma}$ are the upper layer thickness and the reduced-gravity parameter in the basic state of no motion, about which the system is perturbed; v , h , η , and γ are the perturbation meridional (alongshore) velocity, upper layer thickness, sea level, and reduced-gravity parameter; the layer thickness and reduced-gravity parameter are $H = \bar{H} + h$ and $\Gamma = \bar{\Gamma} + \gamma$.

We define an “equivalent layer thickness” (ELT)

$$H' = \bar{H} + h', \quad (6.2a)$$

where

$$h' = h + \left(\frac{\gamma}{2\bar{\Gamma}} \right) \quad (6.2b)$$

is the “equivalent perturbation layer thickness” (EPLT). Equations (6.1) and (6.2) yield the free wave equation

$$\frac{\partial h'}{\partial t^2} = c^2 \frac{\partial h'}{\partial y^2}, \quad (6.3)$$

where $c = (g\bar{\Gamma}\bar{H})^{1/2}$ is the speed of the first-baroclinic-mode Kelvin wave. The solution to (6.3) is

$$h' = \tilde{h}' e^{x/a+i(l_y-\sigma t)}, \quad (6.4)$$

where \tilde{h}' is the “equivalent” amplitude of the Kelvin wave at the coast and $a = \frac{c}{f}$ is the internal Rossby radius of deformation. Equations (6.1), (6.2), and (6.4) yield the required zeroth-order solution

$$h = \tilde{h}' e^{x/a + i(l y - \sigma t)} - \left(\frac{\gamma}{2\bar{\Gamma}} \right), \quad (6.5a)$$

$$v = \left(\frac{g\bar{\Gamma}}{H} \right)^{\frac{1}{2}} \tilde{h}' e^{x/a + i(l y - \sigma t)}, \quad (6.5b)$$

$$\eta = \bar{\Gamma} \tilde{h}' e^{x/a + i(l y - \sigma t)} + \left(\frac{\gamma}{2} \right) H. \quad (6.5c)$$

In the absence of spatial variation in density ($\Gamma = \bar{\Gamma}; \gamma = 0$), we obtain the classical Kelvin wave solution. When density varies in space ($\gamma \neq 0$), the Kelvin wave amplitude is modified (it becomes the “equivalent” amplitude), but there is another change that is significant for sea level at the coast. When salinity, and hence density, decreases (increases) from the open sea towards the coast, i.e., when $\frac{\partial \gamma}{\partial x} > 0$ ($\frac{\partial \gamma}{\partial x} < 0$), sea level at the coast increases (decreases). This change in sea level depends only on γ and, hence, is independent of time. Since the low-salinity water is spread along the coast by currents that decay exponentially away from the coast, i.e., they are coastally-trapped, the perturbation in salinity, and hence γ , decays exponentially away from the coast ($\gamma \propto e^{kx}, k > 0$). Therefore, the time-independent change in sea level predicted by the model also varies exponentially cross-shore.

The Kelvin wave is superimposed on the time-independent increase in sea level. In the linear system described by equations (6.1), we can ignore the Kelvin wave to look at the quasi-steady state. It consists of an increase in sea level and an upsloping of the pycnocline towards the coast (Figure 6.22b), i.e., when there is no Kelvin wave and density decreases coastward, sea level rises at the coast, the pycnocline upslopes, and there is no current in the layer. This result, which is intriguing because a sloping surface and pycnocline are normally associated with a geostrophic alongshore current, can be understood by extending the model to include another active layer.

6.4.2 The $2\frac{1}{2}$ -Layer Model

Consider a $2\frac{1}{2}$ -layer reduced-gravity model (Section A.2), but with no difference in density between the two active layers in the basic state, i.e., $\bar{\Gamma}_1 = \bar{\Gamma}_2 = \bar{\Gamma}$; the perturbation density in the two layers, however, is different, i.e., $\Gamma_1 \neq \Gamma_2$. The model now supports velocity shear in the vertical, permitting the existence of a “shear mode”. As with the $1\frac{1}{2}$ -layer model, the perturbation density varies in the horizontal in the active layers; the interface between the lower active layer and the deep ocean is the model pycnocline. A precise definition of the density field is required because

this model differs from the usual $2\frac{1}{2}$ -layer reduced-gravity model, in which $\bar{\Gamma}_1 \neq \bar{\Gamma}_2$, implying the existence of two baroclinic modes. Our interest is restricted to understanding why the $1\frac{1}{2}$ -layer model does not yield a quasi-steady velocity along with the quasi-steady rise in sea level, and, for this, the introduction of shear in the vertical is sufficient; the assumption that there is no difference in unperturbed density between the two shear layers ($\bar{\Gamma}_1 = \bar{\Gamma}_2$) simplifies the algebra.

We define the reduced-gravity parameters as follows. Let ρ_1 , ρ_2 , and ρ_3 be the densities of the three model layers ($\rho_1 < \rho_2 < \rho_3$). Then, by definition,

$$\Gamma_1 = \frac{\rho_3 - \rho_1}{\bar{\rho}} ; \quad \Gamma_2 = \frac{\rho_3 - \rho_2}{\bar{\rho}},$$

where $\bar{\rho}$ is an average density that is representative of the ocean. In the basic state, $\bar{\Gamma}_1 = \bar{\Gamma}_2 = \bar{\Gamma}$. Hence, we have $\Gamma_1 = \bar{\Gamma} + \gamma_1$; $\Gamma_2 = \bar{\Gamma} + \gamma_2$. Let

$$\bar{\Gamma} = \frac{\rho_3 - \bar{\rho}_{1,2}}{\bar{\rho}}, \quad (6.6a)$$

where

$$\bar{\rho}_{1,2} = \frac{\bar{H}_1 \bar{\rho}_1 + \bar{H}_2 \bar{\rho}_2}{\bar{H}}, \quad (6.6b)$$

and

$$\bar{\rho}_1 = \frac{1}{A} \iint_A \rho_1 dx dy, \quad (6.6c)$$

$$\bar{\rho}_2 = \frac{1}{A} \iint_A \rho_2 dx dy. \quad (6.6d)$$

\bar{H}_1 and \bar{H}_2 are the layer thicknesses in the basic state and A is the area of the model domain. \bar{H}_1 , \bar{H}_2 , and $\bar{\Gamma}$ define the basic state about which the system is perturbed. Since $\rho_2 > \rho_1$, we have $\bar{\rho}_2 > \bar{\rho}_1$. Then,

$$\gamma_1 = \frac{\bar{\rho}_{1,2} - \rho_1}{\bar{\rho}} = \frac{\bar{\rho}_1 - \rho_1}{\bar{\rho}} + \left(\frac{\bar{H}_2}{\bar{H}} \right) \left(\frac{\bar{\rho}_2 - \bar{\rho}_1}{\bar{\rho}} \right), \quad (6.7a)$$

$$\gamma_2 = \frac{\bar{\rho}_{1,2} - \rho_2}{\bar{\rho}} = \frac{\bar{\rho}_2 - \rho_2}{\bar{\rho}} - \left(\frac{\bar{H}_1}{\bar{H}} \right) \left(\frac{\bar{\rho}_2 - \bar{\rho}_1}{\bar{\rho}} \right). \quad (6.7b)$$

This yields $\gamma_1 - \gamma_2 > 0$, as expected. This definition of the density field and reduced-gravity parameters ensures that \bar{H}_1 is a meaningful quantity: it is the depth up to which salinity at the coast

is affected by the runoff from rivers. A consequence of the definition is that $\gamma_2 \neq 0$, but it may be constant.

The zeroth-order, linearized perturbation equations for this $2\frac{1}{2}$ -layer model, equivalent to equations (6.1) for the $1\frac{1}{2}$ -layer model, follow from equations (A.20) and (A.21) on making the same assumptions as for $1\frac{1}{2}$ -layer model.

$$-fv_1 = -g\bar{\Gamma}\frac{\partial}{\partial x}(h_1 + h_2) - \frac{g\bar{H}_1}{2}\frac{\partial\gamma_1}{\partial x} - g\bar{H}_2\frac{\partial\gamma_2}{\partial x}, \quad (6.8a)$$

$$\frac{\partial v_1}{\partial t} = -g\bar{\Gamma}\frac{\partial}{\partial y}(h_1 + h_2) - \frac{g\bar{H}_1}{2}\frac{\partial\gamma_1}{\partial y} - g\bar{H}_2\frac{\partial\gamma_2}{\partial y}, \quad (6.8b)$$

$$\frac{\partial h_1}{\partial t} = -\bar{H}_1\frac{\partial v_1}{\partial y} \quad (6.8c)$$

are the equations for the first layer, and

$$-fv_2 = -g\bar{\Gamma}\frac{\partial}{\partial x}(h_1 + h_2) - \frac{g\bar{H}_2}{2}\frac{\partial\gamma_2}{\partial x}, \quad (6.9a)$$

$$\frac{\partial v_2}{\partial t} = -g\bar{\Gamma}\frac{\partial}{\partial y}(h_1 + h_2) - \frac{g\bar{H}_2}{2}\frac{\partial\gamma_2}{\partial y}, \quad (6.9b)$$

$$\frac{\partial h_2}{\partial t} = -\bar{H}_2\frac{\partial v_2}{\partial y} \quad (6.9c)$$

are the equations for the second layer. The perturbation sea level is given by

$$\eta = \bar{\Gamma}(h_1 + h_2) + \bar{H}_1\gamma_1 + \bar{H}_2\gamma_2. \quad (6.10)$$

Let

$$h = h_1 + h_2, \quad (6.11a)$$

$$\bar{H} = \bar{H}_1 + \bar{H}_2, \quad (6.11b)$$

$$v = \frac{\bar{H}_1 v_1 + \bar{H}_2 v_2}{\bar{H}}, \quad (6.11c)$$

where \bar{H} is the “cumulative layer thickness” in the basic state, h is the “cumulative perturbation layer thickness”, and v is the mean velocity. Then, equations (6.8), (6.9), and (6.11) yield the free wave equation

$$\frac{\partial h'}{\partial t^2} = c^2 \frac{\partial h'}{\partial y^2}, \quad (6.12)$$

where

$$h' = h + \left(\frac{\bar{H}_1^2 \gamma_1 + 2\bar{H}_1 \bar{H}_2 \gamma_2 + \bar{H}_2^2 \gamma_2}{2\bar{\Gamma}H} \right) \quad (6.13)$$

is the “equivalent cumulative perturbation layer thickness” (ECLPT) and $c = (g\bar{\Gamma}H)^{\frac{1}{2}}$. The solution to (6.12) is

$$h' = \tilde{h}' e^{x/a+i(l_y-\sigma t)}, \quad (6.14)$$

where $a = \frac{c}{f}$. Then equations (6.13) and (6.14) imply

$$h = \tilde{h}' e^{x/a+i(l_y-\sigma t)} - \left(\frac{\bar{H}_1^2 \gamma_1 + 2\bar{H}_1 \bar{H}_2 \gamma_2 + \bar{H}_2^2 \gamma_2}{2\bar{\Gamma}H} \right). \quad (6.15)$$

The perturbation sea level is

$$\eta = \bar{\Gamma} \tilde{h}' e^{x/a+i(l_y-\sigma t)} + \left(\frac{\bar{H}_1^2 \gamma_1 + 2\bar{H}_1 \bar{H}_2 \gamma_1 + \bar{H}_2^2 \gamma_1}{2\bar{H}} \right). \quad (6.16)$$

Since we are interested only in the quasi-steady part of the solution, we restrict our attention to it. It is the quasi-steady response that causes the interdecadal changes in sea level, the Kelvin wave being superimposed on it. The quasi-steady component of h is

$$h_s = - \left(\frac{\bar{H}_1^2 \gamma_1 + 2\bar{H}_1 \bar{H}_2 \gamma_2 + \bar{H}_2^2 \gamma_2}{2\bar{\Gamma}H} \right), \quad (6.17a)$$

and the quasi-steady sea level is

$$\eta_s = \frac{\bar{H}_1^2 \gamma_1 + 2\bar{H}_1 \bar{H}_2 \gamma_1 + \bar{H}_2^2 \gamma_1}{2\bar{H}}. \quad (6.17b)$$

Substituting (6.17a) in (6.8a) and (6.9a), we obtain the quasi-steady solutions for the alongshore velocity in the two layers. These are

$$v_{1,s} = \left(\frac{g\bar{H}_2}{2f\bar{H}} \right) \frac{\partial}{\partial x} (\bar{H}_1 \gamma_1 + \bar{H}_2 \gamma_2), \quad (6.17c)$$

$$v_{2,s} = - \left(\frac{g\bar{H}_1}{2f\bar{H}} \right) \frac{\partial}{\partial x} (\bar{H}_1 \gamma_1 + \bar{H}_2 \gamma_2). \quad (6.17d)$$

The introduction of the “shear mode” permits the existence of an undercurrent, but there is no mean velocity, i.e., $v_s = 0$, as in the $1\frac{1}{2}$ -layer model, and

$$\frac{v_{1,s}}{v_{2,s}} = - \frac{\bar{H}_2}{\bar{H}_1}.$$

From equations (6.17), we obtain

$$\frac{\partial \eta_s}{\partial x} \leq 0 \quad \forall \quad \frac{\partial \gamma_1}{\partial x} \leq -\tan \theta_n \frac{\partial \gamma_2}{\partial x}, \quad (6.18a)$$

$$\frac{\partial h_s}{\partial x} \leq 0 \quad \forall \quad \frac{\partial \gamma_1}{\partial x} \geq -\tan \theta_h \frac{\partial \gamma_2}{\partial x}, \quad (6.18b)$$

$$v_{1,s} \leq 0 \quad \forall \quad \frac{\partial \gamma_1}{\partial x} \leq -\tan \theta_v \frac{\partial \gamma_2}{\partial x}, \quad (6.18c)$$

$$v_{2,s} \geq 0 \quad \forall \quad v_{1,s} \geq 0, \quad (6.18d)$$

where

$$\tan \theta_n = \left(\frac{\bar{H}_2}{\bar{H}_1} \right)^2 \left(1 + \frac{2\bar{H}_2}{\bar{H}_1} \right)^{-1}, \quad (6.19a)$$

$$\tan \theta_h = \left(\frac{\bar{H}_2}{\bar{H}_1} \right)^2 \left(1 + \frac{2\bar{H}_2}{\bar{H}_1} \right), \quad (6.19b)$$

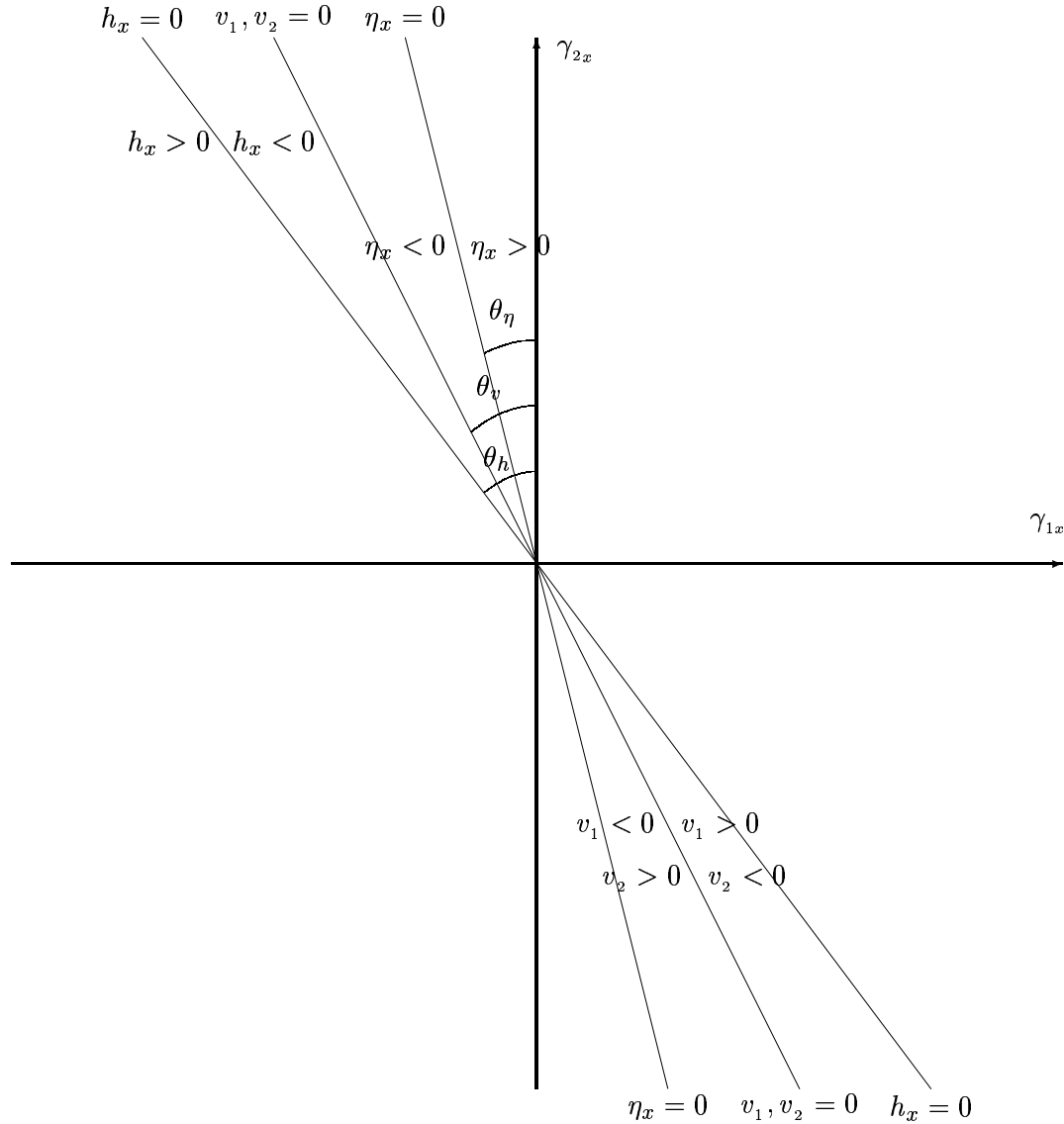
$$\tan \theta_v = \frac{\bar{H}_2}{\bar{H}_1}, \quad (6.19c)$$

with

$$\theta_n < \theta_v < \theta_h. \quad (6.19d)$$

Equations (6.18) and (6.19) imply that the velocities in the two active layers, $v_{1,s}$ and $v_{2,s}$, and the cross-shore gradients of η_s and h_s depend on the layer thicknesses in the basic state, \bar{H}_1 and \bar{H}_2 , and on the cross-shore gradients of both γ_1 and γ_2 . This is shown graphically in Figure 6.23. The solution shows that there exist conditions under which sea level may rise at the coast; this need not, however, be accompanied by a rise of the pycnocline, or by a surface current that flows with the higher sea level on its right, unlike in the simpler solution obtained for the $1\frac{1}{2}$ -layer model. For example, between the solid and dashed lines in the second quadrant in Figure 6.23, sea level falls coastward, but the surface current is still poleward (for an eastern boundary like the Indian west coast); between the solid and dotted lines in the fourth quadrant, sea level rises towards the coast, but so does the pycnocline. An extreme case is that of sea level falling at the coast despite salinity decreasing coastward; this can happen if the density of the lower layer increases coastward at a sufficiently rapid rate (the region to the left of the solid line in Figure 6.23). Thus, there exist a number of possible solutions and it is the prevailing conditions, i.e., the thickness of the layer influenced by runoff (\bar{H}_1), the thickness of the layer below (\bar{H}_2), and the cross-shore gradients of the reduced-gravity parameters in the two layers (γ_1 and γ_2), that determine whether sea level rises at the coast or not.

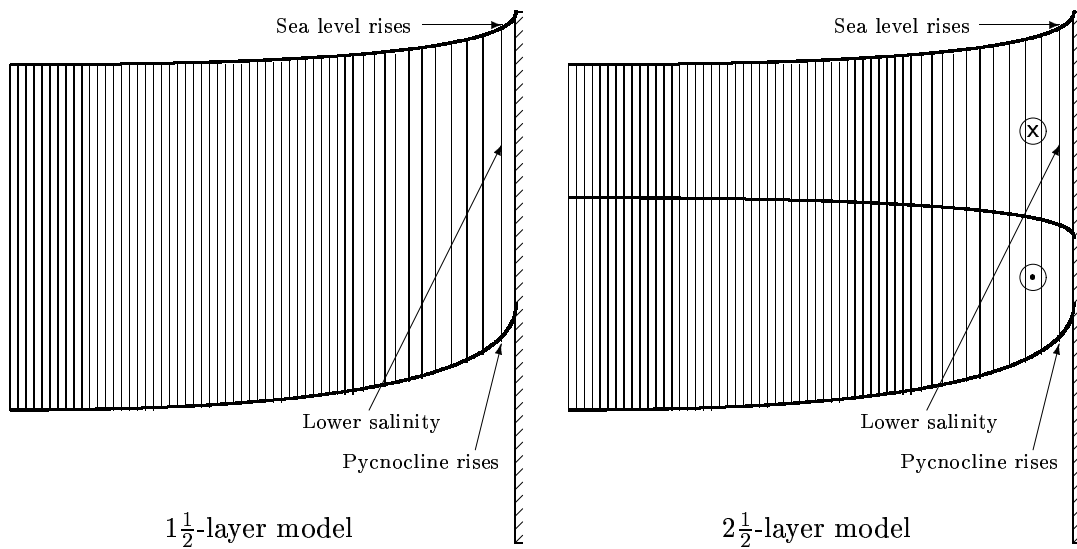
Figure 6.23 A graphical representation of the quasi-steady solution to the $2\frac{1}{2}$ -layer model equations. The possible quasi-steady solutions (the subscript “s” is dropped in this figure for convenience) are shown as a function of γ_{1x} (abscissa) and γ_{2x} (ordinate); the subscript x denotes a partial derivative w.r.t x , the cross-shore co-ordinate. The lines $h_x = 0$ (dotted), $\eta_x = 0$ (solid), and $v_1 = v_2 = 0$ (dashed) mark the boundaries across which the cross-shore gradients of h and η , and the velocities v_1 and v_2 change sign. To the right (left) of the respective lines, η_x and v_1 are positive (negative), and h_x and v_2 are negative (positive). Unless there is a sufficiently large negative gradient of γ_2 , a coastward decrease in the salinity of the upper active layer at an eastern boundary ($\gamma_{1x} > 0$) implies a rise in coastal sea level, a rise of the pycnocline towards the coast, and a surface current (undercurrent) that flows with the coast on its right.



6.4.3 Application to the West Coast of India

Despite the relative complexity of the $2\frac{1}{2}$ -layer solution, it is similar to that for the $1\frac{1}{2}$ -layer model when there is a coastward decrease of salinity in both layers (but with $\gamma_1 > \gamma_2$). The two solutions are shown in Figure 6.24.

Figure 6.24 Schematic of a section normal to the coast, showing the effect of a decrease in the salinity of coastal waters on sea level at an eastern ocean boundary in the northern hemisphere. The panel on the left shows the response in a $1\frac{1}{2}$ -layer model, and that on the right the response in a $2\frac{1}{2}$ -layer model. The cross-shore, time-independent variation in salinity forces a rise in coastal sea level and a time-independent geostrophic circulation with a surface current and an undercurrent. The surface current flows with the lighter water on its right and the undercurrent in the opposite direction. The pycnocline (the interface between the undercurrent and the motionless deeper ocean) slopes up towards the coast. The transports of the two currents cancel to yield a zero net transport. The $1\frac{1}{2}$ -layer model yields only the mean of the surface current and the undercurrent, and hence predicts a zero current associated with the rise in sea level and the pycnocline at the coast. In the figure, the current shown by “x” (“.”) within a circle is into (out of) the plane of the paper, and wider spacing of the hatched lines indicates lower salinity.



At Mumbai, sea level rose by about 11 cm during 1900–1950 and fell by about 4.5 cm during 1950–1980. By how much does the salinity at the coast have to change to force these interdecadal changes in sea level? Our model domain has an eastern boundary and extends to infinity towards west. The changes in salinity due to runoff from rivers affects only a layer of thickness \bar{H}_1 and is restricted to the vicinity of the coast, the slow mixing in the ocean acting over time to reduce the cross-shore density gradient. This cross-shore gradient is quasi-steady because mixing in the ocean is slow; the more rapid changes forced by seasonal Kelvin waves are superimposed on

it. In the lower active layer of thickness \bar{H}_2 , density, and hence γ_2 , is assumed to be constant. Differentiating η_s in (6.17b) then eliminates the contribution from density variations in this layer. Integrating $\frac{\partial \eta_s}{\partial x}$ over $(-\infty, 0]$ for an exponential variation of density in x ($\gamma_1 \propto e^{kx}$, where k^{-1} is a length scale), we obtain

$$\eta_s|_{x=0} = \left(\frac{\bar{H}_1^2 + 2\bar{H}_1\bar{H}_2}{2\bar{H}} \right) \gamma_1|_{x=0}. \quad (6.20)$$

For $\eta_s = 5$ cm and $\bar{H}_1 = \bar{H}_2 = 50$ m, we obtain $\gamma_1 = 0.0013$. If we assume that the change in density is entirely due to a change in salinity, ignoring other processes (for example, temperature changes due to “global warming”, melting of ice caps, etc.), this translates to a decrease of 1.07 PSU in the salinity averaged over the top 50 m. A similar approach, using (6.17a) instead of (6.17b), gives the displacement of the pycnocline at the coast.

$$h_s|_{x=0} = - \left(\frac{\bar{H}_1^2}{2\bar{\Gamma}\bar{H}} \right) \gamma_1|_{x=0}. \quad (6.21)$$

For $\bar{\Gamma} = 0.0035$, the value used in the constant-density reduced-gravity model in Chapter 3, we obtain $h_s = -4.8$ m at the coast. To compute the currents associated with the cross-shore density gradient, we need a measure of the length scale k^{-1} associated with the mixing of salt in the Arabian Sea. Horizontal eddy diffusivities in the Arabian Sea range from 1.3×10^6 (zonal) to 3.1×10^6 cm² s⁻¹ (meridional) [Somayajulu et al., 1996]. Assuming an average value of 2×10^6 cm² s⁻¹, we obtain a length scale of 400 km for a time scale of 25 years, the period over which sea level at Mumbai drops by 4.5 cm. Then (6.17c) implies $v_{1,s} = -v_{2,s} = 0.8$ cm s⁻¹; thus, the background thermohaline circulation forced by the cross-shore density gradient is much weaker than the seasonal WICC superimposed on it.

To summarize, a suitable model to explain the link between sea level and all-India rainfall is the following. The ocean responds as a two-layer system to a cross-shore variation in density. When density decreases coastward in a surface layer, sea level rises at the coast, and this is accompanied by a geostrophic surface current that flows with the lighter water on its right; below the surface current is an undercurrent. The sum of the transport of the surface current and the undercurrent vanishes. Geostrophy requires that the interface between the undercurrent and the motionless deeper ocean (the model pycnocline) slope up towards the coast (Figure 6.24). The slow mixing in the ocean makes this response quasi-steady.

Thus, a coastward decrease (increase) in salinity implies an increase (decrease) in both the annual maximum and the annual minimum of sea level, and hence, an increase (decrease) in sea level throughout the year, as seen at Mumbai. This change in sea level occurs on interannual and interdecadal time scales, much slower than the changes associated with the annual and other

Kelvin waves that are superimposed on it. Though it is the currents associated with these waves that spread the low-salinity water along the Indian coast, the long-term effect of spreading this water is to set up a weak, quasi-steady circulation.

6.4.4 Effect of Interannual Variability of Winds

The above hypothesis links the sub-annual changes in sea level along the coast of India to the variability of the monsoon, with the coastal salinity field playing an intermediate role. In building this hypothesis, we have ignored the large-scale winds over the basin, except for the redistribution of salt due to the currents forced by them. This needs some justification because an increase in the intensity of the monsoon is accompanied by an increase in the strength of the winds; rainfall is not the only measure of monsoon intensity.

An increase in the strength of the winds will force stronger upwelling and stronger downwelling, implying an increase in the maximum and a decrease in the minimum, the range of the seasonal cycle increasing as a consequence. Along the coast of India, the annual mean sea level is significantly correlated with the annual extrema and with the seasonal averages of sea level, and the hypothesis links these to changes in the salinity of coastal waters (Figure 6.22). The increase in the maximum usually is higher than that in the minimum, but a decrease in the maximum is not (Figures 6.8 and 6.9); a decrease in the maximum is, at times, accompanied by an increase in the minimum. This may be because of winds. Also, as shown in Chapter 5, a uniform increase in winds over the basin raises annual mean sea level along the east coast, but lowers it along the west coast. Since an increase in the intensity of the monsoon is accompanied by an increase in the strength of the winds, these two causes, rainfall and winds, force similar changes in sea level along the east coast, but opposing changes along the west coast. Thus, the interannual variability of the large-scale winds associated with the monsoon is bound to affect the correlation between all-India rainfall and sea level.

Interannual changes in the large-scale winds directly affect coastal sea level by forcing interannual Kelvin and Rossby waves. Clarke and Liu [1994] showed that friction due to the presence of the continental shelf [Clarke and van Gorder, 1994] allows Kelvin waves at these periods also to propagate along the coast; not all their energy is lost to westward propagating Rossby waves. Such interannual changes in the winds are bound to influence sea level, especially along the east coast of India, which is affected by Rossby waves forced by Ekman pumping in the open bay and by radiation from Kelvin waves forced by winds in the equatorial Indian Ocean. Since Chennai is to the south of Vishakhapatnam, sea level there will be affected more by these Rossby waves.

That the large-scale winds do have an effect on the sub-annual variability of sea level is apparent from the low correlation between all-India rainfall and sea level at Vishakhapatnam and Chennai; the correlation improves when the data for 1961 is dropped (Table 6.8). The annual sea

level for 1961 is an outlier and distorts the correlations. In 1961, rainfall was among the highest, but sea level at Vishakhapatnam and Chennai were among the lowest observed (Section 6.3.3). The deviation of monthly sea level from the long-term mean is plotted for 1956–1965 in Figure 6.25. The monthly sea levels follow the usual seasonal cycle during the decade, but there is a striking anomaly in 1961. The range of the seasonal cycle is anomalously low along the east coast; at Kochi, data for some months are missing during 1961, and at Mumbai, the effect is not so striking. Despite the high rainfall, the annual maximum decreased at Vishakhapatnam, Chennai, and Mumbai, as did the annual mean; the annual minimum also decreased at Chennai and Mumbai, but hardly changed at Vishakhapatnam (Figures 6.8 and 6.9). This implies that the high rainfall over India did not lower the salinity along the coast. This decrease in annual sea level during 1961–1962 is seen better in Figure 6.26, which shows the deviation of the monthly sea level from the climatology.

One cause is the relatively low rainfall in the catchment areas of the Ganga and the Brahmaputra during 1961 (Figure 6.14); the rainfall on the west coast, however, was in phase with all-India rainfall. Another important difference in 1961 was the anomaly in winds over the equatorial Indian Ocean [Reverdin et al., 1986]. These anomalous winds were driven by a reversal in the gradient of sea surface temperature (SST) along the equator. The SST normally is higher in the east and cooler in the west, where the Somali Current forces strong upwelling. In 1961, however, SST in the eastern equatorial Indian Ocean dropped below that in the west, forcing easterly anomalies in the winds. Such wind anomalies often occur during an El Niño [Reverdin et al., 1986], which also has an impact on monsoon rainfall [Mishra and Gadgil, 1996, and references therein], but 1961 was not an El-Niño year.

An anomaly in the winds over the equatorial Indian Ocean, which are an important forcing mechanism for the EICC [Shankar et al., 1996; McCreary et al., 1996], is likely to force anomalies in the seasonal cycle of the coastal currents off India. Anomalous easterlies would weaken the eastward equatorial jets in May and November [Wyrtki, 1973; O'Brien and Hurlburt, 1974; Jensen, 1993]. The weakening of the May jet would weaken the equatorward EICC that forms in the northern bay during the southwest monsoon, enabling the local Ekman flow to push the runoff offshore into the open bay. The weakening of the November jet would weaken the equatorward EICC during October–January, implying weaker downwelling along the coast. This, coupled with the lower runoff due to the decrease in rainfall in the catchment areas of the Ganga and the Brahmaputra (Figure 6.14) and the offshore movement of the runoff, implies a decrease in the annual mean and extrema according to the hypothesis. More of the runoff is likely to reach Vishakhapatnam because it lies north of Chennai; this is a possible reason for the lack of a decrease in the annual minimum there.

On interdecadal time scales, however, the effect of winds is negligible in comparison with that

Figure 6.25 Deviation of corrected monthly sea level (cm) during 1956–1965 from the long-term mean sea level. On the abscissa, the long and small ticks mark the beginning and end of the years and months, respectively. The monthly sea levels during July 1961 to June 1962 show a different behaviour in comparison to the sea level during the rest of the decade; the anomalous behaviour is maximum along the east coast, but is also seen at Kochi. At Mumbai, however, the anomalies are not striking. 1961 was a year of anomalous easterly winds over the equatorial Indian Ocean. The wind anomalies were similar to those seen during an El Niño, but 1961 was not an El-Niño year. Another possible cause of the anomalies is the lower rainfall in 1961 in the catchment areas of the Ganga and the Brahmaputra; though all-India and West-Coast rainfall were higher than normal, Ganga-Brahmaputra rainfall was lower than normal.

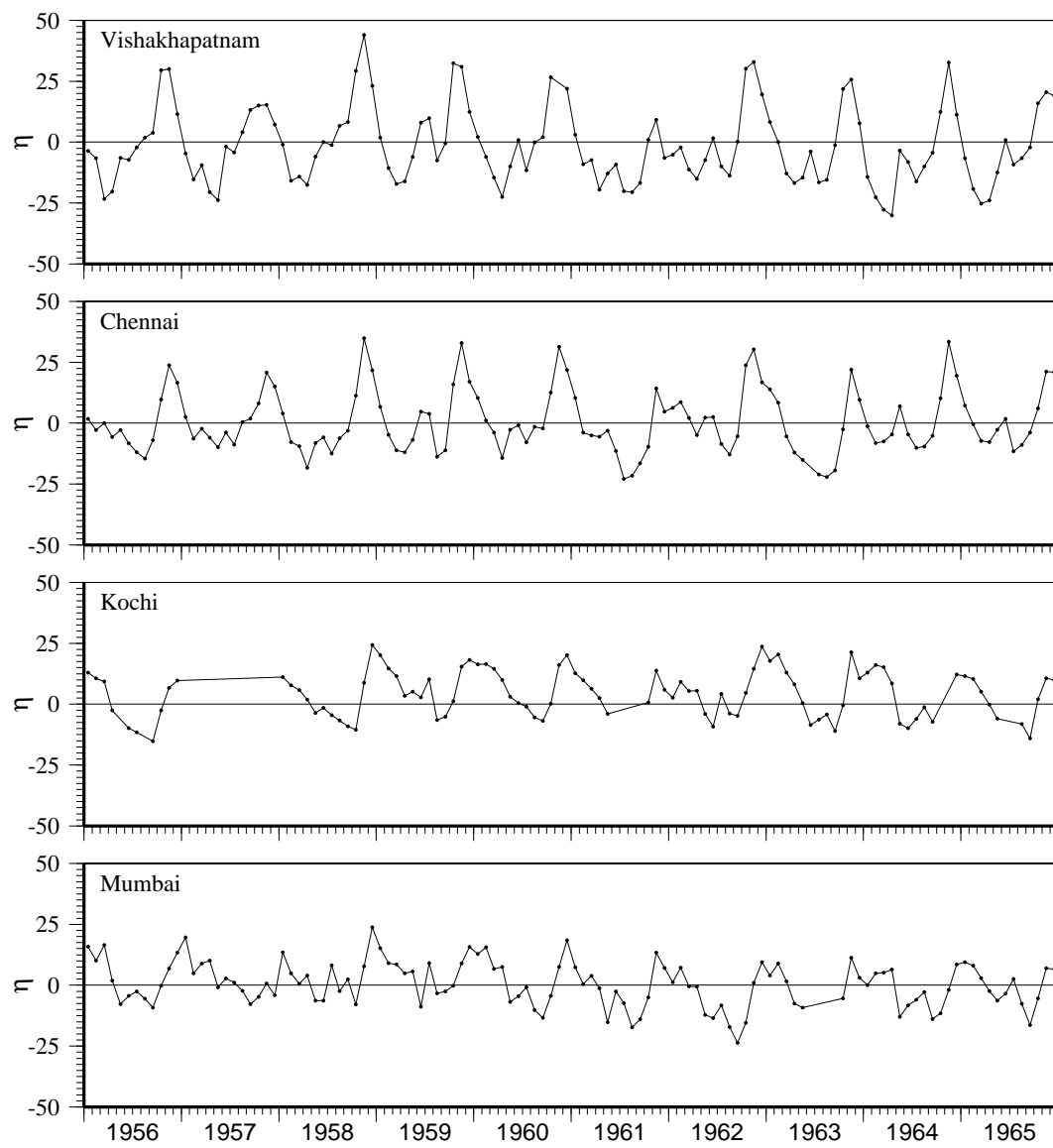
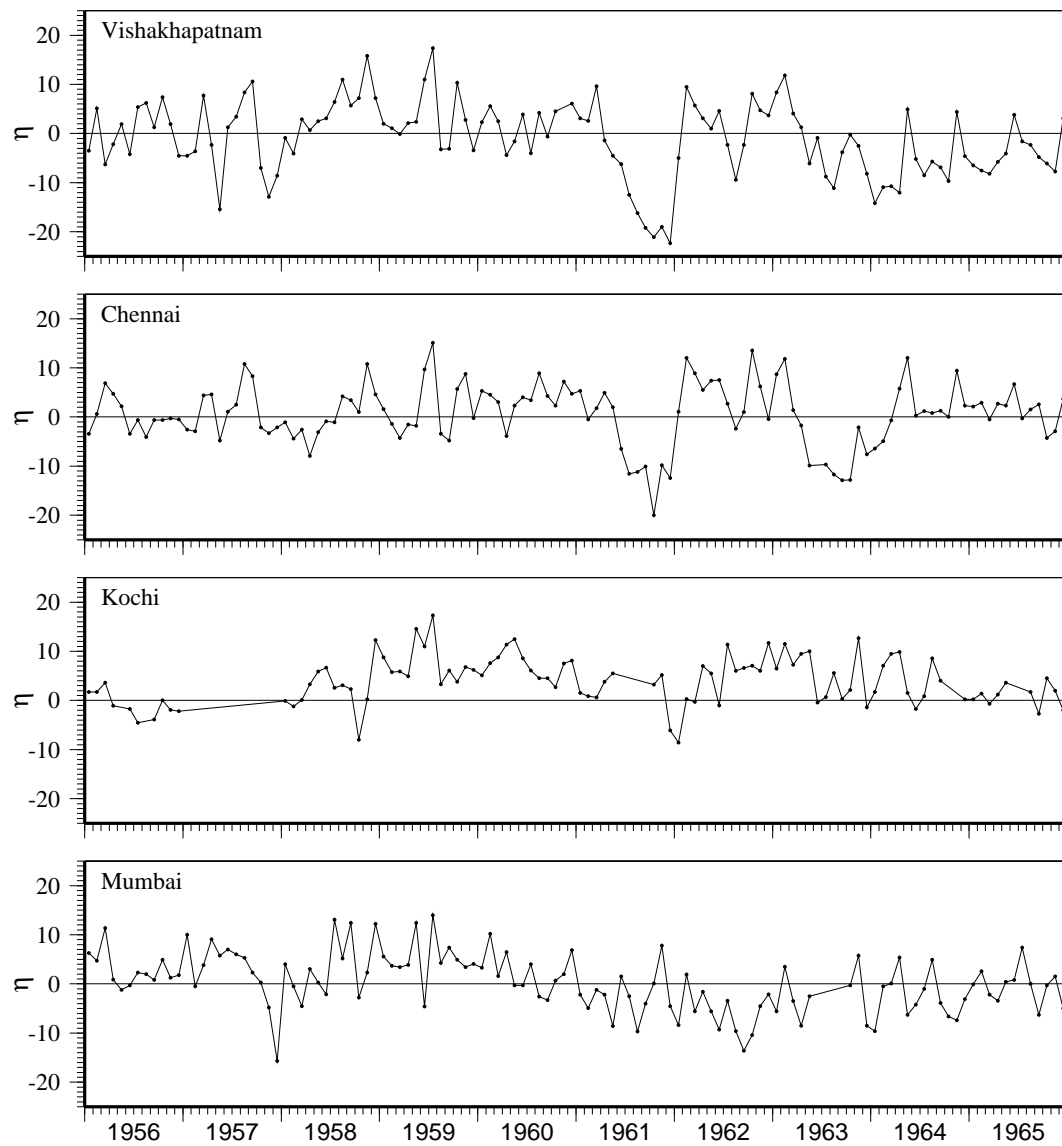


Figure 6.26 Deviation of corrected monthly sea level (cm) during 1956–1965 from the climatology of corrected monthly sea level. On the abscissa, the long and small ticks mark the beginning and end of the years and months, respectively. The monthly sea levels during July 1961 to June 1962 show a different behaviour in comparison to the sea level during the rest of the decade; the anomalous behaviour is maximum along the east coast, but is also seen at Kochi. At Mumbai, however, the anomalies are not striking. 1961 was a year of anomalous easterly winds over the equatorial Indian Ocean. The wind anomalies were similar to those seen during an El Niño, but 1961 was not an El-Niño year. Another possible cause of the anomalies is the lower rainfall in 1961 in the catchment areas of the Ganga and the Brahmaputra; though all-India and West-Coast rainfall were higher than normal, Ganga-Brahmaputra rainfall was lower than normal.



of salinity. The time scale associated with wind-forced changes, determined by the travel time of long baroclinic Kelvin and Rossby waves, is of the order of a few months for the Arabian Sea and the Bay of Bengal [McCreary et al., 1993; Clarke and Liu, 1994]. The effect of a change in salinity survives longer because of the longer time scale associated with the mixing of salt in the ocean; measured values of horizontal eddy diffusivities [Somayajulu et al., 1996] indicate a mixing time of about two years for a length scale of 100 km. Therefore, though monsoon rainfall itself is affected by the monsoon winds, the very low-frequency changes in sea level at Mumbai and elsewhere along the coast of India are mostly because of changes in the salinity of coastal waters caused by variability in monsoon rainfall. Apart from salinity and winds, sea level is affected by ocean temperature and atmospheric pressure; these, however, vary too little in the tropics on these time scales to cause changes of the observed magnitude.

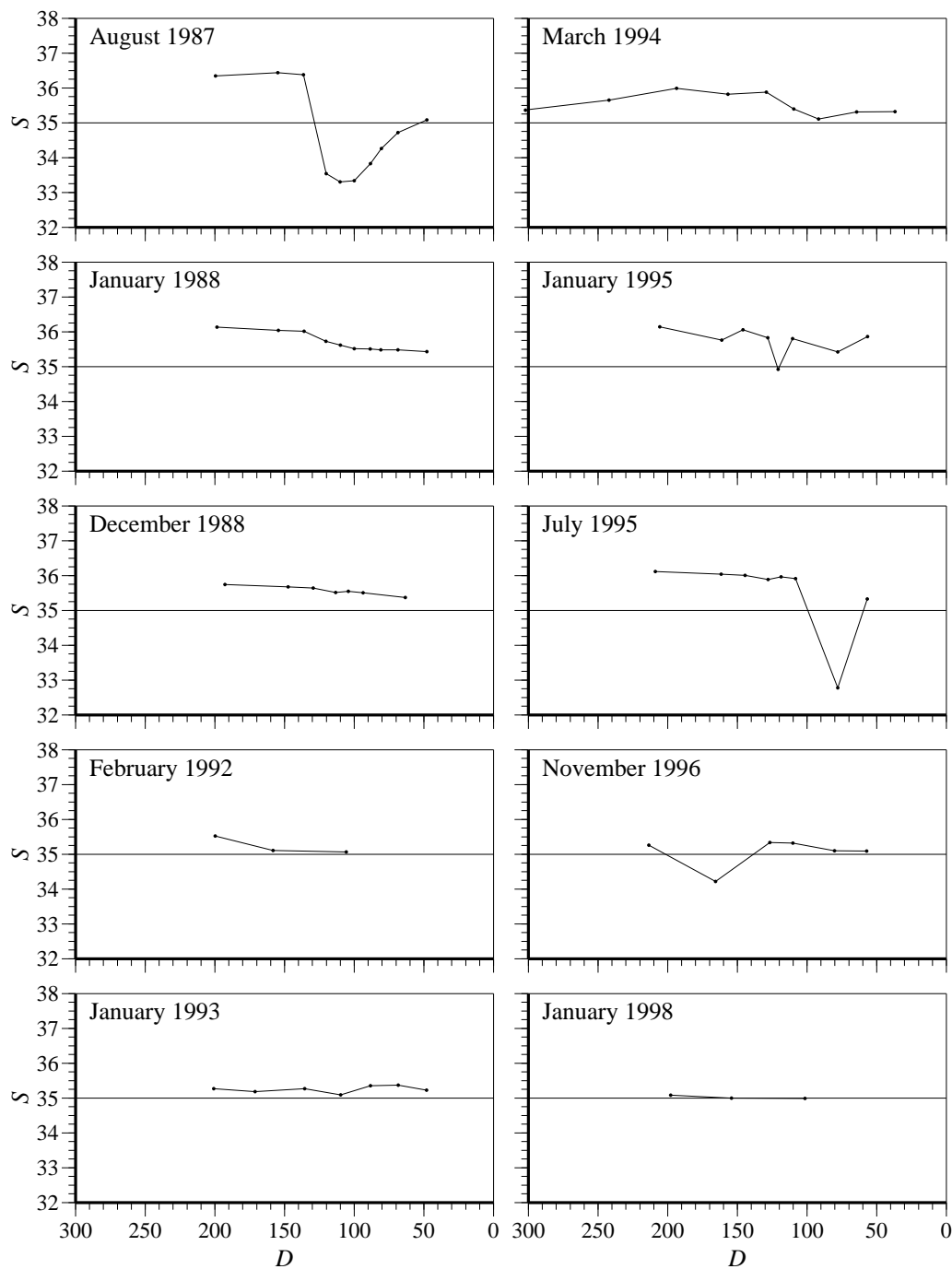
6.5 Implications of the Hypothesis

We have shown that the interdecadal variability of sea level along the coast of the Indian subcontinent is linked to the monsoon rainfall over the subcontinent, the coastal salinity field playing an intermediate role. The most striking feature of this mechanism is the connection between two vastly different time scales, the seasonal and the interdecadal. The bulk of the rainfall over the Indian subcontinent occurs during June–September, and the runoff is carried to the seas around India within a season. The equatorward EICC and the poleward WICC, which transport this low-salinity water along the Indian coast, are also seasonally varying currents. These seasonal phenomena act in concert with the low-frequency variability of monsoon rainfall and the slow mixing of salt in the oceans to force sea-level changes on interdecadal time scales.

A change in the salinity of coastal waters caused by variations in monsoon rainfall, and hence in river runoff, creates a cross-shore density gradient, to which the response is a two-layer, geostrophic circulation with a surface current and an undercurrent. Though this background circulation, on which the seasonal circulation is superimposed, is weak, the associated movements of the sea surface and the isopycnals are observable. When salinity decreases (increases) at an eastern ocean boundary like the Indian west coast, the current at the surface flows poleward (equatorward), there is an opposing undercurrent, sea level rises (falls) at the coast, and the pycnocline, or the interface between the undercurrent and the deeper ocean, slopes up (down) towards the coast. The interdecadal changes in sea level off the Indian coast are thus linked to the dynamics of local coastal currents and to the variability in the rainfall over the Indian subcontinent.

In developing this hypothesis, we were forced to correlate monsoon rainfall directly with sea level, bypassing salinity. This was unavoidable because there is a dearth of data on salinity in the north Indian Ocean. Moreover, the available data are sufficiently scattered in space to preclude

Figure 6.27 Surface salinity along a section normal to the west coast of India. Salinity S (PSU) is plotted as a function of distance D (km) from the coast. The section is off Marmagao, Goa (vertical cross-sections for three cruises along this section are presented in Figure 4.15).



the generation of a time series of salinity along the coast of India. Since the model requires that salinity along the west coast of India change by 1 PSU over a decade, and this is not a small change, a natural question is whether such changes in salinity occur along the coast of India. The only empirical evidence we have is from a hydrographic section normal to the coast off Marmagao in Goa. Hydrographic data for this section based on three cruises were presented in Figure 4.15; these data are for different seasons and two are from the late 1980s, which mark the end of an epoch of low rainfall and high frequency of droughts [Mishra and Gadgil, 1996]. Some cruises since then have added data, and surface salinity from 10 cruises along this section is plotted in Figure 6.27. Four of these sections are during January. There is a difference of about 1 PSU in the salinity, with a high in 1988 and 1995, and a low in 1993 and 1998. This lends credibility to the hypothesis.

This hypothesis, while linking interdecadal changes in sea level to those in the climate of the region, differs from those usually invoked in constructing scenarios of long-term changes in sea level. These hypotheses also link interdecadal sea-level variability to climate change [Gornitz et al., 1982; Wyrtki, 1990], but invoke the rise in temperature in the upper ocean and the melting of polar ice caps. It has been speculated, however, that global climate change is a complex process and will manifest differently in different regions; in the tropics, since ocean temperature is already high, it is expected to change evaporation, and hence, change atmospheric moisture, cloud cover, and rainfall [Wyrtki, 1990]. The rainfall and sea-level observations presented above highlight the complex relationship among the variables that define climate change. They do not, however, allow separation of natural, very low-frequency variability of monsoon rainfall and sea level from that caused by global warming due to anthropogenic effects.

Chapter 7

Summary and Discussion

We have described the variability of sea level along the coast of India on seasonal through inter-decadal time scales, mapping one end of the spectrum of sea-level variability, and have proposed hypotheses to explain the observations. There is significant variability at all these frequencies and the variability is coherent along the coast, which implies that its causes are not purely local; the low-frequency variability of sea level along the coast of India is linked to the large-scale processes in the north Indian Ocean.

In Chapter 3, we presented a theoretical framework for describing this large-scale circulation. Developed over the last decade, the framework invokes equatorial Kelvin and Rossby waves and coastal Kelvin waves, which merge the Bay of Bengal, the Arabian Sea, and the equatorial Indian Ocean into a single dynamical entity, the north Indian Ocean, whose dynamics must be modelled as a whole even to simulate the circulation in its parts. The framework was applied to the dynamics of the Lakshadweep high and low, a high and low in sea level that form off southwest India during the northeast and southwest monsoons, respectively, and propagate westward. Numerical and analytic experiments with a dynamical $1\frac{1}{2}$ -layer reduced-gravity model showed that the high and low are explicable by linear dynamics on an equatorial β -plane and do not owe their existence to nonlinearity: the high and low are the result of the radiation of westward propagating Rossby waves from Kelvin waves propagating poleward along the west coast of India. The Kelvin waves must have a period greater than about 50 days to radiate Rossby waves and force the high and low; at lower periods, they are trapped at the coast. The principal forcing mechanism of the high and low are the winds along the east coast of India and Sri Lanka. The winds along the west coast amplify the low, but not the high; other processes, including equatorial Rossby and Kelvin waves, amplify the high, but not the low. The winds along the coasts of India determine the circulation in the eastern and northern Arabian Sea, including the meandering structure of the Southwest Monsoon Current (SMC) in the Arabian Sea; elsewhere in the basin, other processes dominate.

Though the dynamical reduced-gravity model is successful in simulating the essential features

of the circulation in the north Indian Ocean, including the currents along the coast of India, it fails to simulate the seasonal cycle of coastal sea level, which was dealt with in Chapter 4. The seasonal cycle, corrected for the effect of atmospheric pressure using the Inverse-Barometer approximation, is coherent along the coast, with a range of 45 cm along the east coast and 30 cm along the west coast. Along the east coast, the maximum sea level occurs in November and the minimum during March–April; along the west coast, the maximum occurs in December and the minimum during the southwest monsoon. The wind-forced model fails to simulate the winter peak along the east coast, and as a result, forces a higher range of the seasonal cycle along the west coast than along the east coast. Simulations in which temperature and salinity vary in the active model layer, these fields being prescribed from a climatology, show that the drop in salinity along the east coast after the southwest monsoon raises steric sea level and is the cause of the maximum in November. This low salinity is the result of runoff from the Ganga and the Brahmaputra into the northern Bay of Bengal during the southwest monsoon. Thus, three mechanisms — atmospheric pressure, winds on the scale of the basin, and salinity — contribute to the seasonal cycle of sea level along the coast of India.

A lower frequency, the annual mean sea level, was the subject of Chapter 5. Levelling observations conducted during the Great Trigonometrical Survey of India (1858–1909) showed that the annual mean sea level is higher along the east coast of India than along the west, the difference between Vishakhapatnam and Mumbai being about 30 cm. Simulations with the $1\frac{1}{2}$ -layer reduced-gravity model show that purely wind-forced circulation accounts for half this difference, the other half being due to the gradient in salinity along the coast.

The variability of annual sea level on interannual and interdecadal time scales was dealt with in Chapter 6. Annual mean sea level along the coast is significantly correlated with the annual extrema and seasonal averages. Cross-correlations of annual mean sea level at the stations along the coast are statistically significant, showing that these changes are coherent and are part of a basin-scale response. The annual mean and extrema of sea level are also correlated with annual all-India rainfall, as is the local rainfall at Mumbai with the annual sea level there. These correlations retain their significance when the rainfall and sea-level data are decimated with a 10-year running mean. The interdecadal changes in monsoon rainfall are reflected in sea-level changes at Mumbai, which has the only century-long tide-gauge record in the Indian Ocean; both increase from a low in the first quarter of this century to a high in the 1950s and decrease thereafter.

Our hypothesis is that the seasonal inflow of the monsoon rainfall into the seas around India and the dynamics of the East and West India Coastal Currents (EICC and WICC) provide the link between monsoon rainfall and coastal sea level, the coastal salinity field playing an intermediate role. The seasonal EICC and WICC spread the runoff along the coast, creating a cross-shore gradient in salinity; the time scale associated with this gradient is much longer than a year because

mixing is slow in the ocean, which responds as a two-layer system to this quasi-steady cross-shore gradient in salinity. When salinity, and hence, density, decreases coastward in the upper layer, sea level rises at the coast, and this is accompanied by a weak, geostrophic, surface current that flows with the lighter water on its right; below it is an undercurrent. Geostrophy also requires that the pycnocline slope up towards the coast.

Thus, there are two main conclusions of this thesis.

1. There are three causes of the low-frequency variability of sea level along the coast of India.
 - (a) The large-scale wind-forced circulation of the upper ocean.
 - (b) The large changes in salinity that are a result of the high rainfall over the Indian sub-continent and the surrounding seas.
 - (c) Atmospheric pressure.

The first two causes are important at periods ranging from a season to decades; atmospheric pressure contributes significantly only to the seasonal cycle.

2. We propose a hypothesis connecting the interdecadal changes in sea level along the coast of India to the variability of the monsoon, the major aspect of the climate of the region. This hypothesis is different from those generally proposed to link sea level to climate change; these hypotheses invoke the increase in volume due to the change in temperature of the upper ocean and the addition of freshwater because of the melting of polar ice caps.

The hypothesis predicts that sea level rises (falls) along the coast of India when rainfall over India increases (decreases), changes in the ocean thereby reflecting those in the atmosphere. A corollary is that an increase (decrease) in rainfall leads to a rise (fall) of the pycnocline and thermocline, implying a decrease (increase) in the thickness of the surface mixed layer. One implication of this corollary is that coastal sea level is not a good proxy for the movement of the thermocline. The second implication is for ocean-atmosphere coupling. A solution similar to that obtained for the quasi-steady rise in sea level at a coast can be obtained for the interior ocean away from coastal boundaries, a westward propagating Rossby wave replacing the coastal Kelvin wave that is superimposed on the quasi-steady response. This implies that a similar decrease in the thickness of the mixed layer will occur even away from the coast if salinity changes there. This mechanism operates on long time scales and diffusion acts incessantly to increase the area of the region affected by the change in salinity. It is inevitable that the resulting low-frequency variability in the thickness of the mixed layer should have an effect on atmospheric processes.

This is especially true in the Bay of Bengal, where the changes in salinity are much larger than they are in the Arabian Sea. Changes in salinity in the interior of the bay need not be caused by diffusion alone; the Northeast Monsoon Current (NMC), which marks the dynamical boundary

between the equatorial Indian Ocean and the bay during the northeast monsoon, transports low-salinity water from the Andaman Sea, forcing changes in salinity in the middle of the basin. Since this process acts on advective time scales, like the seasonal redistribution of salt along the coast of India by the EICC and the WICC, an implication is that the effect of monsoon rainfall over India and Myanmar (Burma) will be felt within a season in the mixed layer over a large part of the bay.

The Bay of Bengal is believed to play a major role in the dynamics of the monsoon. The Tropical Convergence Zone (TCZ), which determines the large-scale monsoon rainfall, is maintained by the genesis of disturbances over the warm waters of the bay [Mishra and Gadgil, 1996]. Hence, any change in the structure of the mixed layer in the bay is likely to be fed back to the atmosphere. The details of this coupling between the ocean and the atmosphere are not clear, but it must be similar to the “barrier layer” in the western Pacific Ocean [Sprintall and Tomczak, 1992; Vialard and Delecluse, 1998a,b]. The major difference between the western Pacific and the Bay of Bengal is in the magnitude of changes in salinity; the changes in the bay are much larger. In the western Pacific, salinity modifies the thermodynamics of the mixed layer; in the bay, it probably controls the process.

The importance of salinity in the north Indian Ocean points to the need for more measurements, without which further theoretical studies will be difficult. The hypothesis linking monsoon rainfall and sea level along the coast of India relies on statistical and mechanistic models. We have assumed that the changes in monsoon rainfall lead to changes in salinity, producing the cross-shore salinity gradient that forces changes in sea level. How is this cross-shore salinity gradient set up? What is the source of the low-salinity water along the west coast of India? How important is the local rainfall over the west coast in relation to the inflow of freshwater from the bay? To answer these questions, we have to go beyond mechanistic models and try to model the salt balance, given the fluxes and the river runoff; this in turn, calls for better data on runoff and salinity in the north Indian Ocean in general, and along the coast of India in particular.

Appendix A

The Reduced-Gravity Model

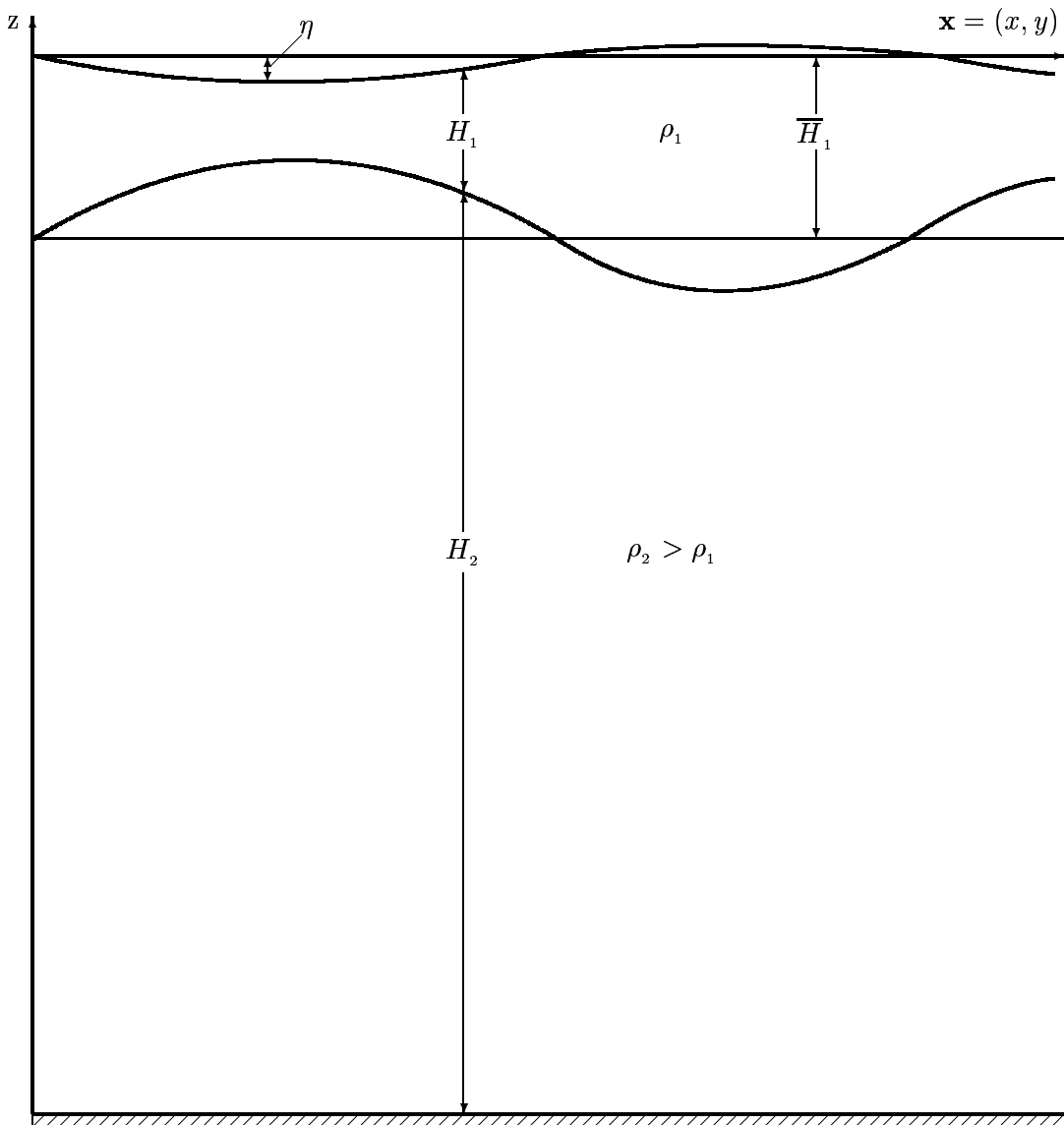
Since our aim in this thesis is to formulate a hypothesis to explain the observed low-frequency variability of sea level along the Indian coast, we simplify the problem to the extent possible, making use of models that are malleable enough to permit simple numerical experiments and, at times, yield analytic solutions. The simplest realistic model of the low-frequency surface circulation of the ocean is the $1\frac{1}{2}$ -layer reduced-gravity model, in which the ocean is a two-layer system, the denser lower layer being much deeper than the relatively shallow upper layer. The assumption that the pressure gradient in the lower layer is vanishingly small makes it motionless (isostatic) and eliminates the fast-moving barotropic mode; only the first baroclinic mode is retained in this model. This is akin to the assumption of a “level of no motion” in computing dynamic heights from hydrographic data. Therefore, the height of the model surface, computed with reference to the motionless layer, is equivalent to the dynamic height, and is the model equivalent of sea level.

Extension of the model to include higher baroclinic modes is simple; an additional active layer results in a $2\frac{1}{2}$ -layer model, and so on. The $\frac{1}{2}$ represents the lowest, motionless model layer. The simplicity and ruggedness of these models makes them malleable; as a result, they are among the most used tools in oceanography. Reduced-gravity models have enjoyed tremendous success in oceanography and have played a major role in the study of El Niño. In the rest of this chapter, we derive the equations for the $1\frac{1}{2}$ and $2\frac{1}{2}$ -layer models and manipulate them to obtain the simpler equations solved in this thesis.

A.1 The $1\frac{1}{2}$ -Layer Model

A schematic vertical cross-section of the $1\frac{1}{2}$ -layer model is shown in Figure A.1. The model ocean has a flat bottom and consists of two incompressible layers, the lower layer being denser

Figure A.1 A schematic vertical cross-section of the $1\frac{1}{2}$ -layer reduced-gravity model. The model ocean has a flat bottom and consists of two incompressible layers, the denser lower layer being much deeper than the relatively shallow upper layer. In the reduced-gravity models used in this thesis, there is no mixing between the layers. In the figure, the subscripts 1 and 2 refer to the two layers. \bar{H}_1 is the mean, or initial thickness of the upper layer, H_i and ρ_i are the instantaneous thickness and density of layer i , and η is the displacement of the surface from the initial, or undisturbed, state. η , the model sea level, is equivalent to the dynamic height computed from hydrographic data. The interface between the layers is the model pycnocline. H_1 , ρ_1 , and η are functions of space and time; ρ_2 is constant.



than the upper layer. Each layer is a material layer, i.e., there is no mixing between the layers¹, and is homogeneous in the vertical (in velocity, temperature, and salinity). The interface between the layers represents the model pycnocline, which, in this model, coincides with the thermocline and the halocline. Thermohaline effects are included by permitting horizontal gradients in temperature and salinity in the active layer, but vertical fluxes of heat and salt across the surface, the interface, and the bottom are neglected.

A.1.1 The Nonlinear Model

We begin with the basic conservation equations for zonal, meridional, and vertical momentum, mass, heat, and salt on an equatorial β -plane; for an incompressible fluid, these are given by [Pedlosky, 1979; Gill, 1982]

$$\frac{du}{dt} - fv = -\frac{1}{\rho} \frac{\partial p}{\partial x} + \frac{1}{\rho} \frac{\partial \tau^x}{\partial z} + A' \nabla^2 u, \quad (\text{A.1a})$$

$$\frac{dv}{dt} + fu = -\frac{1}{\rho} \frac{\partial p}{\partial y} + \frac{1}{\rho} \frac{\partial \tau^y}{\partial z} + A' \nabla^2 v, \quad (\text{A.1b})$$

$$\frac{\partial p}{\partial z} = -\rho g, \quad (\text{A.1c})$$

$$\frac{\partial u}{\partial x} + \frac{\partial v}{\partial y} + \frac{\partial w}{\partial z} = 0, \quad (\text{A.1d})$$

$$\frac{dT}{dt} = A'_T \nabla^2 T + Q_T, \quad (\text{A.1e})$$

$$\frac{dS}{dt} = A'_S \nabla^2 S + Q_S, \quad (\text{A.1f})$$

$$\rho = \rho_0 [1 + \alpha_T (T - T_0) + \alpha_s (S - S_0)]. \quad (\text{A.1g})$$

In (A.1), $\mathbf{v} = (u, v)$ is the horizontal velocity, w the vertical velocity, p the pressure, T the temperature, S the salinity, ρ the density, $\tau = (\tau^x, \tau^y)$ the horizontal shear stress, Q_T and Q_S the sources and sinks of heat and salt, $f = \beta y$ the Coriolis parameter, A' the horizontal eddy viscosity coefficient,

¹This assumption is not necessary. There are many reduced-gravity models that incorporate entrainment and deentrainment, mixed-layer physics, surface fluxes, etc.; among them is the model of McCreary et al. [1993].

A'_T and A'_S the horizontal eddy diffusivity coefficients for heat and salt, α_T and α_S the expansion coefficients, ρ_0 , T_0 , and S_0 determine a reference state about which the system is perturbed, and

$$\frac{d}{dt} = \frac{\partial}{\partial t} + u \frac{\partial}{\partial x} \mathbf{i} + v \frac{\partial}{\partial y} \mathbf{j},$$

where \mathbf{i} and \mathbf{j} are the unit vectors in the zonal and meridional directions. The vertical momentum equation (A.1c) reduces to the hydrostatic equation because we are interested in large-scale flows. Equations (A.1) are integrated in the vertical over the depth of the layer, from $-(H_1 - \eta)$ to η , to obtain the required depth-averaged equations for the active layer.

The pressure at a depth z in the two layers is given by

$$p_1 = p_{\text{atm}} + \rho_1 g (-z + \eta), \quad (\text{A.2a})$$

$$p_2 = p_{\text{atm}} + \rho_1 g H_1 + \rho_2 g [-z - (H_1 - \eta)], \quad (\text{A.2b})$$

where p_{atm} is the atmospheric pressure, whose horizontal variations are ignored. The assumption that the pressure gradient vanishes in the lower layer, i.e., $\nabla p_2 = 0$, then implies that

$$\nabla \eta = \nabla (\Gamma H_1). \quad (\text{A.3})$$

$$\Gamma = \frac{\rho_2 - \rho_1}{\bar{\rho}} \quad (\text{A.4})$$

is the reduced-gravity parameter, $g\Gamma$ is the “reduced gravity”, and $\bar{\rho}$ is an average density that is representative of the ocean (this is equivalent to the Boussinesq approximation). This factor Γ reduces the speed of the internal, or interfacial, wave in the model because it multiplies g . Averaging the pressure gradient term over the layer gives

$$\begin{aligned} \overline{H_1 \frac{1}{\rho_1} \nabla p_1} &= g H_1 \nabla (\Gamma H_1) + \frac{g H_1^2}{2\bar{\rho}} \nabla \rho_1 \\ &= g H_1 \nabla (\Gamma H_1) - \frac{g H_1^2}{2} \nabla \Gamma \\ &= g \Gamma H_1 \nabla H_1 + \frac{g H_1^2}{2} \nabla \Gamma. \end{aligned} \quad (\text{A.5})$$

$\overline{H_1 \frac{1}{\rho_1} \nabla p_1}$ represents a vertical average of the horizontal pressure gradient over the layer.

Using

$$w|_{\eta} = \frac{d\eta}{dt}; \quad w|_{-(H_1 - \eta)} = \frac{d\eta}{dt} - \frac{dH_1}{dt}$$

and assuming that Laplacian friction acts on a column of fluid the way it does on a fluid parcel, we obtain the required governing equations. In vector form, they are

$$\frac{(\partial H_1 \mathbf{v})}{\partial t} + \nabla \cdot (\mathbf{v} H_1 \mathbf{v}) + f \mathbf{k} \times (H_1 \mathbf{v}) = -H_1 \overline{\frac{1}{\rho_1} \nabla p_1} + \frac{\tau}{\bar{\rho}} + A \nabla^2 (H_1 \mathbf{v}) - r(H_1 \mathbf{v}), \quad (\text{A.6a})$$

$$\frac{\partial H_1}{\partial t} = -\nabla \cdot (H_1 \mathbf{v}), \quad (\text{A.6b})$$

$$\frac{\partial \Gamma}{\partial t} = \mathbf{v} \cdot \nabla \Gamma + A_\gamma \nabla^2 \Gamma + Q, \quad (\text{A.6c})$$

where \mathbf{k} is the unit vector in the vertical and $\overline{\frac{1}{\rho_1} \nabla p_1}$ is given by (A.5). Q combines the sources and sinks of heat and salt into a source-cum-sink term for Γ , and $\tau = (\tau^x, \tau^y)$ now represents the wind stress acting at the surface. The bottom friction, or the friction between the two layers, is set to zero. Instead, a friction term, $r(H_1 \mathbf{v})$, is introduced; it is used to define dampers near open boundaries in numerical simulations. Often called Rayleigh friction when linearized, it is also used to add friction to analytic models. It may be thought of as “bottom friction”, but is not necessarily that. (A.6c) combines the equations for conservation of heat and salt. This is done because we do not solve the equations for temperature and salinity in this thesis; we do, however, need this equation because temperature and salinity can vary in the horizontal within the active layer.

From (A.3), the surface dynamic height, or model sea level, is

$$\eta = \overline{\Gamma} h + \overline{H} \gamma, \quad (\text{A.7})$$

the constant of integration being set to zero.

The pressure gradient, given by (A.5), has one depth-dependent term. $g \nabla (\Gamma H_1) = g \nabla \eta$ is the barotropic component and $\frac{g H_1}{2 \rho} \nabla \rho_1$ is the baroclinic component. Despite this, the velocity field is independent of depth and the wind stress projects as a body force on the upper layer; this is based on the assumption that the Reynolds stresses $\overline{u' w'}$ and $\overline{v' w'}$ have a vertical structure such that their depth-dependent part cancels that of the pressure gradient. A necessary condition for this cancellation is that the depth-dependent part of the pressure gradient is its average value in the layer, evaluated by substituting $z = \frac{H_1}{2}$ in the baroclinic term² [McCreary and Kundu, 1988].

Equations (A.6), with $\Gamma = \overline{\Gamma}$, a constant, and $r = \chi_s$, are solved in Section 3.3; this is a dynamical $1\frac{1}{2}$ -layer reduced-gravity model, the only dependent variables being u , v , and H_1 .

²For a detailed discussion on the consequences of this assumption, see Ripa [1992, 1995].

A.1.2 The Linearized Model

Equations (A.6) are linearized by perturbing the system about a basic state of no motion with thickness \bar{H} and “density” $\bar{\Gamma}$ in the upper layer. Let the perturbations in H and Γ be h and γ , respectively, i.e.,

$$H = \bar{H} + h, \quad (\text{A.8a})$$

$$\Gamma = \bar{\Gamma} + \gamma. \quad (\text{A.8b})$$

To linearize, we scale the variables, expand them in powers of an infinitesimal, ϵ , and collect terms of the same order in ϵ ; this yields the required linearized, perturbation equations. We first rewrite the momentum equation for transport, (A.6a), in terms of velocity, i.e., we use (A.6b) to eliminate the factor H_1 . (The only term that does not yield directly to this simplification is the Laplacian friction because it was an *ad hoc* change that allowed us to write the friction term for the transport.) The equation becomes

$$\frac{\partial \mathbf{v}}{\partial t} + \mathbf{v} \cdot \nabla \mathbf{v} + f \mathbf{k} \times \mathbf{v} = -\frac{1}{\rho_1} \nabla p_1 + \frac{\tau}{\bar{\rho} H_1} + A \nabla^2 \mathbf{v} - r \mathbf{v}. \quad (\text{A.9})$$

The variables are scaled as follows.

$$(t, x, y, u, v, Q, \tau, \eta) = (T t', \mathcal{L} x', \mathcal{L} y', \mathcal{U} u', \mathcal{U} v', Q q', \mathcal{F} \tau', \mathcal{H} \eta'), \quad (\text{A.10a})$$

$$H = \bar{H} (1 + \delta^h h'); \quad \Gamma = \bar{\Gamma} (1 + \delta^\gamma \gamma). \quad (\text{A.10b})$$

Then, with the scalings

$$\frac{1}{\beta \mathcal{L} T} = \frac{r}{\beta \mathcal{L}} = \frac{A_\gamma}{A} = \frac{\mathcal{F}}{\beta \mathcal{L} \mathcal{U}} = 1, \quad (\text{A.11a})$$

$$\frac{U}{\beta \mathcal{L}^2} = \left(\frac{U}{g \bar{\Gamma} \bar{H}} \right)^{\frac{1}{2}} = \frac{Q}{\beta \mathcal{L} \bar{\Gamma}} = \frac{\mathcal{H}}{\bar{H}} = \delta^h = \delta^\gamma = \epsilon, \quad (\text{A.11b})$$

$$\frac{A}{\beta \mathcal{L}^3} = \epsilon^2, \quad (\text{A.11c})$$

where $\epsilon \ll 1$ and $f = \beta y$, and with the expansion

$$\theta = \theta_0 + \epsilon \theta_1 + \epsilon^2 \theta_2 + \dots, \quad (\text{A.12})$$

where θ is any of the variables u , v , h , γ , τ , η , or q , we obtain the following zeroth-order perturbation equations.

$$\frac{\partial u_0}{\partial t} - \beta y v_0 = -g \bar{\Gamma} \frac{\partial h_0}{\partial x} - \frac{g \bar{H}}{2} \frac{\partial \gamma_0}{\partial x} + \frac{\tau_0^x}{\bar{\rho} \bar{H}} - r u_0; \quad (\text{A.13a})$$

$$\frac{\partial v_0}{\partial t} + \beta y u_0 = -g \bar{\Gamma} \frac{\partial h_0}{\partial y} - \frac{g \bar{H}}{2} \frac{\partial \gamma_0}{\partial y} + \frac{\tau_0^y}{\bar{\rho} \bar{H}} - r v_0; \quad (\text{A.13b})$$

$$\frac{\partial h_0}{\partial t} = -\bar{H} \left(\frac{\partial u_0}{\partial x} + \frac{\partial v_0}{\partial y} \right); \quad (\text{A.13c})$$

$$\frac{\partial \gamma_0}{\partial t} = Q_0, \quad (\text{A.13d})$$

$$\eta_0 = \bar{\Gamma} h_0 + \bar{H} \gamma_0. \quad (\text{A.13e})$$

In (A.13d), $Q_0 = Q q_0$. The subscript “0” indicates that these are the zeroth-order terms in the expansion (A.12).

Equations (A.13), with $\gamma_0 = 0$, are the linear equations solved in Chapter 3. The Laplacian friction terms, however, are retained in the linear numerical simulations to avoid numerical instabilities.

In the analytic model, we seek wave solutions of the form $\theta_0 \propto e^{i\omega t}$; writing

$$i\omega = \frac{\partial}{\partial t} + r = i\sigma + r \quad (\text{A.14})$$

and dropping the wind stress yields the free wave equations (3.3) for the equatorial β -plane.

For a coastal Kelvin wave propagating along a meridional boundary, $u_0 = 0$. The resulting equations are solved in Section 6.4.1 on an f -plane ($f = f_0$, where f_0 is a constant).

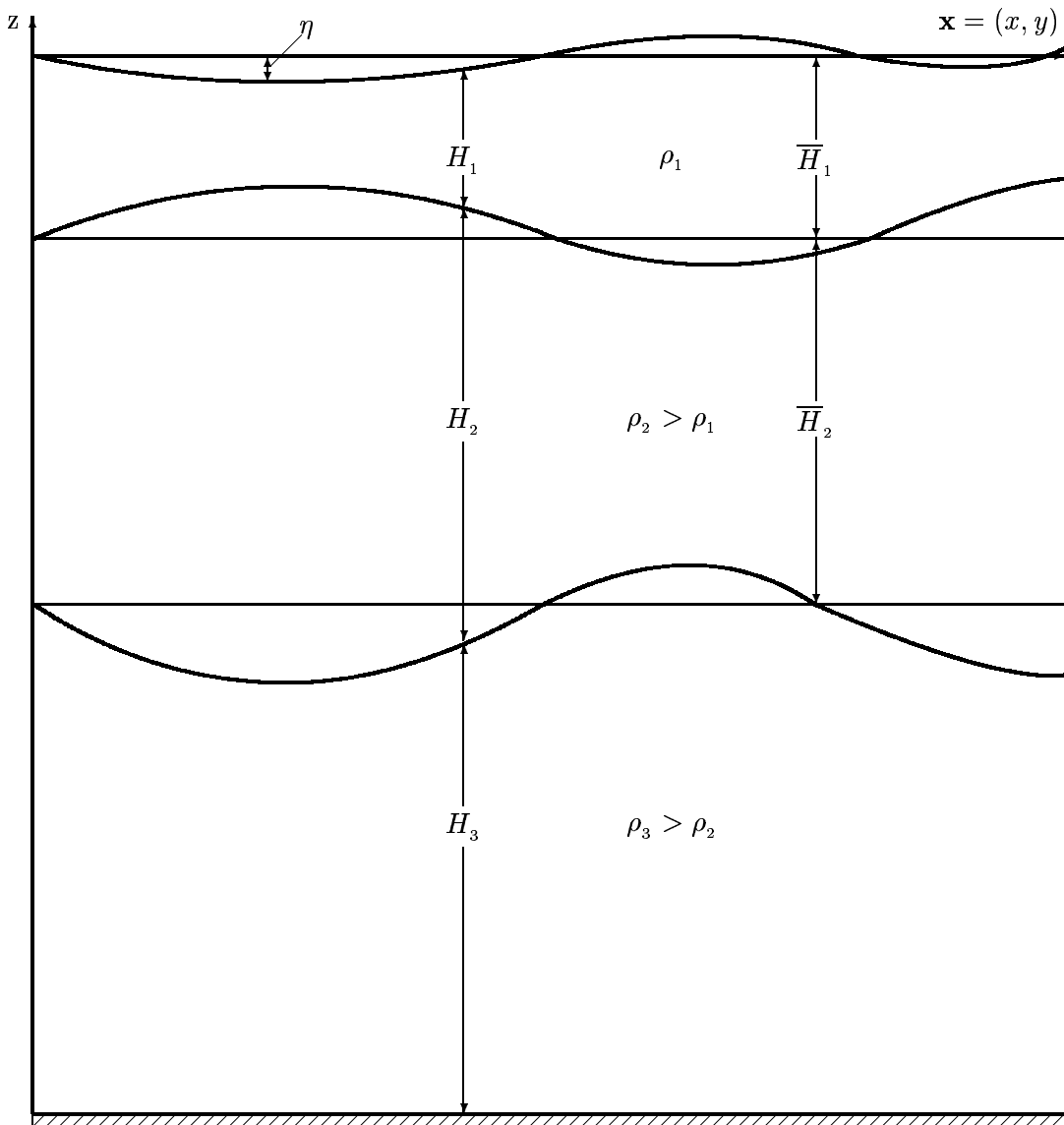
A.2 The $2\frac{1}{2}$ -Layer Model

A $2\frac{1}{2}$ -layer model has two active layers; the third layer is much deeper than these and is motionless (Figure A.2). The equations are similar to those for the $1\frac{1}{2}$ -layer model, except for changes in the pressure gradient terms for the layers. The wind stress projects as a body force on the first layer and the second layer is driven by the resulting changes in the pressure field.

As for the $1\frac{1}{2}$ -layer model, the conservation equations are averaged over the depth of each layer; the limits of integration are $-(H_1 - \eta)$ and η for the first layer and $-(H_1 + H_2 - \eta)$ and $-(H_1 - \eta)$ for the second layer. The pressure at a depth z in the three layers is given by

$$p_1 = p_{\text{atm}} + \rho_1 g (-z + \eta), \quad (\text{A.15a})$$

Figure A.2 A schematic vertical cross-section of the $2\frac{1}{2}$ -layer reduced-gravity model. The model ocean has a flat bottom and consists of three incompressible layers, the lowest layer being much deeper than the relatively shallow layers above. There is no mixing between the layers. In the figure, the subscripts 1, 2, and 3 refer to the three layers. \bar{H}_1 and \bar{H}_2 are the mean, or initial thicknesses, of the top two layers, H_i and ρ_i are the instantaneous thickness and density of layer i , and η is the displacement of the surface from the initial, or undisturbed, state. η , the model sea level, is equivalent to the dynamic height computed from hydrographic data. The interface between the second and third layers is the model pycnocline. H_1 , H_2 , ρ_1 , ρ_2 , and η are functions of space and time; ρ_3 is constant.



$$p_2 = p_{\text{atm}} + \rho_1 g H_1 + \rho_2 g [-z - (H_1 - \eta)], \quad (\text{A.15b})$$

$$p_3 = p_{\text{atm}} + \rho_1 g H_1 + \rho_2 g H_2 + \rho_3 g [-z - (H_1 + H_2 - \eta)], \quad (\text{A.15c})$$

where p_{atm} is the atmospheric pressure, whose horizontal variations are neglected. The assumption that the pressure gradient vanishes in the lowest layer, i.e., $\nabla p_3 = 0$, then implies that

$$\nabla \eta = \nabla (\Gamma_1 H_1 + \Gamma_2 H_2). \quad (\text{A.16})$$

$$\Gamma_1 = \frac{\rho_3 - \rho_1}{\bar{\rho}} \quad \text{and} \quad \Gamma_2 = \frac{\rho_3 - \rho_2}{\bar{\rho}} \quad (\text{A.17})$$

are the “reduced-gravity” parameters for the two layers, and $\bar{\rho}$, as before, is an average density that is representative of the ocean. Averaging the pressure gradient term over each layer gives

$$\begin{aligned} H_1 \overline{\frac{1}{\rho_1} \nabla p_1} &= g H_1 \nabla (\Gamma_1 H_1 + \Gamma_2 H_2) + \frac{g H_1^2}{2 \bar{\rho}} \nabla \rho_1 \\ &= g H_1 \nabla (\Gamma_1 H_1 + \Gamma_2 H_2) - \frac{g H_1^2}{2} \nabla \Gamma_1 \\ &= g H_1 \left(\Gamma_1 \nabla H_1 + \Gamma_2 \nabla H_2 + \frac{H_1}{2} \nabla \Gamma_1 + H_2 \nabla \Gamma_2 \right), \end{aligned} \quad (\text{A.18a})$$

$$\begin{aligned} H_2 \overline{\frac{1}{\rho_2} \nabla p_2} &= g H_2 \nabla [\Gamma_2 (H_1 + H_2)] + \frac{g H_2}{\bar{\rho}} \left(H_1 + \frac{H_2}{2} \right) \nabla \rho_2 \\ &= g H_2 \nabla [\Gamma_2 (H_1 + H_2)] - g H_2 \left(H_1 + \frac{H_2}{2} \right) \nabla \Gamma_2 \\ &= g H_2 \left(\Gamma_2 \nabla H_1 + \Gamma_2 \nabla H_2 + \frac{H_2}{2} \nabla \Gamma_2 \right). \end{aligned} \quad (\text{A.18b})$$

$\overline{\frac{1}{\rho_1} \nabla p_1}$ and $\overline{\frac{1}{\rho_2} \nabla p_2}$ represent a vertical average of the horizontal pressure gradient over the layers.

The required governing equations for the $2\frac{1}{2}$ -layer model, solved numerically in Chapter 4, are

$$\frac{(\partial H_i \mathbf{v}_i)}{\partial t} + \nabla \cdot (\mathbf{v}_i H_i \mathbf{v}_i) + f \mathbf{k} \times (H_i \mathbf{v}_i) = -H_i \overline{\frac{1}{\rho_i} \nabla p_i} + \delta_i \frac{\tau}{\bar{\rho}} + A \nabla^2 (H_i \mathbf{v}_i) - r (H_i \mathbf{v}_i), \quad (\text{A.19a})$$

$$\frac{\partial H_i}{\partial t} = -\nabla \cdot (H_i \mathbf{v}), \quad (\text{A.19b})$$

$$\frac{\partial \Gamma_i}{\partial t} = \mathbf{v}_i \cdot \nabla \Gamma_i + A_\gamma \nabla^2 \Gamma_i + Q_i, \quad (\text{A.19c})$$

where the subscript $i = 1, 2$ refers to layer i and

$$\delta_i = \begin{cases} 1 & \text{if } i = 1, \\ 0 & \text{if } i = 2. \end{cases}$$

Linearization of (A.19) is done as for the $1\frac{1}{2}$ -layer model. The zeroth-order linearized perturbation equations for the $2\frac{1}{2}$ -layer model, equivalent to (A.13) for the $1\frac{1}{2}$ -layer model, are as follows.

$$\frac{\partial u_1}{\partial t} - \beta y v_1 = -g \bar{\Gamma}_1 \frac{\partial h_1}{\partial x} - g \bar{\Gamma}_2 \frac{\partial h_2}{\partial x} - \frac{g \bar{H}_1}{2} \frac{\partial \gamma_1}{\partial x} - g \bar{H}_2 \frac{\partial \gamma_2}{\partial x} + \frac{\tau^x}{\bar{\rho} \bar{H}_1} - r u_1, \quad (\text{A.20a})$$

$$\frac{\partial v_1}{\partial t} + \beta y u_1 = -g \bar{\Gamma}_1 \frac{\partial h_1}{\partial y} - g \bar{\Gamma}_2 \frac{\partial h_2}{\partial y} - \frac{g \bar{H}_1}{2} \frac{\partial \gamma_1}{\partial y} - g \bar{H}_2 \frac{\partial \gamma_2}{\partial y} + \frac{\tau^y}{\bar{\rho} \bar{H}_1} - r v_1, \quad (\text{A.20b})$$

$$\frac{\partial h_1}{\partial t} = -\bar{H}_1 \left(\frac{\partial u_1}{\partial x} + \frac{\partial v_1}{\partial y} \right), \quad (\text{A.20c})$$

$$\frac{\partial \gamma_1}{\partial t} = Q_1 \quad (\text{A.20d})$$

are the equations for the first layer and

$$\frac{\partial u_2}{\partial t} - \beta y v_2 = -g \bar{\Gamma}_2 \frac{\partial (h_1 + h_2)}{\partial x} - \frac{g \bar{H}_2}{2} \frac{\partial \gamma_2}{\partial x} - r u_2, \quad (\text{A.21a})$$

$$\frac{\partial v_2}{\partial t} + \beta y u_2 = -g \bar{\Gamma}_2 \frac{\partial (h_1 + h_2)}{\partial y} - \frac{g \bar{H}_2}{2} \frac{\partial \gamma_2}{\partial y} - r v_2, \quad (\text{A.21b})$$

$$\frac{\partial h_2}{\partial t} = -\bar{H}_2 \left(\frac{\partial u_2}{\partial x} + \frac{\partial v_2}{\partial y} \right), \quad (\text{A.21c})$$

$$\frac{\partial \gamma_2}{\partial t} = Q_2 \quad (\text{A.21d})$$

are the equations for the second layer. In (A.20) and (A.21), we have dropped the subscript “0” for convenience.

The surface dynamic height, or model sea level, is given by

$$\eta = \bar{\Gamma}_1 h_1 + \bar{\Gamma}_2 h_2 + \bar{H}_1 \gamma_1 + \bar{H}_2 \gamma_2, \quad (\text{A.22})$$

where

$$H_1 = \bar{H}_1 + h_1, \quad H_2 = \bar{H}_2 + h_2, \quad (\text{A.23a})$$

$$\Gamma_1 = \bar{\Gamma}_1 + \gamma_1, \quad \Gamma_2 = \bar{\Gamma}_2 + \gamma_2. \quad (\text{A.23b})$$

\bar{H}_1 , \bar{H}_2 , $\bar{\Gamma}_1$, and $\bar{\Gamma}_2$ define the basic state about which the system is perturbed.

Equations (A.20) and (A.21), with the definition (A.14) and $\tau^x = \tau^y = 0$, are solved in Section 6.4.2 for a coastal Kelvin wave on an *f*-plane.

Appendix B

Linear Waves on an Equatorial β -Plane

Theoretical studies of the dynamics of the north Indian Ocean during the last decade have used free and forced long baroclinic waves to describe the circulation in the basin. For the description of low-frequency dynamics, the most important of these waves are the equatorially-trapped Rossby and Kelvin waves and coastally-trapped Kelvin waves, all of which can exist in a reduced-gravity model at the low frequencies of interest. Here, we discuss the characteristics of these waves in brief; the discussion essentially follows Gill [1982] and Shetye [1998].

B.1 Waves Trapped at the Equator

The properties of the equatorially-trapped waves may be found by looking for solutions proportional to $e^{i(kx-\sigma t)}$. When this expression is used in the linearized equations (3.3), the resulting dispersion relation is [Gill, 1982, p. 438]

$$\left(\frac{\sigma}{c}\right)^2 - k^2 - \frac{\beta k}{\sigma} = (2n+1)\frac{\beta}{c}, \quad (\text{B.1})$$

where c is the baroclinic wave speed, σ the frequency, and k the zonal wavenumber. For $n \geq 1$, the waves subdivide into two classes [Gill, 1982]. For the upper branches, $\frac{\beta k}{\sigma}$ is small, and an approximate dispersion relation is

$$\sigma^2 \approx (2n+1)\beta c + k^2 c^2; \quad (\text{B.2})$$

these are the Poincaré waves. For the lower branches, $\frac{\sigma^2}{c^2}$ is small, and an approximate dispersion relation is

$$\sigma \approx \frac{-\beta k}{k^2 + (2n+1)\frac{\beta}{c}}; \quad (\text{B.3})$$

these are the Rossby waves. $n = -1$ yields the Kelvin wave and $n = 0$ yields the Yanai, or mixed planetary-gravity, wave. All these dispersion curves are shown in Figure B.1. Since there is a large gap between the minimum Poincaré wave frequency and the maximum Rossby wave frequency, it is easy to distinguish between them; only the Kelvin and Yanai waves exist in this frequency gap. All these waves are trapped near the equator, and the trapping scale R_{eq} , called the “equatorial radius of deformation” [Gill and Clarke, 1974; Gill, 1982], is of the same order for them.

$$R_{\text{eq}} = \left(\frac{c}{2\beta} \right)^{\frac{1}{2}}. \quad (\text{B.4})$$

For $c = 185 \text{ cm s}^{-1}$, the speed of the baroclinic wave in the linear models used in this thesis, $R_{\text{eq}} \approx 200 \text{ km}$.

At the low frequencies of interest in this thesis, Poincaré waves do not exist and the only equatorially-trapped waves of consequence are the Kelvin and Rossby waves; at these frequencies, the Yanai waves have very short wavelengths and are quickly dissipated.

B.1.1 Equatorially-Trapped Kelvin Waves

The phase and group velocities (c) of these non-dispersive waves is eastward. The particle velocity associated with the waves is along the equator ($v = 0$) and can be eastward or westward. The equatorial Kelvin waves exist within the equatorial waveguide, which extends about 200 km on either side of the equator.

B.1.2 Equatorially-Trapped Rossby Waves

The equatorially-trapped Rossby waves can have both eastward and westward group velocity, though their phase velocity is always westward. The eastward propagating waves, however, have a short wavelength (Figure B.1) and are dissipated quickly. Therefore, they are not important for large-scale dynamics, except in the neighbourhood of a western ocean boundary. The phase speed of the non-dispersive westward propagating Rossby wave is approximately one-third that of the equatorial Kelvin wave. The particle velocity associated with this wave can have both zonal and meridional components. Away from the equator, a local dispersion relation

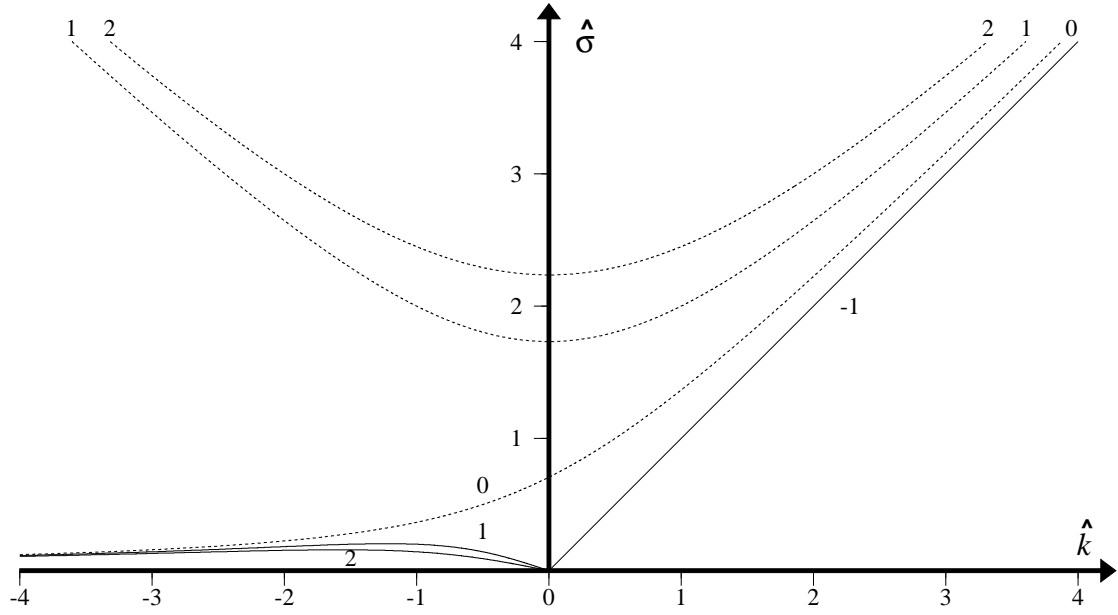
$$c_R = \frac{\sigma}{k} = -\frac{c^2}{\beta y^2} \quad (\text{B.5})$$

can be written for these waves; this states that the local phase velocity of the wave decreases with increasing distance from the equator. They are trapped equatorward of a critical latitude given by

$$y_c = \frac{c}{2\sigma}. \quad (\text{B.6})$$

The equatorial Rossby waves cannot exist poleward of this latitude.

Figure B.1 Dispersion curves for linear waves on an equatorial β -plane, obtained by using different values of n in (B.1). On the ordinate is the non-dimensional frequency $\hat{\sigma} = \frac{\sigma}{(2\beta c)^{\frac{1}{2}}}$ and on the abscissa is the non-dimensional zonal wavenumber $\hat{k} = k \left(\frac{c}{2\beta} \right)^{\frac{1}{2}}$. The curves labelled -1 (solid) and 0 (dashed) correspond to the equatorially-trapped Kelvin and Yanai, or mixed planetary-gravity, waves, respectively. The upper curves (dashed) labelled 1 and 2 are the first two Poincaré wave modes and the corresponding lower curves (solid) are the first two Rossby wave modes [the curves for the Poincaré and Rossby waves are based on the approximate relations (B.2) and (B.3)]. The zonal group velocity of these waves is given by $c_g = \frac{d\sigma}{dk}$ and the zonal phase velocity by $c = \frac{\sigma}{k}$. The zonal group and phase velocity of the Kelvin wave is eastward. The zonal group velocity of the Yanai wave is eastward; its zonal phase velocity is eastward (westward) at positive (negative) wavenumbers. A consequence of the approximation (B.2) is that the dispersion curves for Poincaré waves are symmetric w.r.t. \hat{k} ; hence, the waves with eastward (westward) zonal group velocity also have eastward (westward) zonal phase velocity. At low (high) wavenumbers, i.e., at large (short) wavelengths, the zonal group velocity of the Rossby wave is westward (eastward); its zonal phase velocity, however, is always westward. On the curve for the Rossby wave, the westward (eastward) propagating waves lie to the right (left) of the maximum. Since there is a large gap between the minimum Poincaré wave frequency and the maximum Rossby wave frequency, it is easy to distinguish between them; only the Kelvin and Yanai waves exist in this frequency gap. At positive wavenumbers, the Yanai wave is almost indistinguishable from the Kelvin wave, the only difference being its assymetry about the equator; at high negative wavenumbers, it behaves like the (short) Rossby wave. At the low frequencies of interest, Poincaré waves do not exist. At these frequencies, the eastward propagating Rossby waves and the Yanai wave have short wavelengths and are quickly dissipated; hence, they are not important for the large-scale dynamics in the tropics. Therefore, at the low frequencies of interest in this thesis, the only equatorially-trapped waves of consequence are the westward propagating Rossby waves and the Kelvin wave (solid curves).



B.2 Waves Trapped at a Coast

Since the models used in this thesis have a flat bottom and ignore the effects of the continental shelf, the only coastally-trapped wave of interest is the Kelvin wave, which propagates along a vertical wall.

B.2.1 Coastally-Trapped Kelvin Waves

These waves propagate with the coast on their right in the northern hemisphere [Gill, 1982]. They are non-dispersive and are trapped at the coast with a trapping scale, or “radius of deformation”, given by

$$R_c = \frac{c}{f}, \quad (\text{B.7})$$

where f is the local Coriolis parameter. The coast acts as a waveguide of variable width, R_c decreasing poleward. For $c = 185 \text{ cm s}^{-1}$, the trapping scale is about 75 km at 10°N and 150 km at 5°N . The particle velocity associated with these waves can be in either direction along the coast.

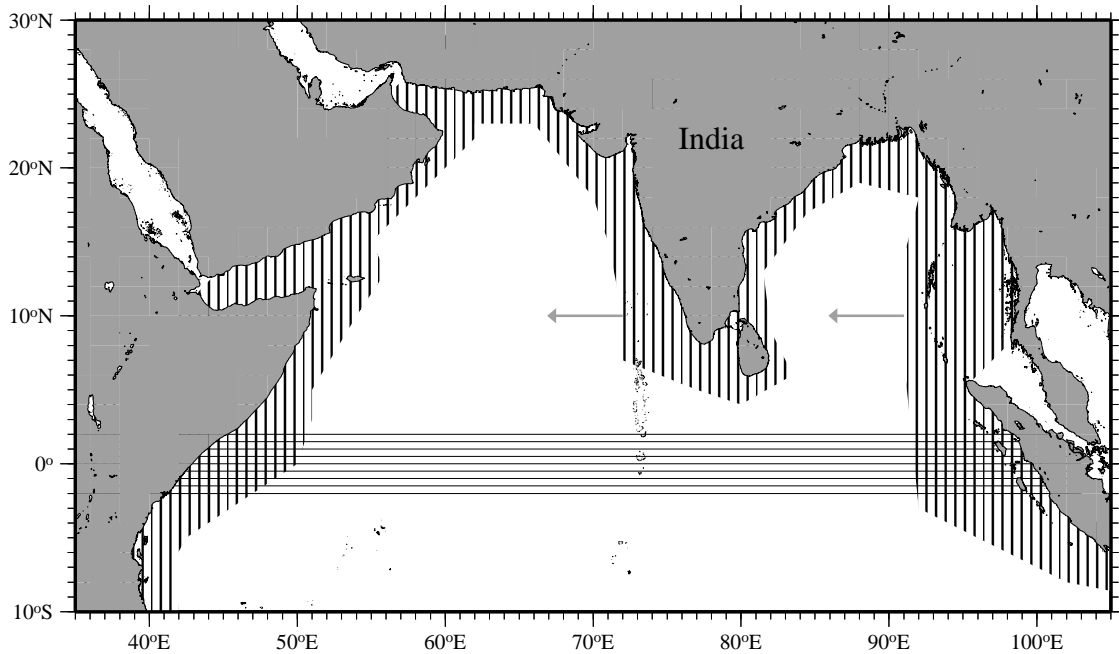
Equatorward of the critical latitude y_c , given by (B.6), a coastal Kelvin wave is not trapped at the coast; it radiates westward propagating Rossby waves as it propagates meridionally and the coastal waveguide turns “leaky” [Shetye, 1998]. In this case, it is not possible to separate the Kelvin wave from the Rossby wave. Since y_c is 42° and 21° for the annual and semiannual harmonics, the coastal waveguide along the eastern boundary of the Bay of Bengal and along the west coast of India is leaky for these frequencies (Figure B.2).

B.3 Observations of Rossby and Kelvin Waves in the Oceans

Equatorial Rossby and Kelvin waves and coastal Kelvin waves are the three waves invoked when describing the large-scale circulation in the north Indian Ocean. They appear prominently in model simulations, which tend to produce a smoother map of sea level and currents than are actually observed. All these waves, however, have been observed in the oceans, either as oscillations of the sea surface, or as oscillations of the thermocline or pycnocline. In association with these fields, there are changes in the currents. The sea-surface temperature (SST) also shows the influence of these waves, the movement of the model interface (the model thermocline) often having been used as a proxy for SST in model studies of El Niño.

A remarkable manifestation of these waves was reported by Jacobs et al. [1994], who used Geosat altimetry and model simulations to track the positive sea-level anomalies generated in the eastern equatorial Pacific by the 1982–83 El Niño a decade later in the subtropical central Pacific. The sea-level high in the eastern equatorial Pacific was generated by the downwelling equatorial

Figure B.2 A schematic of the “leaky” waveguide in the north Indian Ocean [Shetye, 1998]. The horizontal hatching indicates the equatorial waveguide, which extends about 200 km on either side of the equator; the vertical hatching indicates the coastal waveguide. The equatorial waveguide is connected to the Bay of Bengal at its eastern boundary. This link arises as a consequence of the reflection of the equatorial Kelvin wave at the eastern boundary of the basin; the reflected wave is a summation over several meridional modes of the westward propagating Rossby wave, these being required to satisfy the condition of no normal flow at the boundary [Moore, 1968]. The higher meridional modes are equivalent to a coastal Kelvin wave, which carries a part of the incident energy poleward along the coast in both hemispheres. This Kelvin wave is trapped at the coast poleward of the critical latitude; equatorward of this latitude, westward radiation of energy is possible, and the coastal Kelvin wave is inseparable from the Rossby wave. The same phenomenon is seen off the Indian west coast. For the seasonal cycle, it is the annual and semiannual harmonics that are most important. The critical latitudes for these periods are 42° and 21° , respectively; the former lies poleward of the northern boundary of the basin, and the latter is close to it. Hence, both annual and semiannual Kelvin waves are inseparable from westward propagating Rossby waves in the Bay of Bengal and the Arabian Sea, and energy leaks at these periods from the eastern boundary into the open ocean. The arrows show the direction in which energy leaks out of the coastal waveguide.



Kelvin waves triggered by a relaxation in the easterly trade winds. The equatorial Kelvin waves generated Rossby waves on reflection at the eastern boundary of the basin. Moore [1968] showed that the zonal velocity of the Kelvin wave cannot be cancelled by a single meridional mode of the westward propagating Rossby wave; an infinity of modes is needed to satisfy the boundary condition. The higher order modes propagate poleward along the coast and Moore showed that this poleward propagation was equivalent to a coastal Kelvin wave. The Kelvin wave at these latitudes cannot be separated from the Rossby wave because it is equatorward of the critical latitude for the sub-annual frequencies that characterise El Niño; hence, a part of the energy “peels” off the coast as a Rossby wave. Jacobs et al. showed that the Rossby wave generated by the strong El Niño of 1982–83 was still propagating across the subtropical Pacific a decade later, forcing changes in the Kuroshio extension. The coastal Kelvin wave generated by the reflection of the equatorial Kelvin wave has been traced as far as the Canadian border and Alaska [Enfield and Allen, 1980; Chelton and Davis, 1982]. The strength of the signal and the improvement in the measuring instruments made it possible to track the effects of the 1982–83 El Niño, but the basic dynamics of this event was no different from that of other manifestations of the phenomenon.

These waves have been detected in the Indian Ocean too. Perigaud and Delecluse [1992, 1993] detected Rossby wave signals in the south Indian Ocean in Geosat data. Kumar and Unnikrishnan [1995], Unnikrishnan et al. [1997], and Rao [1998] used temperature climatologies to show evidence in thermocline oscillation for the existence of Rossby waves in the north Indian Ocean. Equatorial Kelvin waves too are seen in the altimeter data. Coastal Kelvin waves, however, are difficult to detect in the north Indian Ocean because the wind forcing is strong along most of the coast and distorts the phase of the propagating waves; the free and forced waves cannot be separated, making it difficult to track a signal along the coast. The discussion on forcing mechanisms of the Lakshadweep high and low (Section 3.5), however, hints at the possibility of detecting such signals in daily sea-level data along the Indian west coast during the northeast monsoon, when the local winds are relatively weak and the free waves, forced by winds along the Indian east coast, dominate. Unfortunately, there are no tide-gauge data along the eastern boundary of the Bay of Bengal, which appears to be the best place to look for evidence of free coastal Kelvin waves because the local winds blow into the coast, forcing a very weak Kelvin wave (Section 3.5.2). Therefore, the Kelvin wave signal here must consist of free waves forced remotely from the equatorial Indian Ocean.

We close this discussion here, referring the reader to Gill [1982] and Pedlosky [1979] for more details on these waves.

Appendix C

Estimating the Statistical Significance of Correlations

We say that a linear correlation between two variables x and y is statistically significant at a given level, say $P\%$, when the probability of two series of random numbers having the same correlation is less than $(100 - P)\%$. For example, the correlation is significant at the 95% significance level if there is but a 5% chance that the correlation between two series of random numbers for the same number of degrees of freedom (the number of valid data points at the given lag) would equal or exceed the correlation between x and y . Therefore, the statistical significance of the linear correlations computed in Chapter 6 is estimated as follows.

Suppose the number of degrees of freedom is M . N_s series of random numbers are constructed using a random-number-generator, each series consisting of M terms. Correlations are computed for each combination of these N_s series, taken two at a time; this yields $N_c = \frac{N_s(N_s-1)}{2}$ correlations. The magnitudes (absolute value) of these correlations are sorted to obtain a monotonic sequence C_n of N_c terms, in which correlations are ordered from the lowest to the highest value. Then, C_p is the required correlation at the $P\%$ significance level, where

$$p = \frac{PN_c}{100} + 1.$$

The correlations computed thus match those in Table 7 in Crow et al. [1960].

The same method is used to estimate the significance levels when x and y are filtered with an N -year running mean. The same filter is applied to the N_s series of random numbers and the correlations are computed for these filtered series. The rest of the procedure is as described above. Application of the filter decreases the randomness of the series; the correlations among the filtered series are higher, and hence, the correlation at given significance level is higher than before.

For the correlations computed in Chapter 6, the random-number series were generated using function `ran2` in Press et al. [1989]; M depends on the variables being correlated because

the tide-gauge sea-level and rainfall records are not of the same length; $N_s = 500$; therefore, $N_c = 124750$. Reducing N_s to 150 decreases N_c to 11175, but there is only a minor change in the correlation at a given significance level. Changing the random number seed `iseed` also does not have an influence on these correlations, implying that the random-number series generated by function `ran2` are sufficiently random for our purpose.

Appendix D

Sources of Data and Software

The observations presented in this thesis were obtained from different sources and processed into graphical form using several software packages. The sources of data and software are listed here.

D.1 Data

- The hourly and daily sea level at Mumbai (Figure 1.3) were obtained from the Survey of India. These data were converted to electronic form by Matthew Dias and processed by D. Sundar.
- Monthly sea level data from tide gauges are the major data used in this thesis. These were obtained from the Permanent Service for Mean Sea Level (PSMSL) at the Bidston Observatory, United Kingdom.
- The Comprehensive Ocean-Atmosphere Data Set (COADS) was the source of the climatology of monthly sea-level atmospheric pressure used to correct the climatology of monthly sea level.
- The monthly sea-level atmospheric-pressure data used to correct the time series of monthly sea level in Chapter 6 were obtained from the Global Historical Climate Network (GHCN); the GHCN was also the source of monthly rainfall data for Mumbai, Kochi, Chennai, and Vishakhapatnam.
- All hydrographic data, except the climatologies of Levitus and Boyer [1994] and Levitus et al. [1994] and the salinity data off Marmagao (Figure 6.27), were obtained from the Indian National Oceanographic Data Centre (INODC) at the National Institute of Oceanography, Goa. A. Suryachandra Rao [Rao, 1998] put these data together and checked their quality, making possible the synthesis of the “coastal climatology” presented in Chapter 4. The

climatologies of Levitus and Boyer [1994] and Levitus et al. [1994] were obtained from the National Oceanic and Atmospheric Administration (NOAA), USA. The salinity data off Marmagao were made available by P. V. Narvekar, National Institute of Oceanography, Goa.

- All-India rainfall data were made available in electronic form by (late) Asha Guruprasad, Sulochana Gadgil, and Sajani Surendran, Indian Institute of Science, Bangalore. The 1871–1994 data were synthesized from the rainfall data for 306 stations in 29 meteorological subdivisions in India by Parthasarathy et al. [1995].
- Julian McCreary, Kevin Kohler, and Weiqing Han (Nova Southeastern University, Florida, USA) made available the results of the numerical simulations of McCreary et al. [1993]; these data were used to compute the sea level plotted in Figure 4.4. The climatology of winds, from Hellerman and Rosenstein [1983], and the climatology of ship drifts, from Rao et al. [1989], were also obtained from them.

D.2 Software

- Most of the figures were made with *GMT* (*Generic Mapping Tools*) and *FERRET*; *LATEX 2 ϵ* was used to prepare some of the schematics. *GMT* was written by Paul Wessel and Walter Smith [Wessel and Smith, 1991; Smith and Wessel, 1990]. *FERRET* was developed by the Thermal Modeling and Analysis Project (TMAP) at the Pacific Marine Environmental Laboratory (PMEL) of NOAA, USA; it uses *PlotPlus*, a package developed by Donald Denbo.
- Both *GMT* and *FERRET* use *netCDF*, a data format developed at the University Centre for Atmospheric Research, University of Boulder, Colorado, USA.
- This thesis was typeset using *LATEX 2 ϵ* . The manuscript was typed using *GNU Emacs* and *AUCTEX* on a pentium running *Debian GNU/Linux*. *GNU* was also the source of several other packages that were used; notable among these are *ghostscript*, *gv*, and *ghostview*.

Bibliography

- J. S. Allen. Coastal trapped waves in a stratified ocean. *Journal of Physical Oceanography*, 5: 300–325, 1975.
- D. G. Aubrey and K. O. Emery. Australia — an unstable platform for tide-gauge measurements of changing sea levels. *Journal of Geology*, 94:699–712, 1986.
- K. Banse. Hydrography of the Arabian Sea Shelf of India and Pakistan and effects on demersal fishes. *Deep-Sea Research*, 15:45–79, 1968.
- K. Banse. Overview of the hydrography and associated biological phenomena in the Arabian Sea. In B. U. Haq and J. D. Milliman, editors, *Marine geology and oceanography of Arabian Sea and coastal Pakistan*, pages 271–303. Van Nostrand Reinhold Co, New York, 1984.
- K. Banse. On the coupling of hydrography, phytoplankton, zooplankton, and settling organic particles offshore in the Arabian Sea. *Proceedings of the Indian Academy of Sciences (Earth and Planetary Sciences)*, 103(2):125–161, June 1994. Special issue: Biogeochemistry of the Arabian Sea.
- T. P. Barnett. The estimation of “global” sea level change: A problem of uniqueness. *Journal of Geophysical Research*, 89(C5):7980–7988, September 1984.
- J. G. Bruce. Comparison of near surface dynamic topography during the two monsoons in the western Indian Ocean. *Deep-Sea Research*, 15:665–667, 1968.
- J. G. Bruce, D. R. Johnson, and J. C. Kindle. Evidence for eddy formation in the eastern Arabian Sea during the northeast monsoon. *Journal of Geophysical Research*, 99(C4):7651–7664, April 1994.
- J. G. Bruce, J. C. Kindle, L. H. Kantha, J. L. Kerling, and J. F. Bailey. Recent observations and modeling in the Arabian Sea Laccadive high region. *Journal of Geophysical Research*, 103(C4): 7593–7600, April 1998.

- D. C. Chapman. Numerical treatment of cross-shelf open boundary conditions in a barotropic coastal ocean model. *Journal of Physical Oceanography*, 15:1060–1075, 1985.
- D. B. Chelton and R. E. Davis. Monthly mean sea level variability along the west coast of north America. *Journal of Physical Oceanography*, 12:757–784, 1982.
- A. J. Clarke and X. Liu. Observations and dynamics of semiannual and annual sea levels near the eastern equatorial Indian Ocean boundary. *Journal of Physical Oceanography*, 23(2):386–399, February 1993.
- A. J. Clarke and X. Liu. Interannual sea level in the northern and eastern Indian Ocean. *Journal of Physical Oceanography*, 24(6):1224–1235, June 1994.
- A. J. Clarke and C. Shi. Critical frequencies at ocean boundaries. *Journal of Geophysical Research*, 96(C6):10,731–10,738, June 1991.
- A. J. Clarke and S. van Gorder. On ENSO coastal currents and sea levels. *Journal of Physical Oceanography*, 24(3):662–680, March 1994.
- E. L. Crow, F. A. Davis, and M. W. Maxfield. *Statistics Manual*. Dover Publications, Inc., New York, 1960. Released within the Department of Defense as NAVORD REPORT 3369-NOTS 948.
- A. N. Cutler and J. C. Swallow. Surface currents of the Indian Ocean (to 25°S, 100°E): Compiled from historical data archived by the Meteorological Office, Bracknell, UK. *Report 187*, Institute of Oceanographic Sciences, Wormley, England, 1984. 36 charts, 8pp.
- V. K. Das. Seasonal variation in mean-sea level at Mormugao, west coast of India. *Mahasagar*, 12(2):59–67, 1979.
- A. T. Doodson. Harmonic development of the tide-generating potential. *Proceedings of the Royal Society of London, Series A*, 100:305–329, 1921.
- K. O. Emery and D. G. Aubrey. Tide gauges of India. *Journal of Coastal Research*, 5(3):489–501, Summer 1989.
- D. B. Enfield and J. S. Allen. On the structure and dynamics of monthly mean sea level anomalies along the Pacific coast of north and south America. *Journal of Physical Oceanography*, 10(4): 557–578, April 1980.
- H. S. Ghildyal and A. Kumar. Global mean sea level investigations: Discrepancy between the local mean sea level of the Bay of Bengal and local mean sea level of the Arabian Sea. Technical Paper, Published by the Surveyor General of India, 1984.

- A. E. Gill. *Atmosphere-Ocean Dynamics*, volume 30 of *International Geophysics Series*. Academic Press, Inc., San Diego, CA 92101, USA, 1982.
- A. E. Gill and A. J. Clarke. Wind-induced upwelling, coastal currents, and sea-level changes. *Deep-Sea Research*, 21:325–345, 1974.
- V. Gornitz, S. Lebedeff, and J. Hansen. Global sea level trend in the past century. *Science*, 215: 1611–1614, 26 mar 1982.
- I. S. Gradshteyn and I. M. Ryzhik. *Tables of Integrals, Series, and Products*. Academic Press, fourth edition, 1965. Translated from the Russian by Scripta Technica, Inc. Translation edited by A. Jeffrey.
- S. Hellerman and M. Rosenstein. Normal monthly wind stress over the world ocean with error estimates. *Journal of Physical Oceanography*, 13:1093–1104, 1983.
- G. A. Jacobs, H. E. Hurlbert, J. C. Kindle, E. J. Metzger, J. L. Mitchell, W. J. Teague, and A. J. Wallcraft. Decade-scale trans-Pacific propagation and warming effects of an El Niño anomaly. *Nature*, 370:360–363, 1994.
- T. G. Jensen. Equatorial variability and resonance in a wind-driven Indian Ocean model. *Journal of Geophysical Research*, 98:22,533–22,552, 1993.
- P. V. Joseph. Climatic change in monsoon and cyclones 1891–1974. In *Proceedings of the Symposium on Tropical Monsoons*. Indian Institute of Tropical Meteorology, Pune, 1976.
- S. P. Kumar and A. S. Unnikrishnan. The seasonal cycle of temperature and associated wave phenomena in the Bay of Bengal. *Journal of Geophysical Research*, 100:13,585–13,593, 1995.
- S. Levitus and T. P. Boyer. World Ocean Atlas 1994, Volume 4: Temperature. NOAA Atlas NESDIS 4. 117 pp., 1994.
- S. Levitus, R. Burgett, and T. P. Boyer. World Ocean Atlas 1994, Volume 3: Salinity. NOAA Atlas NESDIS 3. 99 pp., 1994.
- M. J. Lighthill. Dynamic response of the Indian Ocean to the onset of the southwest monsoon. *Philosophical Transactions of the Royal Society of London, Series A*, 265:45–92, October 1969.
- A. R. Longhurst and W. S. Wooster. Abundance of oil sardine (*Sardinella longiceps*) and upwelling on the southwest coast of India. *Canadian Journal of Fisheries and Aquatic Sciences*, 47:2407–2419, 1990.

- M. Madhupratap, S. P. Kumar, P. M. A. Bhattathiri, M. D. Kumar, S. Raghukumar, K. K. C. Nair, and N. Ramaiah. Mechanism of the biological response to winter cooling in the northeastern Arabian Sea. *Nature*, 384:549–552, 12 December 1996.
- J. M. Martin, J. D. Burton, and D. Eisma. *River inputs to ocean systems*. United Nations Press, 1981.
- J. P. McCreary. Modeling wind-driven ocean circulation. Technical Report JIMAR 80-0029, Hawaii Institute of Geophysics, University of Hawaii, Honolulu, Hawaii 96822, December 1980.
- J. P. McCreary. A linear stratified ocean model of the equatorial undercurrent. *Philosophical Transactions of the Royal Society of London, Series A*, 298(1444):603–635, January 1981.
- J. P. McCreary, W. Han, D. Shankar, and S. R. Shetye. Dynamics of the East India Coastal Current, 2. Numerical solutions. *Journal of Geophysical Research*, 101(C6):13,993–14,010, June 1996.
- J. P. McCreary and P. Kundu. A numerical investigation of the Somali current during the southwest monsoon. *Journal of Marine Research*, 46:25–58, 1988.
- J. P. McCreary, P. K. Kundu, and R. L. Molinari. A numerical investigation of the dynamics, thermodynamics and mixed-layer processes in the Indian Ocean. *Progress in Oceanography*, 31: 181–244, 1993.
- S. K. Mishra and S. Gadgil. *Indian Climate Research Programme. Science Plan*. Department of Science and Technology, Government of India, New Delhi, November 1996.
- D. W. Moore. *Planetary-Gravity Waves in an Equatorial Ocean*. PhD thesis, Harvard University, Cambridge, Massachusetts, February 1968.
- L. A. Mysak. Recent advances in shelf wave dynamics. *Reviews of Geophysics and Space Physics*, 18(1):211–241, February 1980.
- S. W. A. Naqvi, M. D. George, P. Narvekar, D. A. Jayakumar, M. S. Shailaja, S. Sardesai, V. V. S. S. Sarma, D. M. Shenoy, H. Naik, P. A. Maheshwaran, K. Krishnakumari, G. Rajesh, A. K. Sudhir, and M. S. Binu. Severe fish mortality associated with ‘red tide’ observed in the sea off Cochin. *Current Science*, 75(6):543–544, September 1998.
- R. S. Nerem, E. J. Schrama, C. J. Koblinsky, and B. D. Beckley. A preliminary evaluation of ocean topography from the TOPEX/POSEIDON mission. *Journal of Geophysical Research*, 99 (12):24,565–24,583, December 1994.

- J. J. O'Brien and H. E. Hurlburt. Equatorial jet in the Indian Ocean: Theory. *Science*, 184: 1075–1077, 1974.
- B. Parthasarathy, A. A. Munot, and D. R. Kothawale. All-India monthly and seasonal rainfall series; 1871–1993. *Theoretical and Applied Climatology*, 49:217–224, 1993.
- B. Parthasarathy, A. A. Munot, and D. R. Kothawale. Monthly and seasonal rainfall series for all-India homogeneous regions and meteorological subdivisions: 1871–1994. IITM Research Report No. RR–065, ISSN 0252-1075, Indian Institute of Tropical Meteorology, Pune, 1995.
- J. Patullo, W. Munk, R. Revelle, and E. Strong. The seasonal oscillation in sea level. *Journal of Marine Research*, 14(1):88–113, January 1955.
- J. Pedlosky. *Geophysical Fluid Dynamics*. Springer-Verlag, New York, first edition, 1979.
- C. Perigaud and P. Delecluse. Annual sea level variations in the southern tropical Indian Ocean from Geosat and shallow-water simulations. *Journal of Geophysical Research*, 97(C12):20,169–20,178, December 1992.
- C. Perigaud and P. Delecluse. Interannual sea level variations in the tropical Indian Ocean from Geosat and shallow water simulations. *Journal of Physical Oceanography*, 23(9):1916–1934, September 1993.
- G. L. Pickard and W. J. Emery. *Descriptive physical oceanography*. Pergamon Press, fourth edition, 1982.
- R. M. Ponte. Variability in a homogeneous global ocean forced by barometric pressure. *Dynamics of Atmospheres and Oceans*, 18:209–234, 1993.
- J. T. Potemra, M. E. Luther, and J. J. O'Brien. The seasonal circulation of the upper ocean in the Bay of Bengal. *Journal of Geophysical Research*, 96(C7):12,667–12,683, July 1991.
- K. V. S. R. Prasad and B. S. R. Reddy. Sea level variations off Madras, east coast of India. *Indian Journal of Marine Sciences*, 14:206–209, December 1985.
- W. H. Press, B. P. Flannery, S. A. Teukolsky, and W. T. Vetterling. *Numerical Recipes. The Art of Scientific Computing (FORTRAN version)*. Cambridge University Press, first edition, 1989.
- D. T. Pugh. *Tides, surges, and mean sea level*. John Wiley and Sons Ltd., 1987.
- A. S. Rao. *Rossby Waves in the Bay of Bengal: Observations and Simulations*. PhD thesis, Andhra University, Vishakhapatnam, India, March 1998.

- R. R. Rao, R. L. Molinari, and J. F. Festa. Evolution of the climatological near-surface thermal structure of the tropical Indian Ocean, 1. Description of mean monthly mixed-layer depth and sea-surface temperature, surface-current, and surface meteorological fields. *Journal of Geophysical Research*, 94:10,801–10,815, 1989.
- G. Reverdin, D. L. Cadet, and D. Gutzler. Interannual displacement of convection and surface circulation over the equatorial Indian Ocean. *Quarterly Journal of the Royal Meteorological Society*, 112:43–67, 1986.
- P. Ripa. Conservation laws for primitive equations models with inhomogeneous layers. *Geophysical and Astrophysical Fluid Dynamics*, 70:85–111, 1992.
- P. Ripa. On improving a one-layer ocean model with thermodynamics. *Journal of Fluid Mechanics*, 303:169–201, 1995.
- B. C. Roy. Activities of Indian Cell for Monitoring and Analysis of Sea level (CMAS). In *IOC-UNEP-WMO-SAREC Planning Workshop on an Integrated Approach to Coastal Erosion, Sea Level Changes and their Impacts*, volume 96 of *IOC Workshop Reports*, pages 37–47, Zanzibar, Tanzania, 17–21 January 1994.
- F. Schott. Seasonal variation of the cross-equatorial flow in the Somali Current. *Journal of Geophysical Research*, 91:10,581–10,584, 1986.
- D. Shankar, J. P. McCreary, W. Han, and S. R. Shetye. Dynamics of the East India Coastal Current, 1. Analytic solutions forced by interior Ekman pumping and local alongshore winds. *Journal of Geophysical Research*, 101(C6):13,975–13,991, June 1996.
- D. Shankar and S. R. Shetye. On the dynamics of the Lakshadweep high and low in the south-eastern Arabian Sea. *Journal of Geophysical Research*, 102(C6):12,551–12,562, June 1997.
- S. S. C. Shenoi, D. Shankar, and S. R. Shetye. On the sea surface temperature high in the Lakshadweep Sea before the onset of the southwest monsoon. *Journal of Geophysical Research*, 104:15,703–15,712, July 1999.
- S. R. Shetye. Seasonal variability of the temperature field off the southwest coast of India. *Proceedings of the Indian Academy of Sciences (Earth and Planetary Sciences)*, 93(4):399–411, 1984.
- S. R. Shetye. The movement and implications of the Ganges-Brahmaputra runoff on entering the Bay of Bengal. *Current Science*, 64(1):32–38, January 1993.

- S. R. Shetye. West India Coastal Current and Lakshadweep high/low. *Sadhana*, 23:637–651, 1998.
- S. R. Shetye and A. M. Almeida. An examination of the factors that influence the monthly-mean sea level along the coast of India. In *IOC/Unesco Workshop on Regional Co-operation in Marine Science in the Central Indian Ocean and Adjacent Seas and Gulfs*, volume 37 of *IOC Workshop Reports*, pages 87–104, Colombo, Sri Lanka, 8–13 July 1985.
- S. R. Shetye and A. D. Gouveia. *Coastal circulation in the north Indian Ocean. Coastal segment (14,S–W)*, volume 11 of *The Sea*, chapter 18, pages 523–556. John Wiley and Sons, Inc, 1998.
- S. R. Shetye, A. D. Gouveia, D. Shankar, S. S. C. Shenoi, P. N. Vinayachandran, D. Sundar, G. S. Michael, and G. Nampoothiri. Hydrography and circulation in the western Bay of Bengal during the northeast monsoon. *Journal of Geophysical Research*, 101(C6):14,011–14,025, June 1996.
- S. R. Shetye, A. D. Gouveia, S. S. C. Shenoi, G. S. Michael, D. Sundar, A. M. Almeida, and K. Santanam. The coastal current off western India during the northeast monsoon. *Deep-Sea Research*, 38(12):1517–1529, December 1991a.
- S. R. Shetye, A. D. Gouveia, S. S. C. Shenoi, D. Sundar, G. S. Michael, A. M. Almeida, and K. Santanam. Hydrography and circulation off the west coast of India during the southwest monsoon 1987. *Journal of Marine Research*, 48:359–378, 1990.
- S. R. Shetye, A. D. Gouveia, S. S. C. Shenoi, D. Sundar, G. S. Michael, and G. Nampoothiri. The western boundary current of the seasonal subtropical gyre in the Bay of Bengal. *Journal of Geophysical Research*, 98(C1):945–954, January 1993.
- S. R. Shetye, S. S. C. Shenoi, A. D. Gouveia, G. S. Michael, D. Sundar, and G. Nampoothiri. Wind-driven coastal upwelling along the western boundary of the Bay of Bengal during the southwest monsoon. *Continental Shelf Research*, 11(11):1397–1408, November 1991b.
- N. Singh. *Variability of moisture and thermal fields over India*. Ph.D. Dissertation, Department of Geophysics, Banaras Hindu University, Varanasi, India, 1994.
- W. H. F. Smith and P. Wessel. Gridding with continuous curvature splines in tension. *Geophysics*, 55:293–305, 1990.
- B. L. K. Somayajulu, M. M. Sarin, and R. Ramesh. Denitrification in the eastern Arabian Sea: Evaluation of the role of continental margins using Ra isotopes. *Deep-Sea Research, Part B*, 43: 111–117, 1996.

- J. Sprintall and M. Tomczak. Evidence of the barrier layer in the surface layer of the tropics. *Journal of Geophysical Research*, 97:7305–7316, 1992.
- B. D. Tapley, D. P. Chambers, C. K. Shum, R. J. Eanes, J. C. Ries, and R. H. Stewart. Accuracy assessment of the large-scale dynamic ocean topography from TOPEX/POSEIDON altimetry. *Journal of Geophysical Research*, 99(C12):24,605–24,617, December 1994.
- M. N. Tsimplis and P. L. Woodworth. The global distribution of the seasonal sea level cycle calculated from coastal tide gauge data. *Journal of Geophysical Research*, 99(C8):16,031–16,039, August 1994.
- A. S. Unnikrishnan, S. P. Kumar, and G. S. Navelkar. Large-scale processes in the upper layers of the Indian Ocean inferred from temperature climatology. *Journal of Marine Research*, 55: 93–115, 1997.
- R. Varadarajulu, M. Harikrishna, and K. H. Rao. Sealevel changes at Paradip, east coast of India. *Indian Journal of Marine Sciences*, 11:32–34, March 1982.
- M. J. Varkey, V. S. N. Murty, and A. Suryanarayana. Physical oceanography of the Bay of Bengal and Andaman Sea. *Oceanography and Marine Biology*, 34:1–70, 1996.
- J. Vialard and P. Delecluse. An OGCM study for the TOGA decade. Part I: Role of salinity in the physics of the western Pacific fresh pool. *Journal of Physical Oceanography*, 28(6):1071–1088, June 1998a.
- J. Vialard and P. Delecluse. An OGCM study for the TOGA decade. Part II: Barrier-layer formation and variability. *Journal of Physical Oceanography*, 28(6):1089–1106, June 1998b.
- P. N. Vinayachandran. *The Bay of Bengal Circulation in an OGCM*. PhD thesis, Indian Institute of Science, Bangalore 560012, India, December 1995.
- P. N. Vinayachandran, S. R. Shetye, D. Sengupta, and S. Gadgil. Forcing mechanisms of the Bay of Bengal circulation. *Current Science*, 71(10):753–763, November 1996.
- P. N. Vinayachandran and T. Yamagata. Monsoon response of the sea around Sri Lanka: Generation of thermal domes and anticyclonic vortices. *Journal of Physical Oceanography*, 28(10): 1946–1960, October 1998.
- P. Wessel and W. H. F. Smith. Free software helps map and display data. *EOS Transactions of the American Geophysical Union*, 72:441, 445–446, 1991.
- K. Wyrtki. *Oceanographic Atlas of the International Indian Ocean Expedition*. National Science Foundation, Washington, D.C., November 1971. 531 pp.

- K. Wyrtki. An equatorial jet in the Indian Ocean. *Science*, 181:262–264, 1973.
- K. Wyrtki. Sea level rise: The facts and the future. *Pacific Science*, 44(1):1–16, January 1990.
- L. Yu, J. J. O'Brien, and J. Yang. On the remote forcing of the circulation in the Bay of Bengal. *Journal of Geophysical Research*, 96(C11):20,449–20,454, November 1991.